APPROACHES TO ANALYZING UNCERTAINTY IN MECHANISTIC ORDINARY DIFFERENTIAL EQUATION MODELS: PROPOGATION, VALIDATION, AND ESTIMATION

by

ISHAAN A. DAVE

(Under the Direction of K. Melissa Hallow)

ABSTRACT

Biological systems are generally complex networks that involve several interactions among components (genes, proteins, cells, other biochemical species, etc.). These networks are the underlying basis of physiological function and fully understanding these networks enables researchers to investigate perturbations within them which can be representative of disease / disease states. Mathematical modeling is a method to quantify these interactions and nuances of these networks using computational and mathematical representations of these systems. These models incorporate data from multiple sources, and combining these data with a physiological understanding of the system can result in large sets of differential equations. When modeling, several sources of variability arise when considering the data used, the system modeled, and the equations used to represent the system. We investigate these issues by investigating concerns of available data by examining identifiability of a renin angiotensin system (RAS) model, narrow the scope of the model by investigating the sensitivity of input parameters and their effects on

predicted outputs and determining the effect of latent variables on variability of responses to therapy in the model. To accomplish this in this dissertation, we 1) extended an existing mathematical model of the RAS to quantify the interplay of therapy, SARS-CoV-2 infection, and chronic diseases or aging between pro-and anti-inflammatory arms of the RAS, 2) developed a mechanistic model of heart failure biomarkers and 3) integrated that model into an existing model of cardiorenal function to describe and explain changes in biomarker levels with drug treatments and reduced kidney function observed in clinical trials. In this dissertation, three different problems (identifiability, sensitivity, and validation) involving the application of ordinary differential equation (ODE) models and understanding of the related uncertainty will be addressed.

INDEX WORDS: Mathematical Modeling, COVID, Renin Angiotensin System, Quantitative Systems Pharmacology, Heart Failure, BNP, NT-proBNP

APPROACHES TO ANALYZING UNCERTAINTY IN MECHANISTIC ORDINARY DIFFERENTIAL EQUATION MODELS: PROPOGATION, VALIDATION, AND ESTIMATION

by

ISHAAN DAVE

BA, Emory University, 2016

MSPH, Emory University, 2017

A Dissertation Submitted to the Graduate Faculty of The University of Georgia in Partial Fulfillment of the Requirements for the Degree

DOCTOR OF PHILOSOPHY

ATHENS, GEORGIA

2023

APPROACHES TO ANALYZING UNCERTAINTY IN MECHANISTIC ORDINARY DIFFERENTIAL EQUATION MODELS: PROPOGATION, VALIDATION, AND ESTIMATION

by

ISHAAN A. DAVE

Major Professor:	K. Melissa Hallow
Committee:	Stephen Rathbun
	John Drake
	Xiao Song

Electronic Version Approved:

Ron Walcott
Vice Provost for Graduate Education and Dean of the Graduate School
The University of Georgia
December 2023

ACKNOWLEDGEMENTS

I would like to thank my advisor, committee members, professors, colleagues, friends, and family who have supported me throughout this journey and made this work possible. I would sincerely express my gratitude and appreciation to Dr. Melissa Hallow for direction and support through my Ph.D. work. The number of hours, encouragement, patience, scholarship, cannot be counted and for that, I am very grateful. I would also like to thank Dr. John Drake, Dr. Stephen Rathbun, and Dr. Xiao Song for serving on my committee as well as their scientific insight.

I would also like to thank my family and friends for their love, support, and encouragement which has allowed me to persevere and given me strength through this journey. A special shoutout to my amazing girlfriend Raveena Patel and friend/colleague/confidant Nicholas Mallis for their unwavering support t

TABLE OF CONTENTS

Page

LIST OF TABLES

Page

LIST OF FIGURES

Page

LIST OF ACRONYMS

RAS – Renin Angiotensin System

QSP – Quantitative Systems Pharmacology

ODE – Ordinary Differential Equation

ARB – Angiotensin Receptor Blocker

HF – Heart Failure

GFR – Glomerular Filtration Rate

SARS-CoV-2 – Severe Acute Respiratory Syndrome-Coronavirus 2

BNP – B-type Natriuretic Peptide

NT-proBNP – N-terminal B-type Natriuretic Peptide

KS Test – Kolmogorov-Smirnov Test

LV EDS – Left Ventricular End-Diastolic Stress

LV EDP – Left Ventricular End-Diastolic Pressure

CHAPTER 1

INTRODUCTION

1.1 Overview of ODE Models

Biological systems are generally complex networks that involve several interactions among components (genes, proteins, cells, other biochemical species, etc.) and sometimes incorporate movement of fluid (e.g. blood) between compartments in that system. Networks like these drive physiological function and understanding behaviors of these networks plays a key role in understanding diseases, specifically when perturbing these networks [1]. These networks range in complexity from molecular and cellular levels to tissue and organism levels and as representations of systems to allow understanding of drug effects and potentially identifying new drug targets [2]. To encompass these interactions and nuances of these networks, computational and mathematical representations of these systems have been developed to explain the response to drugs and disease progression. Mathematical models like these incorporate data from various sources for the relevant agents in system of interest and combined with a physiological understanding of the biological mechanisms at hand and result in large sets of ordinary differential equations (ODEs) to provide a mechanistic understanding of the phenomenon being studied.

With a combined effort of modelers and scientists, these models are a representation of physical relations that exist within a system. In these models, not all parameters and variables (e.g. peptides, proteins, cells, geometries, etc.) are readily available, and thus are developed with knowledge of their importance within the system, but values for them are at best guesses based on

incomplete, scarce, and sometimes inconsistent data. Since these models are a simplification of reality, work must be done to ensure model results are credible.

Within these models there are several sources of uncertainty. For instance, variability exists within the system itself, the errors in the data used to construct the model, and the model itself likely. Therefore, remedying all sources of uncertainty comes at a computational cost since it's not possible to incorporate every piece of information available into a model. A balance between completeness and practicality must be met since it is impossible to incorporate every bit of the physical system into the model. These models may have several inputs and complex relationships among variables, so outputs are solved computationally; increasing the number of inputs and equations requires more computational power. Even though these models are approximations of real-life because they are deterministic in the sense that we can calculate an event with certainty if we have all the parameters fixed at the start (though uncertainty exists in parameter values).

Quantitative systems pharmacology (QSP) models are an effective way to gain mechanistic insight into the complex dynamics and interactions in a biological system and its response to perturbations (usually drug treatment). These models can become quite complicated since many biological components are involved, thus a collaborative effort among scientists is crucial for development and implementation. Allen et al state that for these models to be fit for purpose, they must include enough biological scope and details mechanistically to connect pathways to response from drugs [3]. To encompass these interactions and nuances of these networks, computational and mathematical representations of these systems have been developed to explain the response to drugs and disease progression. Mathematical models like these incorporate data from various sources for the relevant agents in the system of interest and combined with a physiological understanding of the biological mechanisms at hand, result in large sets of ordinary differential

equations (ODEs) to provide a mechanistic understanding of the phenomenon being studied. In this dissertation, three different problems including identifiability, sensitivity and estimation involving the application of ODE models and understanding of the related uncertainty will be addressed.

1.2 Background

1.2.1 COVID and the Interplay with RAS Therapies

Hypertension and diabetes are common comorbidities among hospitalized patients with coronavirus disease 2019 (COVID-19) [4]. ACE inhibitors (ACEi's) and angiotensin receptor blockers (ARBs) are standard of care treatment for these comorbidities, because they reduce cardiovascular events, kidney injury, and other vascular complications of these diseases [5], [6]. There has been a good deal of debate around the use of these drugs in patients with COVID-19. On one hand, it has been speculated that these therapies may increase susceptibility or severity of COVID-19, but conversely, it has also been speculated that they may protect against excess inflammation following COVID-19 infection [7]. The limited clinical data currently available do not seem to support evidence of harm [8], [9], [10]. De Abajo et al conducted a case-control study with 12,529 patients from seven hospitals in Madrid and found no significant increased risk of COVID-19 hospitalization with use of ACEi's or ARB (monotherapy or combinations). Similarly, they found no association for risk of COVID hospitalization and neither long- nor short-term renin angiotensin system (RAS) blocker use. In a similar case-control study of 69,793 study, Son et al found similar results. Lastly, Trifiro et al found no increase in risk of all-cause mortality when using ACEi's vs. calcium channel blockers. These 3 studies combined strengthened the recommendation to not withdraw/switching ACEi/ARB treatments in COVID-19 infected

patients. The American College of Cardiology, Heart Failure Association of America, and American Heart Association have issued a joint statement urging continued use of ACEi's or ARBs as standard of care, while also urging additional research into any potential interactions with COVID-19 infection [11]. However, the speculation and uncertainty among patients and healthcare providers regarding the most used antihypertensive drug classes in the United States could have significant public health consequences [12].

The debate around protective or harmful mechanisms of ACEi's/ARBs arise from speculation about their interactions with ACE2, the membrane-bound protein by which the severe acute respiratory syndrome-coronavirus 2 (SARS-CoV-2) virus invades the body [13]. ACE2 plays a normal physiological role as an enzyme in the renin angiotensin system (RAS; **Figure 1a**). In the classic arm of the RAS angiotensin I (AngI) is converted to AngII by ACE and then binds to the AT1 receptor, promoting vasoconstriction, sodium retention, and inflammation. AngII binding to the AT2 receptor appears to counter some of these effects [14]. A second arm opposes the effects of AT1. In this arm, AngI and AngII are converted to Ang(1-7) by neprilysin and ACE2, respectively. Ang(1-7) suppresses inflammation by binding to the mas receptor (a G-protein coupled receptor of Ang(1-7) associated with anti-inflammatory effects of the RAS) [15].

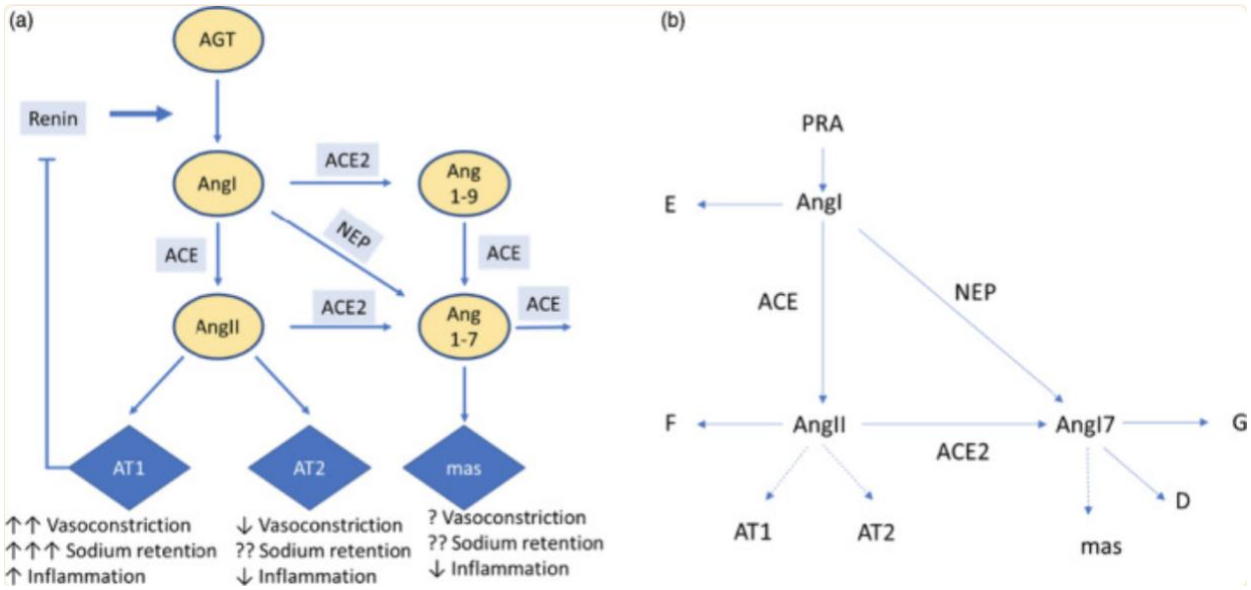

Figure 1.1. *The renin-angiotensin system and (a) Schematic representation of renin-angiotensin system (RAS) mathematical model. Equations for each rate reaction are given in* ***Table 2****. The RAS system illustrated in schematically in a can be represented mathematically as a set of processes summarized in (b), and the reaction rates A–G are given in* ***Table 2****. Each enzyme reaction in this system is assumed to follow Michaelis-Menten kinetics (Eq. 2.1) with a Michaelis constant K m defined by Eq. 2.2.*

It has been hypothesized that ACEi's/ARBs could increase risk or severity of COVID-19 by increasing ACE2 expression and thus providing more routes for viral entry [16]. However, ACE2 has not been established as a rate-limiting step for viral entry. In addition, a recent review of experimental studies found little consistency among studies reporting changes in ACE2 expression with ACEi/ARB treatment [17]. Some studies found increased ACE2 expression/activity with ACEi or ARB treatment, whereas a plurality showed little to no effect, and a few even showed decreased expression.

On the other hand, it has also been hypothesized that ACEi's/ARBs could mitigate the severity of COVID-19 by suppressing inflammation. Although much is unknown about the pathophysiology of COVID-19, the degree of severity appears to depend on the strength of the

host's inflammatory response triggered by the infection [18]. Suppression of the classic AngI-AngII-AT1 pathway may shift the balance toward the anti-inflammatory Ang(1-7)-mas arm of the RAS. Infusion of Ang(1-7) has been shown to reduce acute lung injury and inflammation in animal models of acute respiratory distress syndrome, whereas downregulation of pulmonary ACE2 is associated with increased lung injury severity [19-22].

Part of the challenge in understanding the effect of ACEi's and ARBs on the inflammatory balance in COVID-19 is that ACE2 expression is altered by other factors. Hypertension, diabetes, and aging have all been shown to alter ACE2 expression [23-26]. The SARS-CoV-2 virus itself also induces ACE2 shedding and downregulation after cellular entry, and ACE2 expression is also downregulated by the SARS-CoV-2 virus itself, which may play a role in the excessive inflammatory response in some patients [27]. SARS viruses have a higher affinity to ACE2 and shed ACE2 with higher efficiency than other coronaviruses, and the structure of SARS-CoV-2 suggests that it binds with higher affinity than other SARS viruses [28]. This may contribute to both its increased transmissibility and then subsequently to increased disease severity.

The speculated suppression of the inflammation with ACEi's and ARBs in COVID-19 is based on qualitative directional effects on the RAS components, and the integrative consequences of infection, aging, chronic disease, aging, and therapies on the effectors of this system (AT1, AT2, and mas binding) have not been quantified.

1.2.2 Heart Failure and Natriuretic Peptides

i. Heart Failure

Chronic heart failure (HF) affects approximately 6.2 million people per year (on nearly 380,000 death certificates) and costs the US around $30 billion per year, according to the CDC.

Heart failure is primarily defined by ejection fraction – amount of blood pumped out at each heartbeat – and is broken down into 2 types, reduced ejection fraction (rEF), and with preserved ejection fraction (pEF). Patients with HF-rEF have ejection fractions less than 40%, where those with HF-pEF are anything greater than 40%. A challenge in diagnosing heart failure comes from the fact that there are no good measures to diagnosis or measure severity of heart failure. Any tests for HF are neither sensitive nor specific. Common comorbidities of heart failure include hypertension, diabetes, and renal dysfunction.

Heart failure with reduced ejection fraction (HF-rEF) is usually caused by impaired contractility of the left ventricle but does not occur acutely. A slowly progressing disease is usually initiated by a myocardial infarction and soon after, the heart enlarges and is weakened and soon is unable to adequately pump blood throughout the body. To combat this, the kidney sends more blood to the heart, but the heart is unable to produce enough cardiac output to distribute it. This causes increased preload in the left ventricle (initial stretching of the ventricle before contraction) at the end of diastole which leads to chamber enlargement to retain the blood. This filling of the chamber characterizes the eccentric hypertrophy that occurs where the volume overload causes the cardiomyocytes to become thinner and elongate, thus reducing their ability to contract and increases the stiffness of the heart.

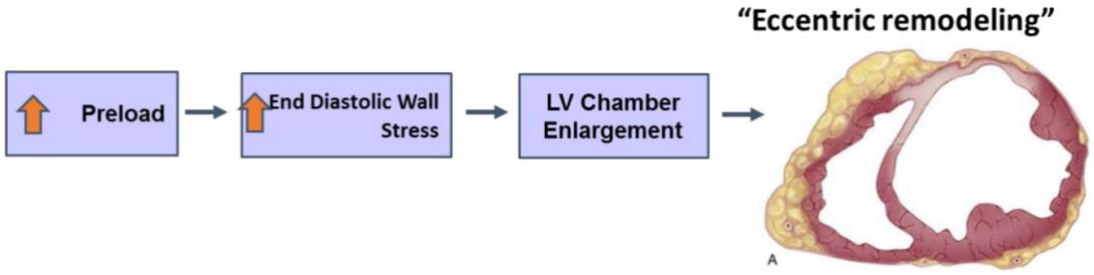

Figure 1.2. *Eccentric Remodeling*

Another characteristic of HF-rEF is cardiomyocyte cell death. In HF, troponin-T levels are increased which damages cardiomyocytes. Since these are already stretched in response to chamber enlargement, damaging them leads to even less functionality in the left ventricle. Moreover, diabetes and continued pressure overload lead to further cardiomyocyte cell death, a classical characteristic of HF-rEF. Another defining characteristic of HF is left ventricular stiffness. It is unknown whether stiffness increases or decreases. Titin drives changes in stiffness, and when it is sliced, studies have shown that the resulting mRNA isoforms that are produced, N2B and N2BA, are indicative of reductions in LV stiffness (particularly production of N2BA). Lastly, unsurprisingly, a common presentation in HF-rEF patients is cardiac inflammation due to cardiomyocyte damage. As previously mentioned, this is triggered by a myocardial infarction, which causes cytokines and chemokines to flood to the site to aid in the healing process of the damaged cells leading to an inflammatory storm within the heart. In terms of vascular changes in HF-rEF, nitric oxide availability is decreased while oxidative stress increases, and the decrease in cardiac output promotes vasoconstriction which causes endothelial dysfunction. Endothelial vasodilation is usually a strong predictor in HF-rEF of cardiac hospitalization and death.

ii. Natriuretic Peptides

As previously mentioned, heart failure is increasingly becoming a problem in the US and EU. Because HF is such a costly problem and a major public health burden, accurate diagnosis and thorough monitoring of HF patients is important since the mortality/morbidity of cardiac failure is very high – the median survival time is 4 years [29]. Measuring ventricular dysfunction accurately is extremely important in diagnosing heart failure and measuring concentrations of BNP (B-type natriuretic peptide) and NT-proBNP (N-terminal B-type natriuretic peptide) is usually

done in the initial assessment. These peptides are derived from their parent molecule, proBNP, which is released by cardiomyocytes in the left ventricular in response to elevated cardiac wall stretch due to fluid overload. The Framingham Cohort Study was one of the first studies to determine BNP and NT-proBNP's success as a predictor of mortality / hospitalization, and moreover, according to the American College of Cardiology Foundation / American Heart Association (ACCF / AHA), and European Society of Cardiology (ESC), BNP and NT-proBNP are the most valuable and reliable biomarkers to diagnosing HF and cardiac dysfunction. The peptides are very important in determining severity, treatment strategy and prognosis of heart failure.

The ESC 2016 guidelines recommend that all patients with suspected HF have their natriuretic peptides levels checked to identify acute HF. The non-acute thresholds for BNP and NT-proBNP are 35 pg/mL and 125 pg/mL, respectively, while in the acute setting, the cutoff values for BNP and NT-proBNP are 100 pg/mL and 300 pg/mL. If BNP is < 100 pg/mL, HF is considered unlikely, if BNP is between 100 and 500 pg/mL, clinical judgement should be used to diagnose HF, and for BNP > 500 pg/mL, HF and cardiac dysfunction is highly likely and rapid initiation of therapy is suggested [30]. According to the International Collaborative of NT-proBNP (ICON), age-dependent cutoffs are likely more useful for diagnosing HF. Generally, 300pg/mL+ is the age-independent cutoff, but for patients younger than 50 years old, HF should be diagnosed if NT-proBNP > 450pg/mL; patients between 50 and 75, if NT-proBNP > 900pg/mL; and for patients older than 75, if NT-proBNP > 1800 pg/mL [31].

Not only are BNP and NT-proBNP important in the diagnosis of cardiac dysfunction and heart failure, but they are also valuable in assessing severity and prognosis of HF. Improvement

(reduction) in BNP and NT-proBNP levels usually indicates improvements in clinical systems, there is a positive correlation between risk of death and peptide concentrations, and they were the strongest predictors of sudden cardiac death after adjusting for other clinical variables. Their utility stems from guiding management and as prognostic indicators to help inform clinicians about therapy strategy and effectiveness [32].

iii. Role of Kidneys in Natriuretic Peptides

The prohormone proBNP is released by cardiomyocytes in response to elevated stretch [33, 34], and is quickly cleaved to form biologically active BNP and inactive NT-proBNP (N-terminal proBNP). Both peptides are cleared by renal filtration, although BNP is also cleared by non-renal mechanisms (endopeptidase degradation and receptor-mediated clearance through NPR-C (Natriuretic Peptide Receptor-C)). BNP and NT-proBNP are low molecular weight proteins (3.464 and 8.4 kDa, respectively), with estimated atomic radii of 1.12 nm and 1.5 nm, respectively, well below the glomerular filter pore radius of 37 nm [35]. They are similar in size to inulin (6.179 kDa) and cystatin-C (13.3 kDa), which are commonly used in measuring GFR because they are freely filtered. Fractional excretion rates of BNP and NT-proBNP in human subjects are consistent with free glomerular filtration [36]. There is no evidence for renal metabolism or reabsorption. Thus, both biomarkers are likely cleared renally by free filtration across the glomerulus.

When plasma NT-proBNP and BNP concentrations increase, then it may reflect increased production due to elevated cardiac wall stress, but if GFR is abnormal or is changing as well, then it may also reflect reduced clearance due to decreased renal function. Both biomarkers have consistently been shown to increase with decreasing GFR [36-39]. NT-proBNP is more strongly affected than BNP, presumably because NT-proBNP is cleared only by renal mechanisms while

BNP is cleared by additional mechanisms. As a result, the ratio of NT-proBNP to BNP also increases and the concordance between the two biomarkers is reduced as GFR decreases [40].

The effect of renal function on natriuretic peptide concentrations has important implications for their clinical interpretation and use. Heart failure and kidney dysfunction often coexist and also both progressively worsen. Accounting for the effect of kidney function on biomarker concentrations may increase their sensitivity as both diagnostic and monitoring tools. In addition, many therapies evaluated for treating heart failure have both acute and long-term effects on GFR. For instance, SGLT2 (sodium glucose cotransporter 2) inhibitors and RAAS (renin angiotensin aldosterone system) blockers cause an initial drop in GFR upon initiation of therapy, but subsequently slow the rate of GFR decline. These GFR changes may at least partially confound the interpretation of observed natriuretic peptide changes if not accounted for [41].

Therapies for heart failure (ACEi's, ARBs, beta blockers, digoxin, among others) usually act by reducing the workload on the heart. A misconception is they alter contractile function, but this is usually not the case – they reduce workload on the heart by reducing things such as heart rate and blood volume. Since the heart is being remodeled due to fluid buildup, these therapies work to slow or reverse the cardiac remodeling process. Drugs affecting the RAS (and natriuretic peptides) achieve therapeutic effect by at least partially acting through the kidneys to control water/sodium homeostasis and reduce volume retention. The therapies listed reduce the risk of mortality and morbidity in HF-rEF (effect on HF-pEF is not as beneficial); the mechanisms by which these drugs affect cardiorenal function are still incompletely understood.

1.2.3. Current State of HF-rEF Modeling

Computational models can be used to represent physiology, pathophysiology, and pharmacology with mathematical equations incorporating a sufficient level of detail and can be

used to understand and predict the response to therapy and help understand the mechanisms underlying clinical observations. Guyton's model described the "whole-body" human circulatory system and blood pressure dynamics by modeling cardiovascular, renal, and neurohormonal regulation of hemodynamics and demonstrated how other physiological systems respond when another is function abnormally. In addition, Guyton's model measured cardiac function as a time-averaged cardiac output and did not allow for calculations of blood pressure or ejection fraction [42]. Several updates over the years have improved the ability of the model to calculate key biomarkers and functioning with LV mass and remodeling and incorporating the geometry of the heart. Previous models used the idea of "elastance" where ventricular volume and pressure was approximated with a single function for all heart conditions, which limits the ability of the model to relate blood/volume dynamics to stresses in cardiac tissue and the remodeling that follows [43-46]. At a more extreme level of complexity, finite element methods modeled the beating of the heart and described the geometry in great detail – but required a large computational cost in terms of speed and amount of information necessary to inform model parameters. Between the levels of complexity lie the Bovendeerd and Cox models which derived the pressure-volume relationship using simplified geometry as a function of stress plus strain in cardiac tissue [47]. They also linked macro characteristics to the properties of individual cardiomyocytes, thus allowing for understanding / simulating myocardial remodeling at a single cell level. The cardiac model developed in Hallow's lab combines the frameworks of the Bovendeerd and Cox models to describe ventricular wall mechanics. None of the cardiac models previously mentioned incorporate renal function.

Guyton and Coleman were among the first to use mathematical modeling to demonstrate pressure-natriuresis phenomenon [42]. The models have become more sophisticated since the

1970's and range in scope but hadn't linked renal function to sodium and volume control. Hallow et al. developed an integrated model of renal function to simulate renal hemodynamics, volume control, and sodium/water balance and combined it with their previous cardiac model to develop an integrated cardiorenal model to simulate cardiac and renal hemodynamics for a wide range of heart conditions [48]. These improvements have allowed researchers to investigate the effects of therapies (in HF patients specifically) on blood pressure, renal hemodynamics, and body fluid regulation.

i. Virtual Patients and Populations

Mthematical models are quantitative means to incorporate data from several sources to predict outcomes computationally without the need for costly and time-consuming experiments. Of course, computational models are not perfect representations of phenomena, but they can give researchers a qualitative understanding of effects, especially in response to therapies. Population-based and individual subject models exist to account for uncertainty and variability, but in quantitative systems pharmacology (QSP) models, the term "virtual subjects/patients" (VPs) are model parameterizations that can be used to analyze uncertainty. While one VP is not enough to understand variability, virtual cohorts or populations (VPops) can be constructed to cover a range of conditions and biomarkers; e.g., varying levels of heart failure measured by ejection fraction and BNP/NT-proBNP. From these virtual populations, subsets can be selected or weighted to match a clinical distribution. Sometimes, full variability of clinical distributions cannot be realized through model parameterizations because of complex nonlinearities and constraints within the QSP model [3]. , Several methods have been proposed to compare distributions of Vpops to clinical data. In addition, several metrics have been developed to measure the "distance" between the distributions of a virtual patient population and a clinical dataset. For our analyses, we

introduce a new method to select a clinically representative set of virtual patients and measure distance between our VP's and clinical observed data using a Kolmogorov Smirnov test (KS-test), which measures the maximum distance between the empirical distribution function of a sample with the cumulative distribution (CDF) of the reference sample, or the difference between the empirical distributions of two samples.

Allen et al. proposed a method to optimize parameter sets to generate Vpop's that mostly covered the range of observed NHANES data. However, Allen's method is iterative in the sense that it would require generating several sets of virtual patients multiple times until an optimal set was achieved [49]. This iterative process requires substantial computational resources and can be time consuming, especially if the model is especially large (contains large sets of differential equations). He then improved on this method by incorporating alternative optimization algorithms (simulated annealing and Metropolis-Hastings) which allowed for fewer virtual patients to cover a clinical population. But like the previous issue, computational cost is a large issue. We developed a method that allows researchers to select virtual patient populations that closely mimic real, clinical data to inform future simulations and better understand inter-individual variability in responses to therapy. With the ability to create virtual patients and populations to match distributions of clinical data and the goal of predicting outcomes, we want to use these ODE models to validate our QSP model by reproducing data seen in published literature. For instance, QSP models could be used to reproduce results from a clinical trial by simulating biomarker trajectories over time. Using ensembles of VP's is sufficient to explore the range of possible responses.

Catheterization can be used to measure pressure and diagnose a variety of heart problems. However, this procedure is extremely delicate and high risk, so measuring natriuretic peptides, specifically b-type natriuretic peptide (BNP) and N-terminal pro b-type natriuretic peptide (NT-

proBNP) can serve as surrogate measures for pressure. BNP and NT-proBNP are derived from their parent molecule, proBNP, which is produced in response to increased wall stress (usually from fluid buildup). Using these relationships and surrogate measures of pressure, the goal of this objective is to use the integrated cardiorenal model to gather a set of virtual patients with a wide range of HF-rEF patients and simulate the effects of an angiotensin receptor blocker (valsartan) and compare trajectories of BNP and NT-proBNP to a published clinical trial.

After comparing trajectories to a clinical trial, it is necessary to understand which parameters in the model are most influential in explaining the variability in response to therapy. Several methods exist to "select" parameters including, but not limited to random forests, Latin Hypercube Sampling, or Sobol Sensitivity. All of these methods require some permutation of the inputs to understand how the response varies as a function of those permutations, but among the most innovative is the Sobol analysis which requires systematic permutations of the inputs and decomposes the variance of the output to determine how influential inputs are in explaining that the variance. In short, Sobol measures how much the overall variance in the outputs changes when a parameter is held constant. Sobol indices are measured in percentages which makes interpretations simple and straight forward. Sobol sensitivity analyses are able to analyze each parameter individually (first order) as well as how the variances change when analyzing with all parameters together (total order).

1.3 Motivation for Aims

The motivation for the 3 specific aims is described below:

1.3.1 Motivation for Aim 1: Mathematical Analysis of Interplay between COVID-19 Infection and RAS Therapies and Effect on Pro- and Anti-Inflammatory Arms of the RAS

Therapies such as ACE inhibitors (ACEi's) and angiotensin receptor blockers (ARBs) inhibit the renin-angiotensin-aldosterone system (RAS). At the height of the 2020 COVID pandemic, use of those therapies was heavily debated due to potential interactions with ACE2, an enzyme that links the pro- and anti-inflammatory arms of the RAS, but also is an entry by which severe acute respiratory syndrome-coronavirus (SARS-CoV-2) invades cells. It has been hypothesized that use of ACEi's and ARBs could increase risk of severe COVID-19 infections by increasing ACE2 expression; thus, providing more entry routes for the virus, but also could mitigate severity by suppressing inflammation. The quantitative effects among RAS therapies, SARS-CoV-2 infection, and diseases chronic diseases/aging on the balance between the pro- and anti-inflammatory arms of the RAS are unknown.

1.3.2 Motivation for Aim 2: Relationship between Kidney Function and Natriuretic Peptides and a Mathematical Analysis on their Response to Therapy

BNP and NT-proBNP are diagnostic biomarkers in heart failure, but their utility is hindered because both biomarkers are affected by renal function. Since both biomarkers are cleared by the kidneys (a function of GFR), their concentrations increase non-linearly with decreased renal function and it can be difficult to define diagnostic and therapeutic thresholds with GFR changing over time. BNP and NT-proBNP are cleaved from their parent molecule, proBNP, which is released by cardiomyocytes in response to elevated stretch on the heart. When concentrations increase, it may be increased due to elevated wall stress, or changes in GFR. NT-proBNP is more strongly affected than BNP, likely because NT-proBNP is *solely* cleared by renal mechanisms, while BNP is cleared by additional, non-renal mechanisms.

It is important to account for renal function on these peptides since heart failure and kidney dysfunction often coexist and both progressively worsen. Many therapies for heart failure reduce loads on the heart, but also have acute and/or long-term effects on GFR; so a better understanding of how GFR affects peptide concentrations may improve interpretability.

1.3.3 Motivation for Aim 3: Validating Natriuretic Peptides' Response to Therapy with a Cardiorenal Model

Since kidney function is usually present with heart failure, researchers often underestimate the drug effect on cardiac stress because they fail to account for changes in GFR. Angiotensin receptor blockers (ARBs) reduce inflammation / stresses on the heart by inhibiting binding to the AT2 receptor in the RAS. The effect of ARB's on BNP (a surrogate measure of pressure in the heart) has been studied in a large clinical trial but fails to account for the effect of GFR. It is hypothesized that standard of care therapies' effects on GFR lead to underestimations of drug effects on cardiac stress. However, the quantitative contribution between stresses on the heart vs. effect on the kidneys and variability of responses to therapy is unknown.

1.4 Hypothesis, Objectives, and Specific Aims

The purpose of the research aims is to provide novel insights into uncertainties surrounding mathematical modeling of various health and disease contexts.

1.4.1 **Specific Aim 1: Extend an existing mathematical model of the RAS to quantify the interplay of therapy, SARS-CoV-2 infection, and chronic diseases or aging between pro- and anti-inflammatory arms of the RAS.**

The objective of this aim is to develop a tool to evaluate the effects of parameter uncertainty and analyze the relative changes in pro- and anti-inflammatory pathways under different treatments (e.g. ACE inhibitor or Angiotensin Receptor Blocker (ARB)), disease states (e.g. diabetes, hypertension, COVID-19), and combinations of therapy, comorbidities and timing of infection. We hypothesize that the anti-inflammatory response induced by RAAS therapy outweighs the potential increase in risk of severe infection due to increased ACE2 expression. Once the model was extended, parameter estimation and model fitting was conducted by fitting to published data. Model simulations were performed to analyze parameters most influential in predicting change in measures of inflammation in the RAAS. From there, the propagation of uncertainty was analyzed by comparing differences in shifts to and from the pro- and anti-inflammatory arms of the RAAS under several simulation conditions.

1.4.2 **Specific Aim 2: Develop a mechanistic model of heart failure biomarkers to describe and explain changes in natriuretic peptides and reduced kidney function observed in clinical trials.**

The objective of this aim is to develop a relationship between NT-proBNP or BNP with GFR and cardiac stress that can be defined mechanistically and mathematically based on their production and clearance rates and validate the biomarkers' response to therapy. To derive the

relationships, we described the processes involved in production and clearance of natriuretic peptides.

1.4.3 **<u>Specific Aim 3:</u> Integrate biomarker model into a larger cardiorenal model and validate the response of natriuretic peptide biomarkers to therapy by simulating a published clinical trial.**

The objective of this aim is to integrate the model developed in Aim 2 into a larger cardiorenal model and predict the response of the natriuretic peptides (BNP and NT-proBNP) to therapy. In addition, to characterize the response, we generated virtual patient populations that realistically represent patients in real-world clinical trials. We tested the model's ability to reproduce the biomarker response to therapy observed in the VAL-HEFT study and improve interpretability of biomarkers in heart failure patients.

CHAPTER 2

Uncertainty Quantification and Propagation – RAS Blockade and COVID-19: Modeling Mas and AT1 Receptor Occupancy as Indicators of Pro- and Anti-Inflammatory Balance

Dave, I., Hallow, K.M. To be submitted to Clinical Pharmacology.

2.1 Abstract

ACE inhibitors (ACEi's) and angiotensin receptor blockers (ARBs) are standard-of-care treatments for hypertension and diabetes, common comorbidities among hospitalized patients with coronavirus disease 2019 (COVID-19). Their use in the setting of COVID-19 has been heavily debated due to potential interactions with ACE2, an enzyme that links the pro-inflammatory and anti-inflammatory arms of the renin angiotensin system, but also the entryway by which severe acute respiratory syndrome-coronavirus 2 (SARS-CoV-2) invades cells. ACE2 expression is altered by age, hypertension, diabetes, and the virus itself. This study integrated available information about the renin angiotensin aldosterone system (RAAS) and effects of SARS-CoV-2 and its comorbidities on ACE2 into a mechanistic mathematical model and aimed to quantitatively predict effects of ACEi/ARBs on the RAAS pro-inflammatory/anti-inflammatory balance. RAAS blockade prior to SARS-CoV-2 infection is predicted to increase the mas-AT1 receptor occupancy ratio up to 20-fold, indicating that in patients already taking an ACEi/ARB before infection, the anti-inflammatory arm is already elevated while the pro-inflammatory arm is suppressed. Predicted pro-inflammatory shifts in the mas-AT1 ratio due to ACE2 downregulation by SARS-CoV-2 were small relative to anti-inflammatory shifts induced by ACEi/ARB. Predicted effects of changes in ACE2 expression with comorbidities of diabetes, hypertension, or aging on mas-AT1 occupancy ratio were also relatively small. Last, predicted changes in the angiotensin (Ang(1-7)) production rate with ACEi/ARB therapy, comorbidities, or infection were all small relative to exogenous Ang(1-7) infusion rates shown experimentally to protect against acute lung injury, suggesting that any changes in the ACE2-Ang(1-7)-mas arm may not be large enough to play a major role in COVID-19 pathophysiology.

2.2 Methods

2.2.1 Model overview

The RAS system illustrated in schematically in **Figure 1A** can be represented mathematically as a set of processes summarized in **Figure 1B**, and the reaction rates A-G are given in **Table 2.2**. Each enzyme reaction in this system is assumed to follow Michaelis-Menten kinetics

$$[E] + [S] \underset{K_{off}}{\overset{K_{on}}{\rightleftarrows}} [ES] \xrightarrow{K_{cat}} [P], \qquad \text{Eq. 2.1}$$

where [E] and [S] represent enzyme and substrate concentrations respectively, [ES] represents concentration of the enzyme-substrate complex, and [P] is the product formed, with a Michaelis rate constant K_m defined by

$$K_m = \frac{[E][S]}{[ES]} \qquad \text{Eq. 2.2}$$

The enzyme activity V, or rate of product formation, is given by

$$V = K_{cat}[ES] = \frac{K_{cat}[E][S]}{K_m} \qquad \text{Eq. 2.3}$$

where K_{cat} is the catalytic rate constant. The catalytic efficiency is defined as

$$Eff_{substrate,enzyme} = \frac{K_{cat}}{K_m} \qquad \text{Eq. 2.4}$$

For conversion of angiotensinogen (AGT) to AngI by renin, AGT is normally available in excess, and renin is the rate-limiting components. Thus, the rate of formation of Angiotensin I (AngI) is given by plasma renin activity (PRA) and for simplicity, AGT is not considered in the model. For all other enzyme-substrate pairs in Figure 1, K_m, K_{cat}, and $Eff_{substrate,enzyme}$ have been measured in [50] (**Table 2.2**).

Rate	Description	Formula
A	ACE conversion of AngI to AngII	$Eff_{ACE,AngI}[ACE][AngI]$
B	ACE2 conversion of AngII to Ang(1-7)	$Eff_{ACE2,AngII}[ACE2][AngII]$
C	NEP conversion of AngI to Ang(1-7)	$Eff_{NEP,AngI}[NEP][AngI]$
D	ACE conversion of Ang(1-7) to other forms	$Eff_{ACE,Ang17}[ACE][Ang17]$
E	AngI degradation by enzymes other than ACE and NEP	$K_{AngI}[AngI]$
F	AngII degradation by enzymes other than ACE2	$K_{AngII}[AngII]$
G	Ang(1-7) degradation by enzymes other than ACE	$K_{Ang17}[Ang17]$

Table 2.1. *Reaction Rate Formulas for the RAS Model in Figure 1b*

For all enzyme-substrate pairs, K_m is on the order of micromoles, while normal substrate concentrations [S] is on the order of picomoles (**Table 2.2**). Since $K_m >> [S]$, then according to Eq. 2.2, [E] must be much greater than [ES], so that [E] is approximately equal to the total enzyme concentration $[E]_t$. This also means that even if substrate concentrations change several folds of magnitude, [E] remains approximately constant. Therefore, enzyme activities for each enzyme substrate pair (Eq. 2.3) can be written as

$$enzyme\ activity = Eff_{substrate,enzyme}[E]_t[S] \qquad \text{Eq. 2.5}$$

As a simplification, the pathway from AngI to Ang(1-9) to Ang(1-7) is not included in this model. This is justified because the catalytic efficiency for AngI-ACE2 is an order of magnitude lower than AngI-ACE and AngI-NEP, and the catalytic efficiency of Ang(1-9)-ACE is also an order of magnitude lower than AngI-NEP or AngII-ACE2 [50, 51]. Therefore, very little Ang1-7 is expected to form from the AngI-Ang(1-9) arm of the pathway, relative to the AngI-NEP and AngII-ACE2 pathways. Any AngI conversion to Ang(1-9) is lumped in with other routes of AngI degradation.

Parameter	**Definition**	**Value**	**Units**	**Source**	**Species**
$Eff_{ACE,AngI}$	Catalytic efficiency of ACE conversion of AngI to AngII	648	/pM/hr	[50].	*In vitro* (human cDNA transfected in CHO cells)
$Eff_{ACE2,AngII}$	Catalytic efficiency of ACE2 conversion of AngII to Ang(1-7)	7920	/pM/hr	[50, 51].	*In vitro* (human cDNA transfected in CHO cells)
$Eff_{ACE,Ang(1-7)}$	Catalytic efficiency of ACE conversion of Ang(1-7) to other peptides	1260	/pM/hr	[50].	*In vitro* (human cDNA transfected in CHO cells)
$Eff_{NEP,AngI}$	Catalytic efficiency of NEP conversion of AngI to Ang(1-7)	2232	/pM/hr	[50].	*In vitro* (human cDNA transfected in CHO cells)
$K_{d,AT1}$	AT1 receptor dissociation constant	552	pmol/L	[52]	Primate (in vitro COS-7)
$K_{d,AT2}$	AT2 receptor dissociation constant	552	pmol/L	assumed	

$K_{d,mas}$	Mas receptor dissociation constant	930	pmol/L	[53]	mice
h_{renin}	Renin half-life	0.1733	hr		human
PRA(0)	Baseline Plasma Renin Activity	3587	pmol/L/h	[54]	human
AngI(0)	Baseline Angiotensin I plasma concentration	10.5	pmol/L	[54]	human
AngII(0)	Baseline Angiotensin II plasma concentration	6.6	pmol/L	[54]	human
Ang(1-7)(0)	Baseline Angiotensin (1-7) plasma concentration	3	pmol/L	[54]	human
b_{renin}	Fitting exponent for AT1 feedback on renin	0.8	-	Estimated [55]	human
$Ratio_{ACE-NEP}$	Ratio of ACE expression to NEP expression	9	-	Fitting to [56]	rats
$Ratio_{ACE-ACE2}$	Ratio of ACE expression to NEP expression	32	-	Fitting to [56]	rat

Table 2.2. RAS Model parameters

Rate equations for each peptide are then given by Eq. 2.6-8:

$$\frac{d(AngI)}{dt} = PRA - A - C - E \quad \text{Eq. 2.6}$$

$$\frac{d(AngII)}{dt} = A - B - F \quad \text{Eq. 2.7}$$

$$\frac{d(Ang17)}{dt} = C + B - D - G \quad \text{Eq. 2.8}$$

Fractional receptor occupancy for AT1, AT2, and mas are given by

$$f_{AT1} = \frac{AngII}{K_{d,AT1}+AngII} \quad \text{Eq. 2.9}$$

$$f_{AT2} = \frac{AngII}{K_{d,AT2}+AngII} \quad \text{Eq. 2.10}$$

and

$$f_{mas} = \frac{Ang(1-7)}{K_{d,mas}+Ang(1-7)} \quad \text{Eq. 2.11}$$

respectively, where K_d is the dissociation constant for each receptor-ligand pair, given in **Table 2.2** These forms assume that the clearance of AngII and Ang1-7 by binding to receptors is small and is encapsulated in the degradation terms F and G, respectively.

As described previously [55, 57], plasma renin concentration (PRC) is given by

$$\frac{d(PRC)}{dt} = SEC_{renin} - \frac{\ln(2)}{h_{renin}} * PRC \quad \text{Eq. 2.12}$$

where SEC_{renin} and h_{renin} are the renin secretion rate and half-life, respectively. Binding of Ang II to the AT1 receptor produces highly non-linear feedback on renin secretion, given by

$$SEC_{renin} = SEC_{renin,0} * \left(\frac{f_{AT1}}{f_{AT10}}\right)^{-b_{renin}}, \quad \text{Eq. 2.13}$$

where f_{AT10} is the equilibrium fractional AT1 receptor occupancy, and $b_{,renin}$ is a fitting constant. PRA can be related to PRC by the conversion factor 0.06 (ng/ml/hr)/(pg/ml).

2.2.2 Parameter Estimation and Model Constraints

A subset of model parameters is known with some degree of certainty from clinical or experimental measurements (**Table 2.2**). Concentration ranges for renin, AngI, AngII, and Ang(1-7) in humans have been measured clinically. Catalytic efficiencies for each enzyme substrate pair as well as receptor binding affinities have been measured experimentally [50]. The half-life of renin is known, and nominal renin secretion rate $SEC_{renin,0}$ can thus be determined from Eq. 2.12.

This leaves another subset of six unknown parameters: [ACE], [ACE2], and [NEP], K_{AngI}, K_{AngII}, and K_{Ang17}. Some studies have measured ACE and ACE2 concentrations, but with widely varying results. Expression varies across tissues, so obtaining a value that represents total ACE and ACE2 expression is difficult. Neprilysin and ACE2 are membrane-bound proteins and circulating levels may only reflect ectodomain shedding of these enzymes, not tissue levels [58, 59]. Plasma levels are not easily measurable and may not reflect tissue levels. However, if the relative ratio of ACE to NEP and ACE to ACE2 expression are known, then, as shown later, these remaining model parameters can be determined from equilibrium conditions.

Another aspect of estimation of parameters in ODE models is identifiability. When considering identifiability, we are assessing whether it is possible to estimate unique parameters values from data, given the model structure. Another way to put it, we want to make sure we are using the appropriate data when estimating parameter sets. In short, the parameters in the model can be uniquely estimated only if the parameters of a model are identifiable.

Guillaume et al list the sources of identifiability as 1) the model structure – non-uniqueness can occur given the choice of quantities included in the model; 2) the dataset used to estimate parameters – ideally having complete enough information to inform all necessary parameters; and

3) the choice of model and observation error – random noise could absolutely result in non-uniqueness of parameters.

First, we needed to estimate parameters for our RAS model. Doing so can sometimes require solving a simple inverse problem – given a set of data, calculating the set of parameters that most resembles the observed data. A common way to estimate parameters involves optimizing an objective/loss function to quantify how well the model fits the data. We use a least squares

$$\boldsymbol{\theta^* = argmin_\theta \sum_{i=1}^{m} (y_i - f_i(\theta))^2} \qquad \textbf{Eq (2.14)}$$

approach to minimize the distance between our model predictions and the observed data, where m is the number of observations, and f is the solution to the differential equation using numerical methods since no closed form exists.

For our identifiability analysis of the 6 unknown parameters ([ACE], [ACE2], and [NEP], K_{AngI}, K_{AngII}, and K_{Ang17}, we first identified values that produced an adequate fit. All parameters were positive values, so at first, all parameters were scaled so they were in the same order of magnitude (e.g. K_{Ang17} divided by 1000). This was done to ensure the gradient of the parameters vary across equal scales so that changes in a parameter with large values don't outweigh changes in a parameter on a much smaller scale. Then, to allow parameter to vary from negative infinity to infinity, we used the exponential of each parameter in the model ([ACE], [ACE2], and [NEP], K_{AngI}, K_{AngII}, and K_{Ang17}), so they could be reported as log([parameter]). For parameters that varied between 0 and 1 (ACE and NEP enzyme inhibition), the logit scale was used. We then used these rescaled parameters to run the optimizer to minimize the distance between our model and data points.

The data used in our least squares approach came from a study (Yamamoto et al.) where four Wistar-Kyoto rats were injected with AngI and time courses of AngI, AngII, and Ang(1-7) were

recorded over a period of 3 minutes with use of a control, an ACEi, a NEPi, and their combination. Summary level data was recorded for each outcome at 15 seconds, and every 30 seconds between 30 and 180 seconds. Our objective function then, was the total sum of the distance between the model prediction and the data points at each timepoint for each combination of peptide and drug used. To ensure equal weights across compounds, Ang17 differences were multiplied by 5 to be measured on a similar scale to AngI and AngII since its values were between 0 and 3 while, AngI and AngII were between 0 and 20. The transformed parameters were then able to be reported between negative infinity and infinity as well as their standard errors.

To run the optimizer, we provided an initial guess for each parameter to be used, then once a seemingly optimal parameter set was estimated, the resulting Hessian and standard errors were calculated. Hessians were calculated by determining the second order partial derivatives of the objective function, then finding the negative inverse of the Hessian gives us the covariance matrix, which can then be used to calculate the standard errors (by taking the square root of the diagonals). From there, to ensure we had the best fit and there were no better fits, we performed a Latin Hypercube Sampling technique (N = 50) to vary starting points for each parameter. The fit and objective functions were analyzed for each sample to determine consistency across fitted parameters. Finally, one of the optimized runs was overlaid on to Yamamoto's data to visually inspect how the model fit the data.

2.2.3 Determining ACE-NEP and ACE-ACE2 ratios

Enzyme levels vary across tissues, disease states, and species [60, 61]. Nevertheless, we aimed to estimate a reasonable starting value for these ratios by fitting the model to experimental measurements by Yamamoto and colleagues [56]. In their experiments, an ACE inhibitor, a neprilysin inhibitor, or both an ACE inhibitor and neprilysin inhibitor were administered to 16-week-old male Wistar-Kyoto (WKY) and spontaneously hypertensive (SHR) rats. Twenty minutes later, a 2 nmol bolus injection of radiolabeled AngI was administered, and concentration of radiolabed AngI, AngII, and Ang(1-7) every 15-30 seconds over the next 3 minutes. Only data from WKY rats were used in this analysis. To simulate this study, all peptide concentrations are initially set to zero. Since only radiolabeled peptides were measured, neither renin production nor renin activity are reflected in the available data, and thus PRA is set to zero. ACE inhibition and NEP inhibition were modeled as a constant fractional reduction in their respective enzyme concentration. The study protocol is simulated, and enzyme concentrations ([ACE], [ACE2], and [NEP]), peptide degradation rate constants (K_{AngI}, K_{AngII}, K_{Ang17}), and ACEi and NEPi fractional inhibition were estimated by fitting the digitized data using a least squares method.

Because the experimental study was conducted in rats, it may not be reasonable to assume that the absolute concentrations and rate constants translate to humans. However, we assumed that the estimated ratio of [ACE] to [ACE2] and [ACE] to [NEP] may translate, and these ratios were used in all further simulations. Based on the estimated ACE to ACE2 and ACE to NEP ratios, remaining parameters were determined from steady-state conditions when steady-state concentrations of renin, AngI, AngII, and Ang(1-7) are known.

2.2.4 Model Evaluation

To further qualify the model, we evaluated its ability to reproduce observed changes in plasma AngI, AngII, and Ang(1-7) concentrations in response to an ACE inhibitor in a previously published human clinical trial [54]. In this double-blind, placebo-controlled crossover study, 17 healthy men were treated with enalapril or placebo for two weeks. During the first week they were given a low-sodium diet, and during the second week they were given a high sodium diet. Plasma AngI, AngII, and Ang(1-7) were measured at the end of each week.

To simulate this study, baseline concentrations of AngI, AngII, and Ang(1-7) were set to the average of the reported values during the placebo high- and low-salt periods. Catalytic efficiencies were specified according to [50], and the ratio of ACE to NEP and ACE to ACE2 were initially set to the values estimated by fitting to data in [56], as described above. Parameters governing renin secretion and AT1 feedback on renin were specified as previously described [55]. The study protocol was then simulated. To represent the effects of different Na^+ intakes, the rate of renin secretion (SEC_{renin0}) was adjusted to give the observed differences in AngI between the high- and low-salt groups during the placebo period.

As shown in **Figure 2.1**, the simulation predicted the increase in AngI and Ang(1-7) and decrease AngII following ACE inhibition well. This provides validation that the model reasonably describes the behavior of the RAS system in humans.

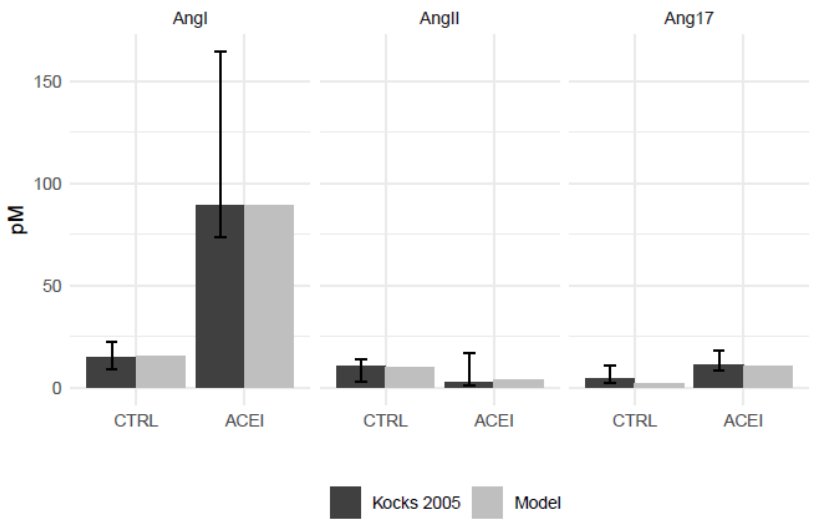

Figure 2.1. *Model validation: The model produces the observed changes in in plasma AngI, AngII, and Ang(1-7) concentrations in 17 human subjects on a low-salt diet. Data from [54].*

2.2.5 Simulation Settings

i. Effect of changes in ACE2 receptor expression on mas, AT1, and their ratio, before and after ACEi or ARB therapy

A literature review was conducted to understand the range of changes in ACE2 expression due to aging, diabetes, or hypertension that have been observed experimentally or clinically. Based on this review, a range of ACE2 concentrations from 0.01 to 2.5 times normal was determined to be a reasonable operating range. Changes in mas and AT fractional occupancy, as well as their ratios, were simulated over this range of ACE2 values, before and after addition of an ACE inhibitor or an ARB. We have previously estimated that ACE inhibition with common ACE inhibitors is 90-95%. For ARBs, inhibition of AT1 ranged from 88 to 97%, depending on the drug and dose [55]. In this study, a value of 93% inhibition was used for both.

ii. Response to SARS-CoV-2 Infection

SARS-CoV-2 infection was simulated as a 95% decrease in ACE2, representing a "worst-case" scenario for ACE2 downregulation. Because all enzymes of the RAS have some natural variability and may be affected by disease states, the effects of SARS-CoV-2 infection was simulated in 200 "virtual subjects" created by sampling ACE2, ACE, NEP, and renin secretion from a log-normal distribution with means given in **Table 2.2**. The parameter distributions and resulting distribution in RAS peptides are characterized in **Figure 2.2** and **2.3**.

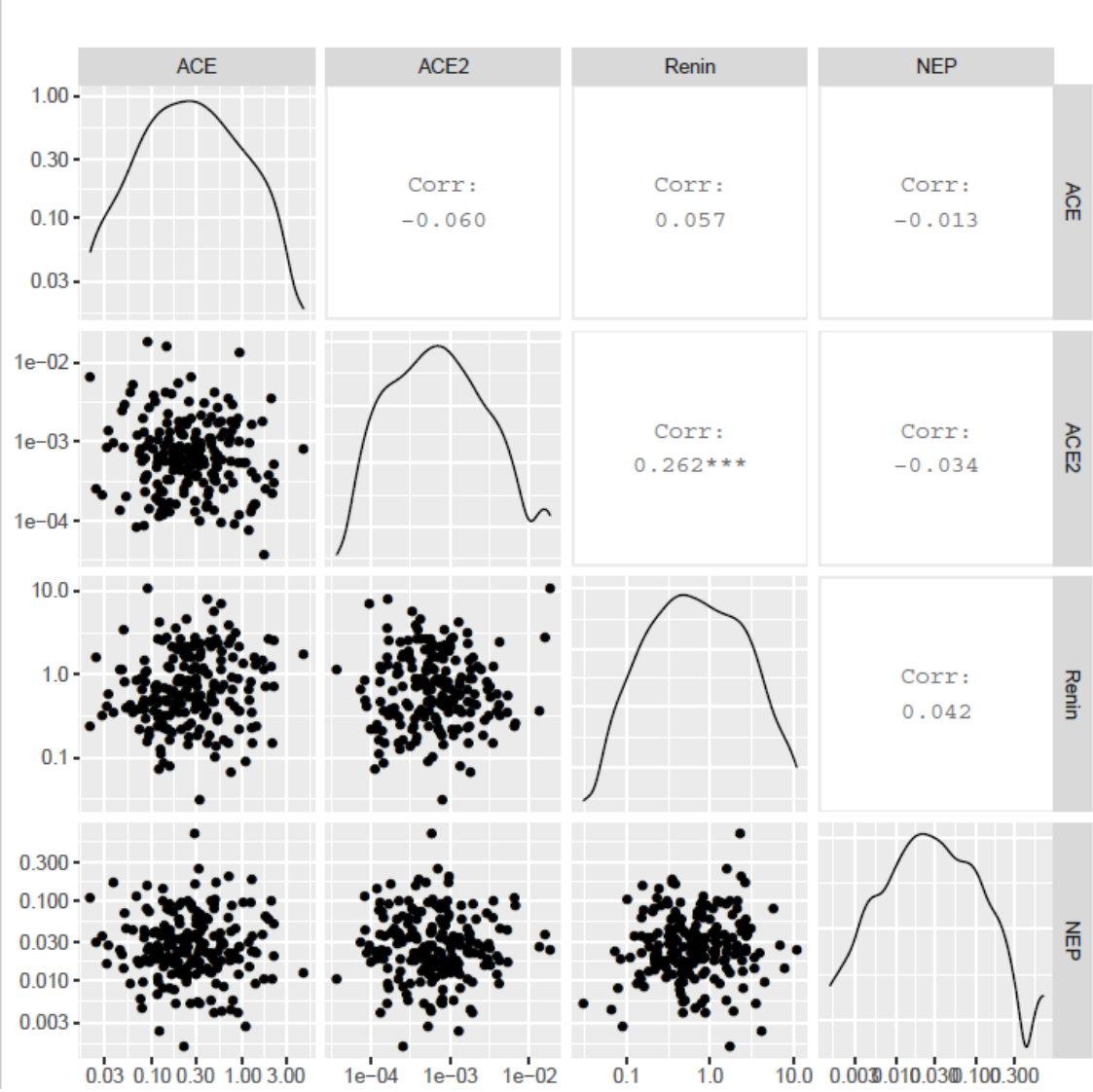

Figure 2.2. *Distribution of enzyme concentrations (pM) for 200 virtual patients.*

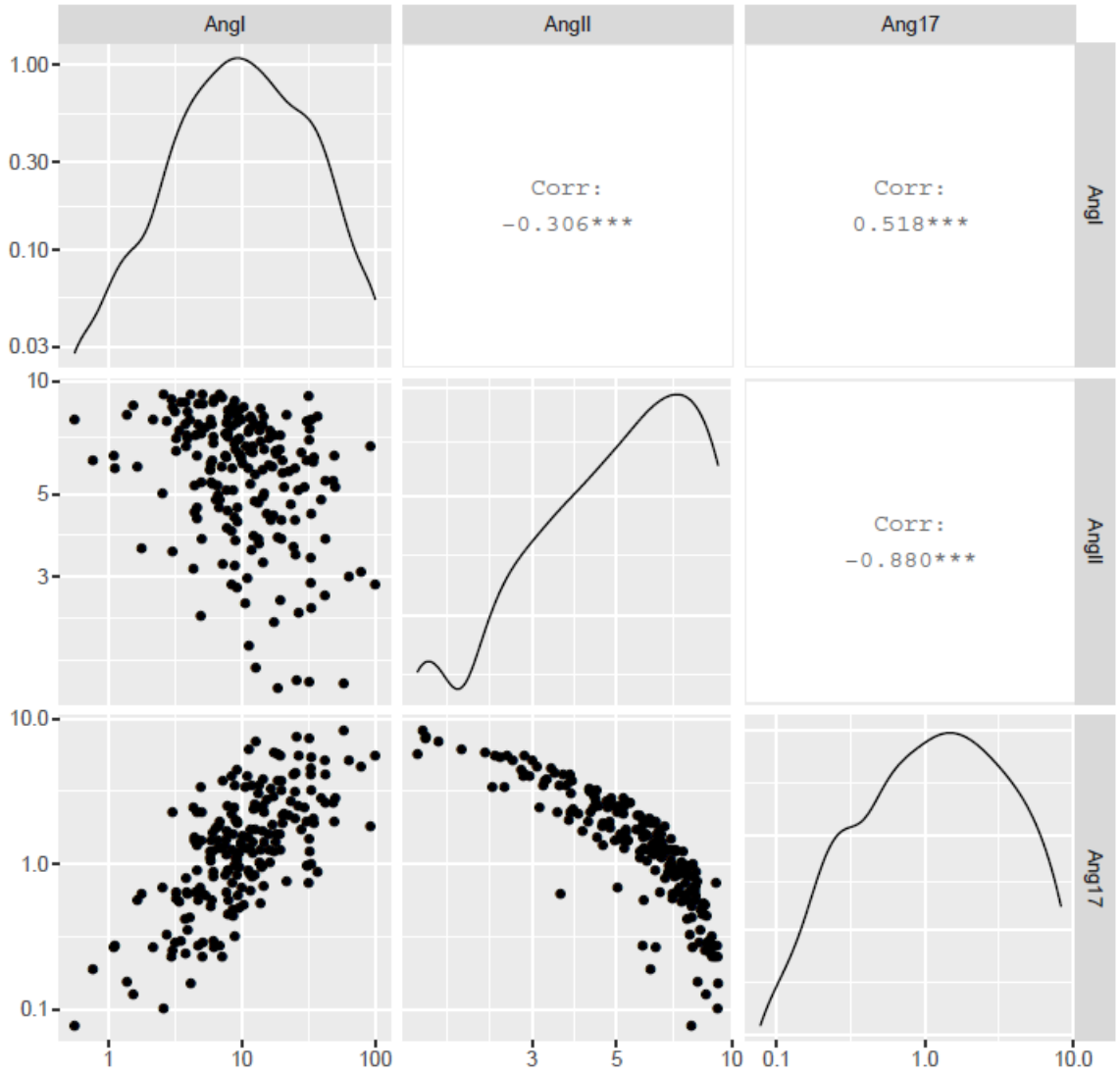

Figure 2.3. *Distribution of RAS peptide concentrations in 200 virtual patients, resulting from parameters shown in Figure 2.2.*

2.2.6 Sensitivity Analysis

To analyze sensitivity in the RAS model that incorporates ACE2 (and is relevant to COVID), A sensitivity analysis using a Latin Hypercube Sampling was conducted to determine the parameters most influential in predicting change in AT1, AT2, and mas receptor occupancies

with varying ACE2 levels and with RAS therapy. As previously stated, Latin Hypercube Sampling is a method that generates values for a set of parameters, each with a specified distribution. Most input parameters were informed by literature data, but parameters whose distributions were not specified were either defined so that 90% of sampled values fell between the range of minimum and maximum values found in literature, or the coefficient of variation was equal to 0.25. Two hundred fifty parameter sets were generated to represent 250 virtual patients. Because the relationship between some inputs and outputs are nonmonotonic or nonlinear, partial rank correlation coefficients were calculated at steady state to quantify how variation in the input parameters contributes to changes in receptors' occupancies. Parameters with the highest sensitivity were further investigated to understand how that parameter's uncertainty influenced the predicted changes in mas-AT1 receptor occupancy ratio. Other sensitivity methods exist, but LHS was used for easy interpretability and fast convergence.

2.3 Results and Discussion

2.3.1 Model Fitting and Validation

Figure 2.4 shows an optimized model fit to data from four rats from Yamamoto *et al [62]*. Yamamoto's data overlaid with a simulation using a model simulation with an optimized set of parameters is shown in **Figure 2.4**. As shown in **Figure 2.4**, the simulation predicted well the increase in AngI and Ang(1-7) and decrease in AngII following ACE inhibition observed in [54]. All parameters were able to be estimated with precision (see **Table 2.3)**. The concentration of ACE was estimated to be at least one order of magnitude larger than the concentrations of NEP and ACE2, with ACE-NEP and ACE-ACE2 ratios of 9 and 32, respectively. These ratios were used in all further simulations. Also of note, K_{AngI} was estimated to be an order of magnitude less than

$Eff_{ACE\text{-}AngI}$[ACE] or $Eff_{NEP\text{-}AngII}$[NEP] (66.5 vs. 397 and 150, respectively). This indicates that most AngI was converted through ACE or NEP, and the reaction rate E in **Figure 1.1b** and Eq. 2.6 is negligible. Therefore, E was considered zero for the rest of this analysis. When analyzing identifiability of our model parameters, we examined the parameter values and objective functions for each of the 50 different starting points and saw nearly all of them settled at the same parameter values / objective function values (**Figure 2.5)**. This provides validation that the model reasonably describes the RAS in humans.

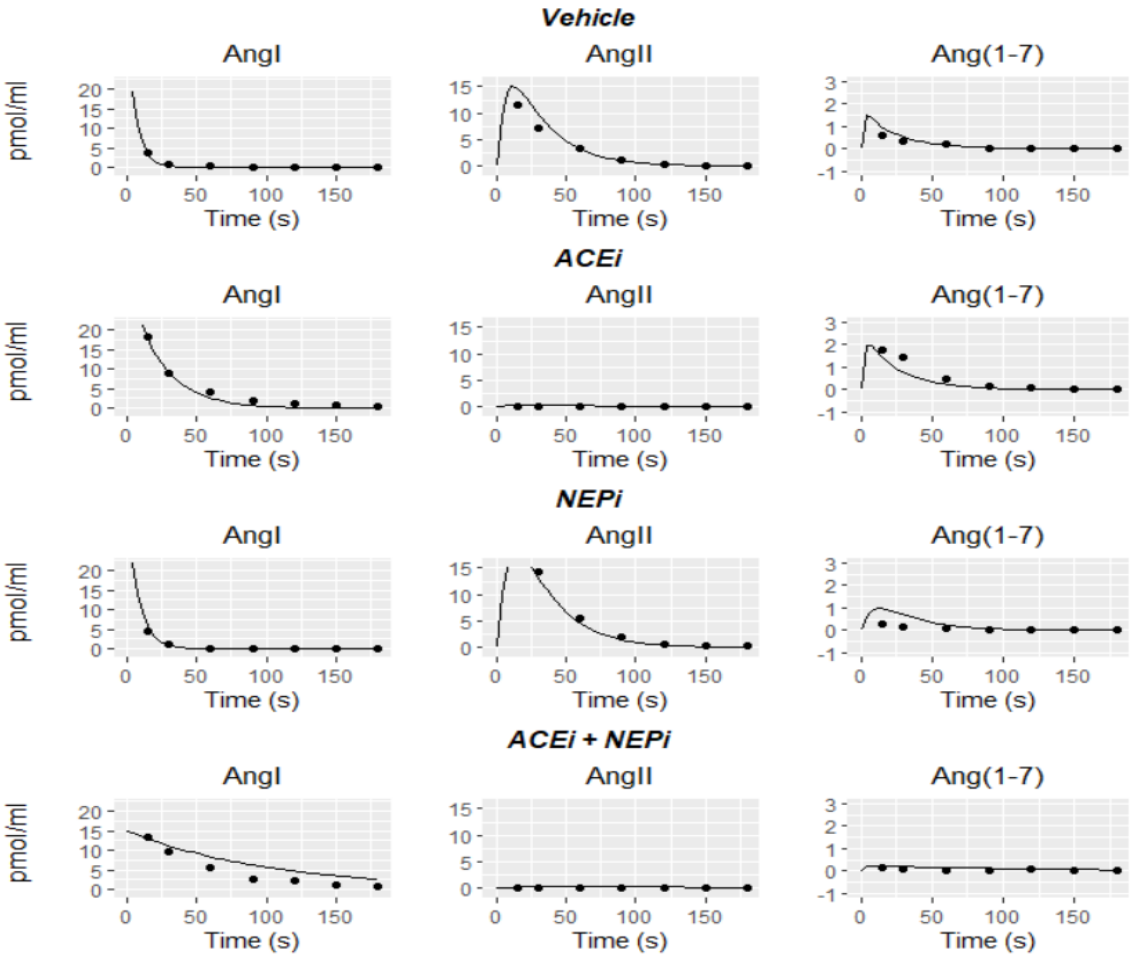

Figure 2.4. *Model calibrated to fit to radiolabeled concentrations of AngI, AngII, and Ang(1-7) following a bolus injection of radiolabeled Ang I, 20 minutes after treatment with vehicle (Row 1),*

ACE inhibitor (Row 2), neprilysin inhibitor (Row 3), or both a neprilysin and ACE inhibitor (Row 4) in four WKY rats [56].

Parameter	Transformed (SE)	Rescaled (95% CI)	Units
Log([ACE])	-0.14 (0.06)	0.87 (0.77 – 0.98)	pM
Log([ACE2])	-5.80 (0.36)	0.003 (0.001 – 0.006)	pM
Log([NEP])	-3.45 (0.21)	0.03 (0.02 – 0.05)	pM
Log(K_{AngI})	4.20 (0.15)	66.50 (49.90 – 88.63)	hr^{-1}
Log(K_{AngII})	4.64 (0.11)	103.05 (82.32 – 129.01)	hr^{-1}
Log(K_{Ang17})	6.24 (0.25)	515.13 (317.95 – 834.59)	hr^{-1}
Logit (ACE inhibition)	-6.18 (3.48)	0.2 (0.001 – 65.5)	%
Logit(NEP inhibition)	-2.83 (1.31)	0.06 (0.004 – 0.44)	%

Table 2.3. *Estimated model parameters for WKY rats.*

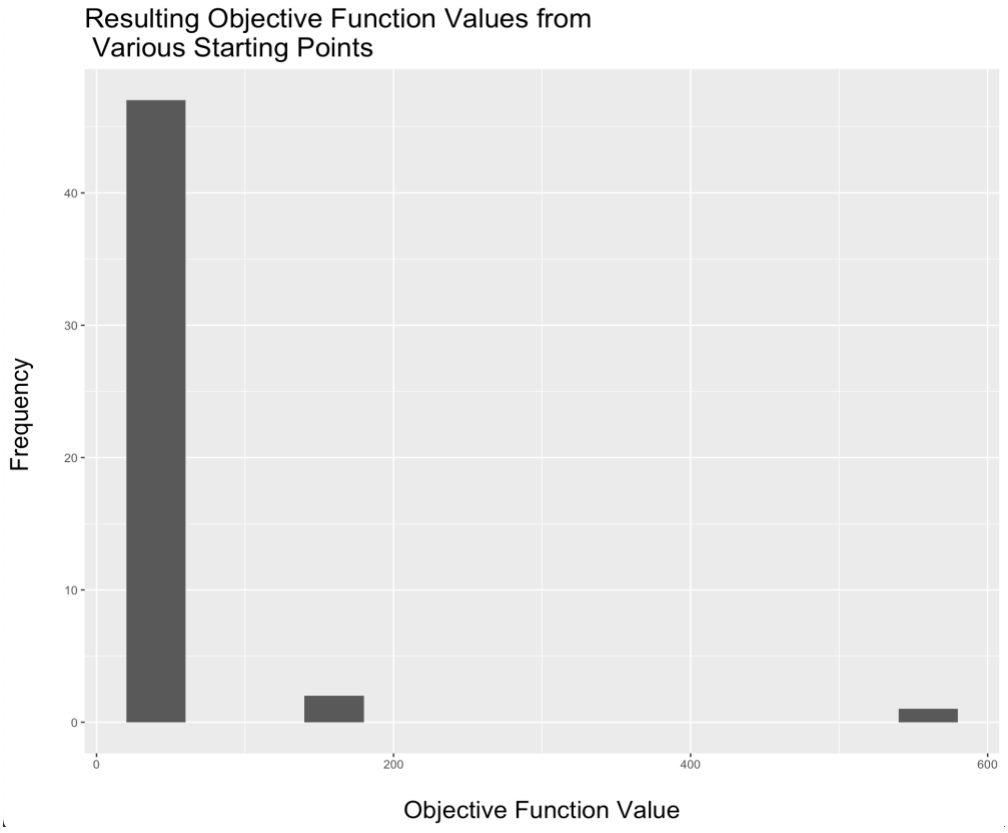

Figure 2.5. *Objective function values resulting from each of the 50 starting points. 94% settled at the minimum calculated value of 20.8, while there were three outliers that were unable to find the minimum.*

2.3.2 Literature review of effects of diabetes, hypertension, aging, and SARS-CoV-2 infection on ACE2

Table 2.4 summarizes studies that have reported changes in ACE2 protein expression, activity, or mRNA in diabetes, hypertension, with age, or after SARS-CoV-2 infection. Unfortunately, no studies of ACE2 changes in human lung tissue were found. In diabetes, small increases in human serum ACE2 were reported. However, it is unclear how changes in serum ACE2 relate to changes in functional membrane-bound ACE2. In diabetes, studies in human kidneys and in rodent lungs, kidneys, and cardiac tissue all showed either a decrease or no change in ACE2 mRNA. However, reported changes in ACE2 protein and activity varied widely, from a 60% decrease to a 2.5-fold increase. Fewer studies were found investigating ACE2 in hypertension. One study found a 20% increase in human serum ACE2 activity, whereas another found a 40–65% decrease in kidney ACE2 protein and mRNA. With aging, two studies found that ACE2 increased during teen years. The only study including adult humans found no difference between young and old adults. Two rodent studies found that ACE2 decreased 67–78% and 50–75% in the lungs and aorta, respectively.

Taken together, these studies do suggest that ACE2 expression can change with disease and aging, decreasing as much as 80% and increasing as much as 2.5-fold. However, the existence and direction of this change is not consistent across studies. Thus, rather than modeling a specific effect of diabetes, hypertension, or aging on ACE2, we sought to understand the effect of a range of changes in ACE2 on the balance between mas and AT1 receptor occupancy.

Two studies have demonstrated that ACE2 is downregulated by earlier SARS coronaviruses, although studies have not yet been published for SARS-CoV-2. Kuba *et al*. found that ACE2 was decreased to levels similar to ACE2 knockouts in Western blot infected mice lungs,

whereas Glowacka *et al.* found that ACE2 shedding was increased 5 times, indicating that membrane ACE2 availability was decreased [27],[63]. Based on these findings, SARS-CoV-2 infection was simulated as a 95% decrease in ACE2 expression.

Condition	**Species**	**Tissue**	**Study**	**Measurement**	**Observed Change**
Diabetes	Human	Lung	Not available		
		Serum	[64]	ACE2 activity	increased 5-18%
		Serum	[65]	ACE2 activity	increased 20%
		Kidney	[66]	ACE2 mRNA and protein	decreased 56-60%
			[67]	ACE2 mRNA	no change
			[68]	ACE2 protein	increased (semi-quantitative, small sample size)
	Rodents	Lung	[60]	ACE2 activity	no significant change
		Lung	[60]	ACE2 protein	increased 25-40%
		Kidney	[60]	ACE2 protein	decreased 40-65%
			[23]	ACE2 activity and protein	Increased 2-fold
			[23]	ACE2 mRNA	decreased 60%
		Cardiac	[23]	ACE2 activity	no change
		Kidney	[69]	ACE2 protein	increased 2.5-fold
Hypertension	Human	Lung	Not available		
		Serum	[65]	ACE2 activity	increased 20%
	Rodents	Kidney	[70]	ACE2 protein and mRNA	40-65% decrease
Age	Human	Lung	Not available		
		Serum	[71]	ACE2 protein	increased during teen years (max age in study: 24)
		Nasal	[72]	ACE2 gene expression	lower in children, no difference between younger and older adults, maximum age in study: 60
	Rodents	Lung	[25]	ACE2 protein	decrease 67-78% in older rats

		Aorta	[26]	ACE2 protein	decreased 50-75% in older mice
SARS-CoV	In Vitro	Vero E6 cells	[63]	ACE2 shedding	Increased 5X (increased indicates decreases membrane availability)
	Mice	Lung	[21]	ACE2 protein	Nearly undetectable with western blot after infection

Table 2.4. *Literature-reported effects of diabetes, hypertension, aging, and SARS-CoV-2 infection on ACE2*

2.3.3 Relationship between ACE2 concentration and mas-AT1 balance, with and without ACEi/ARB therapy

Figure 2.6 (green curves) shows the simulated effects of upregulation or downregulation of ACE2 expression based on either disease effects or pre-existing conditions. At normal ACE2 levels, AT1 and AT2 receptor occupancy are predicted to be nearly twice mas receptor occupancy (9% vs. 5%). A 2.5-fold increase in ACE2 increases the mas/AT1 ratio 66%, while decreasing ACE2 expression down to zero decreases the mas/AT1 ratio 46%. These changes are driven primarily by changes in mas occupancy, with weaker changes in AT1. AT2 occupancy decreases 14% as ACE2 varies from 0 to 2.5 times normal.

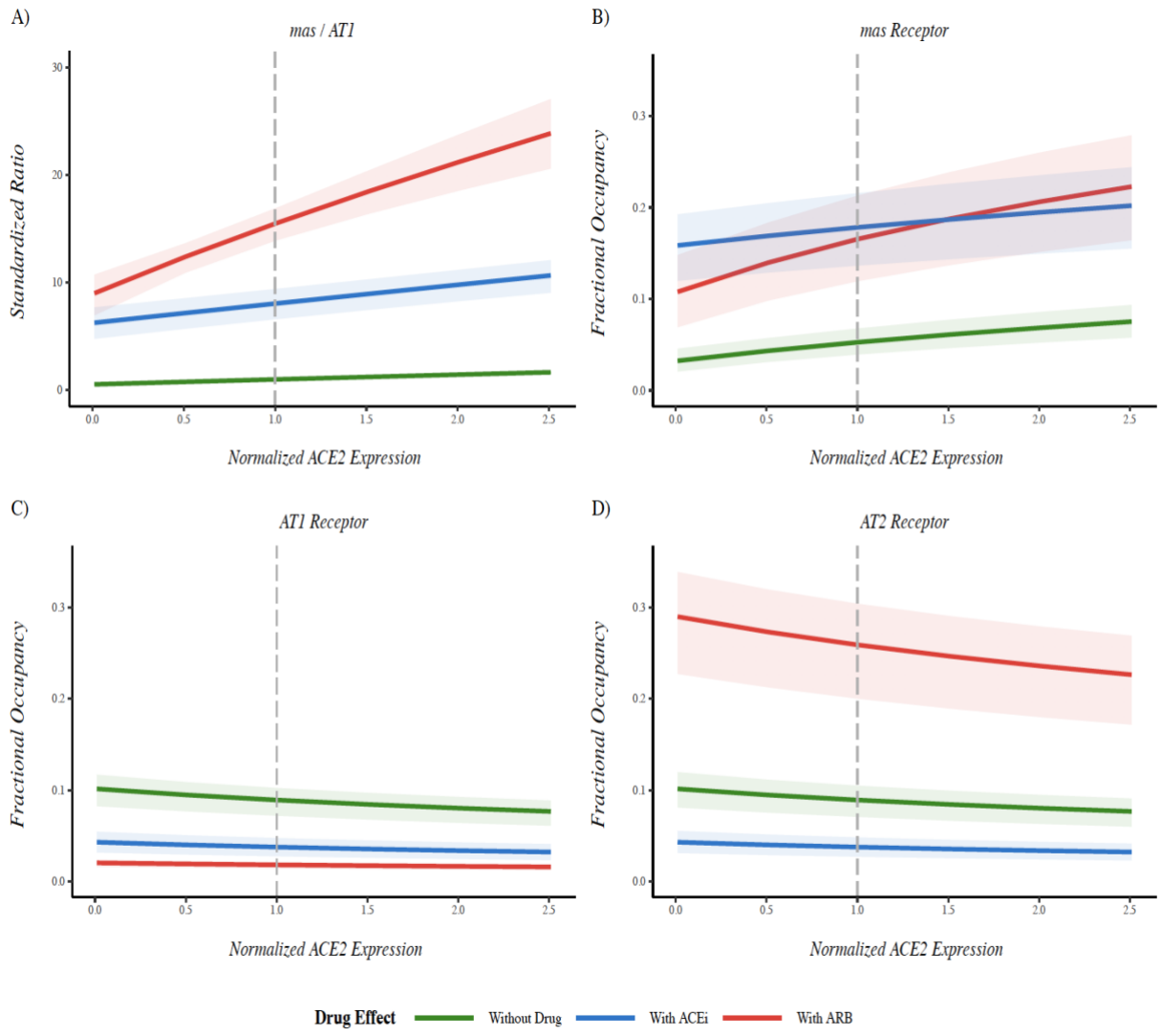

Figure 2.6. *Simulated effects of changes in ACE2 concentration, with and without ARB or ACEi treatment on (a) mas-AT1 receptor occupancy ratio, (b) mas receptor occupancy, (c) AT1 receptor occupancy, and (d) AT2 receptor occupancy. Gray dashed line is the "normal" ACE2 level. All values are standardized by their value at normal ACE2 in the absence of ARB/ACEi therapy. ACEi, ACE inhibitor; ARB, angiotensin receptor blocker.*

Relative to the receptor occupancy changes with ACE2 described above, inhibition of ACE has a much larger effect on mas, AT1, and AT2 receptor occupancy (**Figure 2.6**, blue curves). At normal ACE2 levels, ACEi increases mas receptor occupancy from 5% to 18%, while decreasing both AT1 and AT2 receptor occupancy from 9% to 3%. This resulted in a much larger 7-fold

change in the mas-AT1 receptor binding ratio, compared with the effect of changing ACE2. In the presence of an ACEi, a 2.5-fold increase in ACE2 increased the mas-AT1 ratio to 132% of the ACEi-normal ACE2 level, and 6.4 times the no-treatment-normal-ACE2 level.

ARB therapy is also predicted to have a much larger effect on mas, AT1, and AT2 receptor occupancy than changes with ACE2 concentration (**Figure 2.6**, red curves). At normal ACE2 levels, ARB therapy increases mas receptor occupancy from 5% to 17%, while decreasing AT1 from 9% to 2%, resulting in a 14-fold increase in mas-AT1 receptor binding ratio, compared with the effect of change ACE2. At normal ACE2 levels, ARB therapy did not increase mas receptor occupancy quite as much as ACEi but did increase AT2 receptor occupancy much more than ACEi.

In the presence of an ARB, the effects of changes in ACE2 on mas receptor occupancy are even more dramatic than with ACEi. Still, an increase or decrease in ACE2 concentration does further increase or decrease the mas-AT1 ratio. In the presence of an ARB, a 2.5-fold increase in ACE2 concentration from normal levels increases the mas-AT1-ratio 54%.

The primary conclusion of this analysis is that ACEi/ARB therapy has a much more dramatic effect on shifting the balance of the RAS from the pro-inflammatory AT1 to the anti-inflammatory mas arm, relative to any physiologically relevant changes in ACE2 expression.

2.3.4 Parameter Sensitivity

We next sought to evaluate the sensitivity of these conclusions to assumptions regarding model parameter values. **Figure 2.7** below illustrates the sensitivity of the key model outputs (i.e., changes in AT1, AT2, and mas receptor occupancy), to each model parameter. **Figure 2.7a** considers the sensitivity when ACE2 expression is changed in the absence of treatment, whereas **Figure 2.7b**, **c** considers the sensitivity when ACEi or ARB treatment are added at normal

ACE2 levels. For all three cases, initial Ang(1-7) and AngII concentrations emerged as sensitive parameters relatively speaking, given their deeper colors in the correlation heatmap below. However, these parameters are well-constrained by available clinical and experimental data. Unsurprisingly, all responses to therapy were sensitive to the drug's fractional target inhibition. We have shown previously that while fractional inhibitions with ARBs and ACEi may vary slightly across drug and dose, they are generally well-constrained to be within the range of 90–98%. The change in AT2 and mas receptor occupancy with an ARB was also sensitive to b_{renin}, the strength of negative feedback of AT1 on PRA, which we have also found to be well-constrained between 0.6 and 0.9 [55], [57]. Among parameters with more limited information available for constraining them, $K_{d,\,mas}$ (the binding affinity of Ang(1-7) for the mas receptor) was important for all three cases, while $Eff_{ACE2,AngII}$ (catalytic efficiency of ACE2 for converting AngII to Ang(1-7) was sensitive for changes in AT1 and AT2 with ACE2, but not with ACEi or ARB therapy.

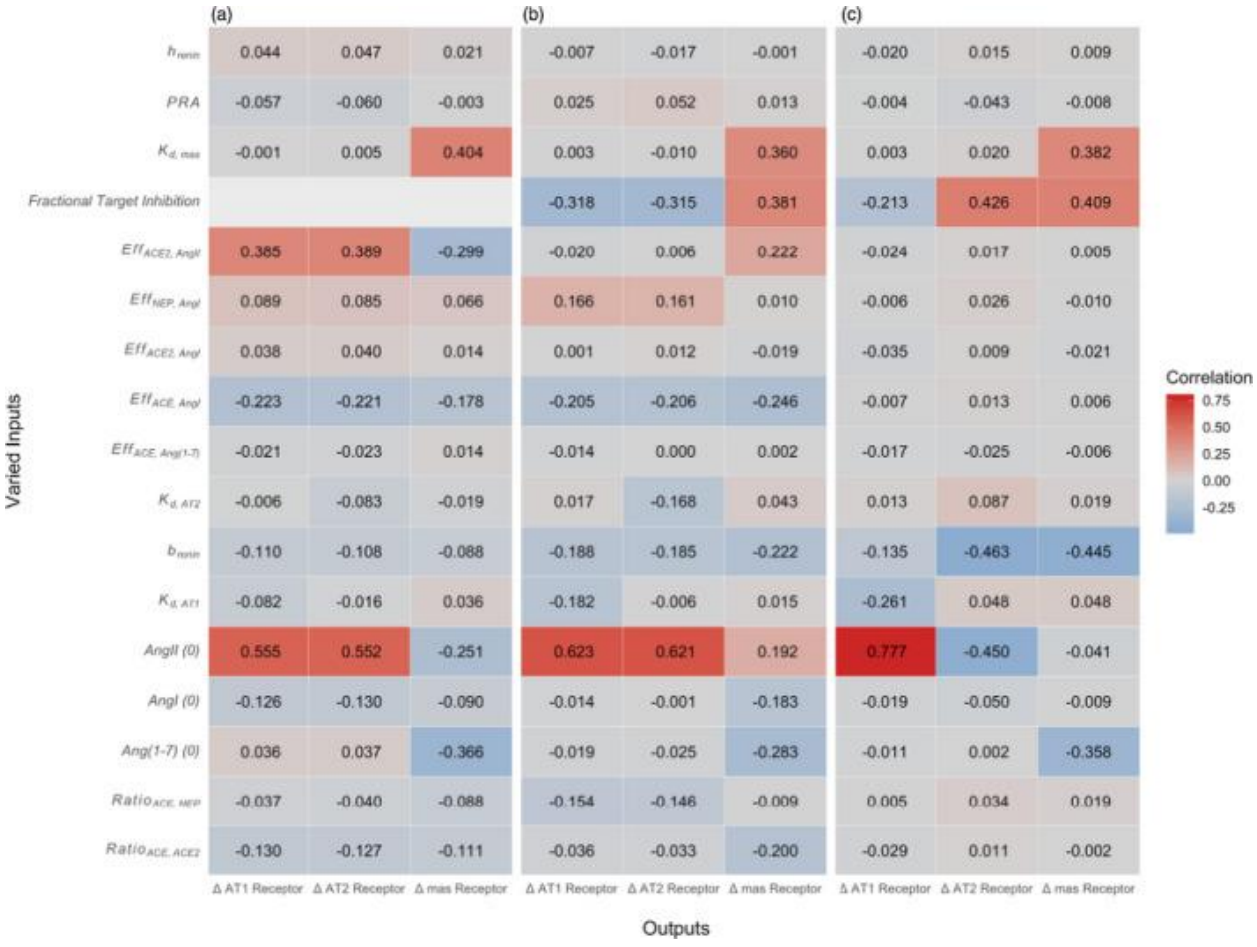

Figure 2.7. *Parameter sensitivity of changes in receptor occupancy with (**a**) a change in ACE2 with no therapy, (**b**) initiation of ACE inhibition, and (**c**) initiation of ARB inhibition. Brightest colors indicate highest correlation between parameter and receptor occupancy.*

To further examine the impact of each of the parameters identified as sensitive, we repeated the earlier simulations of changes in mas-AT1 occupancy, but this time using extreme values of the sensitive parameter (0.05 – 5X).

2.3.5 Effects of ACE2 downregulation by SARS

As shown in **Figure 2.8**, the predicted effects of 95% ACE2 downregulation induced by SARS on AT1, mas, and the mas-AT1 ratio were small relative to the effects of ACEi and ARB

therapy. Both ACEi's and ARBs increased mas while decreasing AT1, thus dramatically increasing the ratio of two. Although ACE and ARBs are predicted to have similar effects on the mas-AT1 ratio, ACEi's are predicted to increase mas to a greater extent, whereas ARBs are predicted to suppress AT1 further.

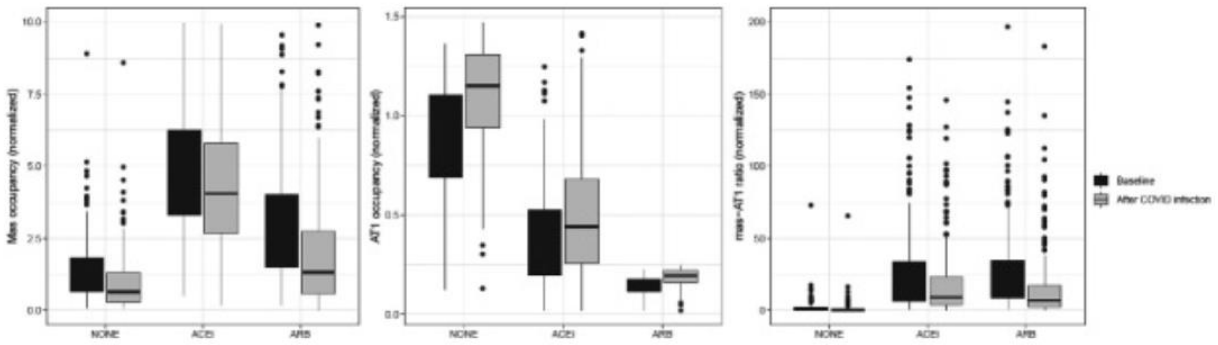

Figure 2.8. *Simulated effect of ACE2 downregulation by severe acute respiratory syndrome-coronavirus 2 (SARS-CoV-2) infection on (left) mas occupancy, (middle) AT1 occupancy, and (right) mas-AT1 ratio, in a population of virtual patients with variable ACE, ACE2, NEP, and renin expressionunder no therapy, ACi therapy and ARB therapy. Points represent simulations outside the interquartile range.*

This suggests that although ACEi's or ARBs may shift the balance toward the anti-inflammatory arm of the RAS, this effect may not be sufficient to produce a therapeutic effect. This may explain why several observational studies have found no difference in outcomes between subjects with COVID-19 who are or are not on RAS therapies [73] Viral downregulation of ACE2 is predicted to decrease mas and increase AT1 binding, but the magnitude of the effect is small relative to the opposing effects of background therapy with ACEi's and ARBs, which elevate mas and decrease AT1 occupancy. ACEi's, ACE inhibitors; ARBs, angiotensin receptor blockers; COVID-19, coronavirus disease 2019.

ACEi/ARBs have been thought to potentially increase ACE2. However, this is not supported by a recent systematic review of published studies, which showed varying and inconsistent effects of ACEi's/ARBs on ACE2 expression [17]. In addition, a recent meta-analysis of cohort and case-control studies found no difference in severe or lethal COVID-19 between untreated subjects and those receiving an ACEi inhibitor or an ARB [73]. Taken together with these reviews and analyses, this study provides further support for the continuation of ACEi/ARB treatment in patients for whom they are indicated.

Still, interactions among ACEi's/ARBs, ACE2, and SAR-CoV-2 are complex, and may be dependent on factors that may vary across individuals, including the ACE/ACE2 ratio, viral load, and the body's immune response, among others. In addition, higher levels of circulating/soluble ACE2 levels may neutralize some SARS-CoV-2 virus, which could reduce availability to bind to membrane-bound ACE2. Thus, these potential interactions deserve further investigation.

Figure 2.9 explores the effect of variability in four RAS enzymes (ACE, ACE2, NEP, and renin) on the mas-AT1-ratio. Mas-AT1 ratio is positively correlated with ACE, negatively correlated with NEP, and is not correlated ACE2 or renin. ACE and NEP are correlated with appear to affect the baseline mas-AT1 ratio (prior to infection) much more than ACE2 or renin. This is true both before and after treatment with ARBs and ACEi's. There is no obvious effect of enzyme expressions on the magnitude of change in mas-AT1 ratio with infection.

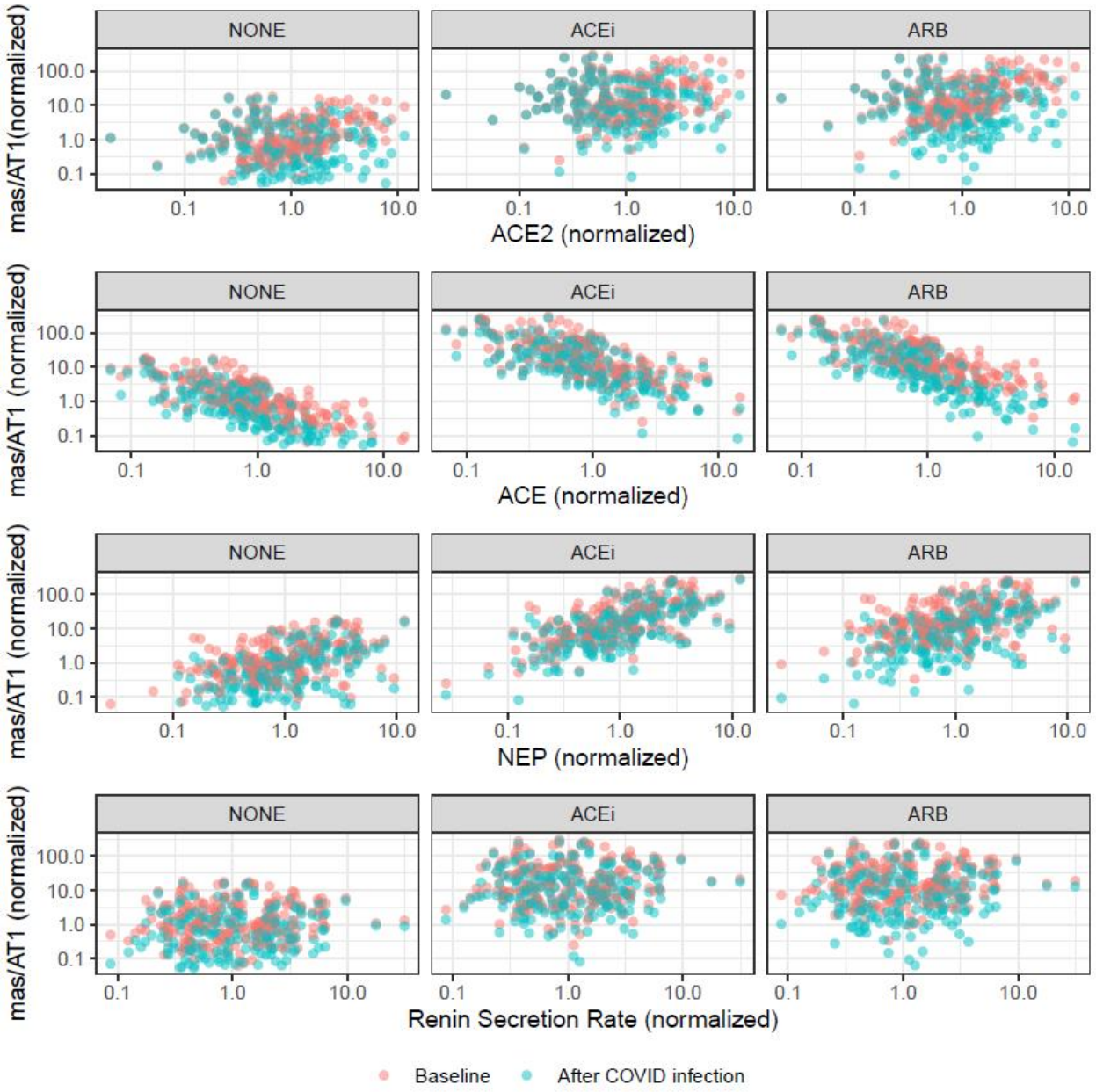

Figure 2.9. *Effect of RAS enzyme expression on baseline mas-AT1 receptor occupancies, and on the response to viral ACE2 downregulation, with and without background ACEi/ARB therapy. All data plotted on log scale.*

This suggests that changes in ACE2 expression due to comorbidities, like diabetes, hypertension, or aging, may be less important than the effects of these comorbidities on other enzymes in the RAS, particularly ACE and NEP. As described earlier, we estimated that ACE

expression is 10 and 30 times higher than NEP and ACE2 expression. ACE expression has been shown to change with disease [23], [74]. Thus, even though ACE2 is the enzyme involved in SARS-CoV-2 infection of the cell, ACE expression levels may be more important in determining the relative pro-inflammatory or anti-inflammatory balance of a subject prior to infection.

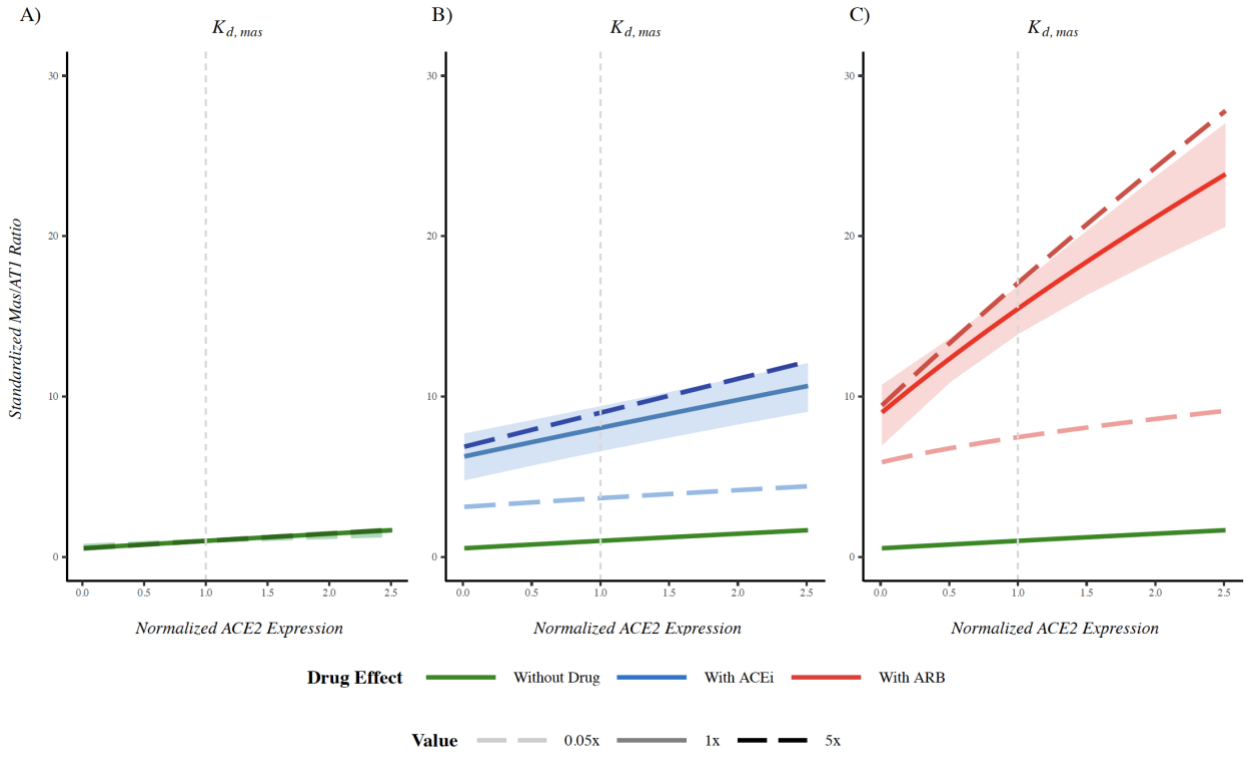

Figure 2.10. *Effect of uncertainty in $K_{d,mas}$ on predicted changes in the mas-AT1 ratio with A) changes in ACE2 concentration alone, B) ACEi therapy , or C) ARB therapy. All values are standardized by their value at normal ACE2 in the absence of ARB/ACEi therapy. Shaded bands represent predicted values using the standard deviation of $K_{d,mas}$ reported in [53].*

Figure 2.10 shows the effect of uncertainty in $K_{d,mas}$, chosen for illustration because its value is informed by very limited experimental data (one *in vitro* study, Santos *et al*. 2003). Although the magnitude of this parameter does have some influence on the magnitude of predicted changes in mas-AT1-ratio, the effects are not sufficient to alter the conclusions of this study. In other words,

even if the value we used is several-fold different from the true value, our conclusions would not differ. Thus, the sensitivity analysis provides confidence that the predictions and conclusions of this study robust to uncertainty in parameter values.

A secondary important observation is that although ARBs and ACEi's produce similar changes in mas occupancy, ARBs increase AT2 occupancy while ACEi's decrease it. These drug-induced changes in AT2 occupancy were also large relative to the effect of ACE2 changes. Because AT2 is associated with reduced inflammation, it is possible the ARBs may further protect from inflammation relative to ACEi's. However, there are limited data available to inform the clinical relevance of changes in AT2 occupancy.

2.3.6 Implications of changes in the mas-AT1 balance for acute lung injury in COVID-19

Although we can predict the change in mas receptor occupancy, directly relating the magnitude of change to the potential for protection or exacerbation of lung injury is more challenging. However, Ang(1-7) infusion studies have shown a dose-dependent protective effect against experimental lung injury [75], [76], [77]. Thus, benchmarking predicted rates of Ang(1-7) formation against the rates of Ang(1-7) infusion in these studies may provide a quantitative indication of whether the simulated changes are likely to be large enough to impact lung inflammation and injury.

Changes in mas receptor occupancy occur due to changes in the rate of Ang(1-7) formation from AngI and AngII, either due to a change in enzyme expression (i.e., by SARS-CoV-2) or in the rate of formation of the enzyme substrates, AngI and AngII (i.e., by ACEi's and ARBs). **Figure 2.11** shows the simulated Ang(1-7) production rates, before and after infection, with and without ACEi or ARB therapy, relative to the Ang(1-7) infusion rates used in experimental studies.

Although the Ang(1-7) production rate was increased by therapy and decreased by the virus, in all cases, the changes were much smaller than the rates necessary to produce benefits in experimental lung injury, and were similar to a rate which was found by Zambelli *et al*. to produce no benefits [75]. This suggests that although ACEi's or ARBs may shift the balance toward the anti-inflammatory arm of the RAS, this effect may not be sufficient to produce a therapeutic effect. This may explain why several observational studies have found no difference in outcomes between subjects with COVID-19 who are or are not on RAS therapies [73].

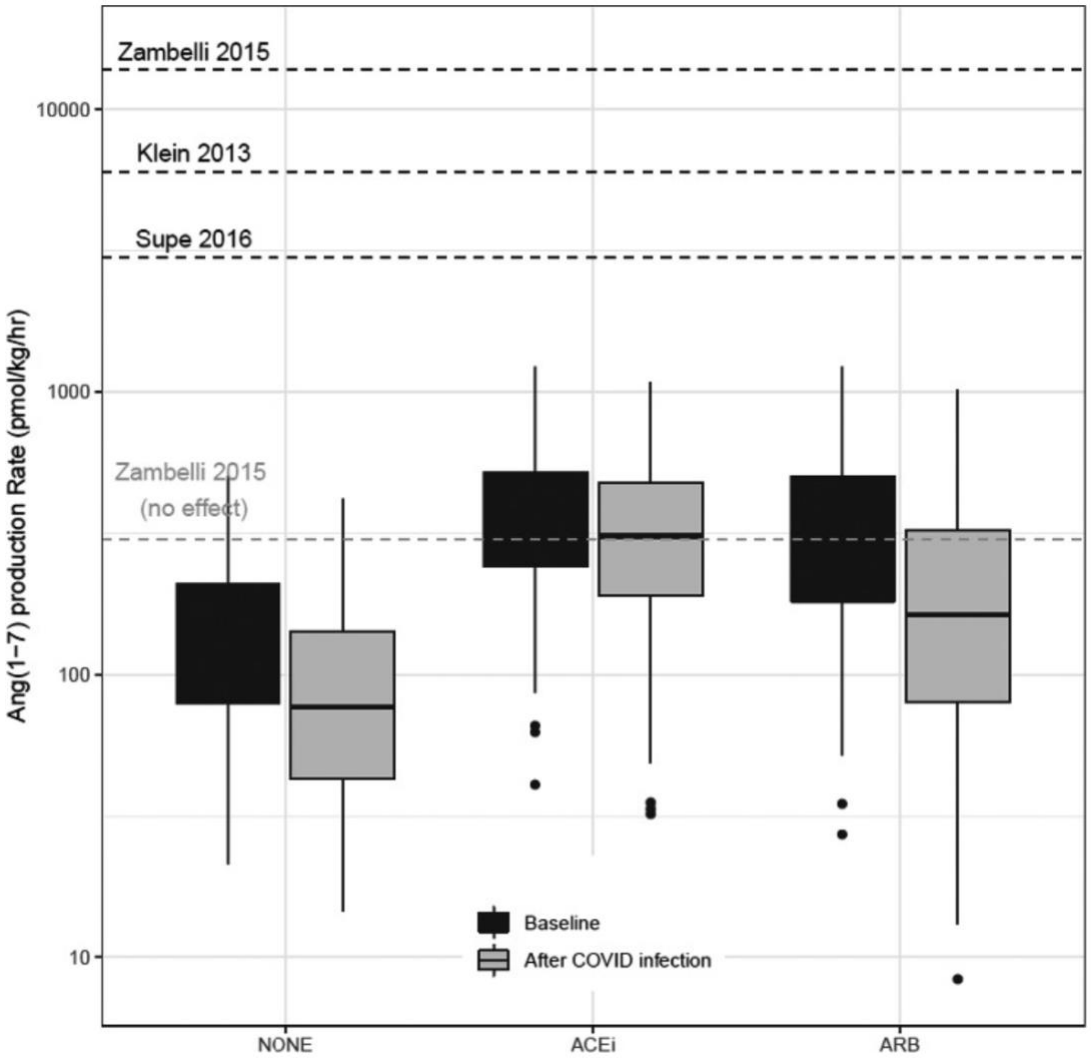

Figure 2.11. *Simulated changes in Ang(1-7) production rate (bars) without or with ACEi or ARB treatment, and with infection-induced ACE2 downregulation, relative to rates of Ang(1-7) infusion rates found to elicit protection from lung injury in experimental models (dashed lines [75-77]).*

ACEi/ARBs have been proposed to potentially increase ACE2. However, this is not supported by a recent systematic review of published studies, which showed varying and inconsistent effects of ACEi's/ARBs on ACE2 expression [17]. In addition, a recent meta-analysis of cohort and case-control studies found no difference in severe or lethal COVID-19 between untreated subjects and those receiving an ACEi inhibitor or an ARB [73]. Taken together with

these reviews and analyses, this study provides further support for the continuation of ACEi/ARB treatment in patients for whom they are indicated. Interactions among ACEi's/ARBs, ACE2, and SAR-CoV-2 are complex, and may be dependent on factors that may vary across individuals, including the ACE/ACE2 ratio, viral load, and the body's immune response, among others. In addition, higher levels of circulating/soluble ACE2 levels may neutralize some SARS-CoV-2 virus, which could reduce availability to bind to membrane-bound ACE2. Thus, these potential interactions deserve further investigation.

2.3.7 Key uncertainties, knowledge gaps, and limitations

One objective of this study was to evaluate the key uncertainties and knowledge gaps in quantifying the effects of ACEi's/ARBs in COVID-19. Some parameters, such as plasma renin activity, AngI, AngII, and Ang(1-7) have well-defined clinical ranges. Renin half-life has been measured in multiple studies, whereas the values for enzyme catalytic efficiencies and receptor binding affinities were based on single *in vitro* studies. Expression of ACE, ACE2, and neprilysin varies across tissue and cell types, and across species, and thus are much more difficult to quantify. Thus, it was necessary to determine these enzyme concentrations using mathematical constraints and estimating their ratios by fitting experimental data for peptides that are more easily measurable. Since it is not immediately apparent whether the unknown parameters are identifiable given the experimental data, identifiability of the model parameters was investigated to 1), estimate unknown parameter values, and 2) to determine if the estimates were unique given the set of experimental data. We saw that our model parameters were indefinable since nearly every estimation starting point settled at the same objective function value with the exception of 3 outliers (**Figure 2.5**). We saw there was the highest degree of certainty in values for AngI, AngII, Ang(1-7), and PRA, whereas uncertainty is greatest for the ACE-ACE2 and ACE-NEP ratios.

Although there is uncertainty around these enzyme ratios, sensitivity analysis showed that predictions of changes in AT1, AT2, and mas receptor occupancy are robust to inaccuracies in parameter values (**Figure 2.7**). Thus, the conclusions of this analysis are unlikely to be impacted if the values used for these ratios are not accurate.

In addition to parameter uncertainty, several limitations should be considered. Model parameters were constrained based on plasma levels of RAS peptides, and local tissue differences and tissue RAS were not considered. Our simulations are able to predict changes in mas-AT1 ratio but do not have the capability to predict the impact of changes in this ratio on COVID-19 pathophysiology. Generic ARB and ACEi were modeled, and we did not consider differences within drug classes or with different doses. Interindividual variability in RAS parameters was not considered. Last, the AngI-Ang(1-9) was not explicitly modeled, but is lumped in other forms of AngI degradation. This is justifiable because very little Ang(1-7) is expected to be formed from Ang(1-9).

The model did not account for potential negative cooperativity between the two binding sites of ACE. Negative cooperativity between these binding sites would mean that ACE reactions follow Hill rather than Michaelis-Menten kinetics. Adding a Hill coefficient with a value of 0.5 (negative cooperativity) had a small numeric effect (< 12%) on predicted receptor occupancies but did not impact the conclusions of the study.

This analysis did not address the potential impact of therapy-induced changes in AT1 and AT2 receptor expression. Limited available data show weak and inconsistent effects of ACEi's on AT1 expression, but consistently show that ARBs reduce AT1 expression [78], [79]. For AT2, data for defining both the binding affinity as well as therapy-induced changes in expression and the clinical consequences of changes in AT2 activity and expression are even more limited.

2.4 Conclusion

Given the ongoing debate surrounding the use of ACEi's and ARBs in the setting of COVID-19, this study aimed to integrate available information about the RAS, effects of SARS-CoV-2 infection, and its comorbidities on the RAS to provide quantitative predictions of the effects of ACEi's and ARBs on the pro-inflammatory/anti-inflammatory balance of the RAS. There are several key conclusions from this analysis. First, our simulations indicate that ACEi/ARB treatment prior to SARS-CoV-2 infection increases the ratio of mas to AT1 receptor occupancy many fold. Thus, in patients already taking an ACEi/ARB before infection, the anti-inflammatory arm of the RAS would already be much more dominant. Second, effects of changes in ACE2 expression with comorbidities of diabetes, hypertension, or aging on the mas-AT1 receptor ratio are relatively small, compared with the effects of ACEi's/ARBs. Changes in ACE expression are predicted to be more important than ACE2 in determining the baseline inflammatory/pro-inflammatory balance of the RAS. Third, pro-inflammatory shifts in the mas-AT1 ratio due to ACE2 downregulation by SARS-CoV-2 infection are predicted to be small relative to anti-inflammatory shifts induced by ACEi/ARB. Last, predicted changes in the Ang(1-7) production rate with ACEi/ARB therapy, comorbidities, or infection were all small relative to the exogenous Ang(1-7) infusion rates shown experimentally to protect against acute lung injury, suggests that changes in the ACE2-Ang(1-7)-mas arm may not be large enough to play a major role in COVID-19 pathophysiology.

CHAPTER 3

Describing Relationships between Natriuretic Peptides and GFR and Incorporating Them into a Larger Cardiorenal Model to Validate the Response to Therapy

Introduction

Heart failure (HF) affects over 6 million per year and costs the US approximately $30 billion annually according to CDC. A defining feature of heart failure is ejection fraction (EF), which is the amount of blood pumped out with each heartbeat. This dissertation discusses HF with reduced ejection fraction (HF-rEF) where patients' ejection fraction is less than 40%. Preserved ejection fraction is any EF greater than 40%. The main cause of HF-rEF comes from the heart's reduced contractility over a long period of time. As a slowly progressing disease usually triggered by a myocardial infarction, the heart enlarges and weakens, thus losing its ability to adequately pump blood throughout the body. Diagnosing HF severity is difficult since there are not any tests for HF that are neither specific nor sensitive enough. Accurate diagnosis is crucial though because it is so costly given the intrusiveness of measuring pressures within the heart. One possible way to diagnose HF is by measuring ventricular dysfunction by measuring concentration of natriuretic peptides (NP's), BNP and NT-proBNP, which are released in response to cardiac stretch due to fluid overload. The Framingham Cohort Study along with the ACCF, AHA, and ESC have all determined that BNP and NT-proBNP are important for initially determining severity and treatment strategy and prognosis of heart failure. Since these NP's are produced in the heart, they

are cleared by the kidneys. However, treatments such as ACEi's and ARBs act to reduce heart and blood volume by slowing the cardiac remodeling process as well as controlling water/sodium homeostasis and reducing volume retention via the kidney. Thus, the first part of this study aimed to incorporate information on cardiac stress as well as kidney dysfunction and their effects on NP concentrations in a mechanistic ODE model to improve interpretability when using NP's as diagnostic and HF monitoring tools.

3.2 Methods

In this analysis, we showed that the relationship between NT-proBNP or BNP and GFR can be defined mechanistically and mathematically, based on consideration of their production and clearance rates. We derive a very simple equation that can be used to quantify the contribution of GFR to NT-proBNP and to correct NT-proBNP for differences in GFR. We develop a similar relationship for BNP that also accounts for its non-renal clearance. We then show that these simple relationships can reproduce clinically observed increases in the ratio of NT-proBNP to BNP with decreasing eGFR across multiple clinical studies.

In this analysis, we make the following assumptions:

1) pro-BNP, the precursor to BNP and NT-proBNP, is secreted by the heart and instantaneously cleaved into BNP and NT-proBNP. Thus, both peptides are produced at the same molar rate Q.
2) Both BNP and NT-proBNP are freely filtered across the glomerulus at a rate that is proportional to GFR and to their respective plasma concentrations.
3) NT-proBNP is cleared solely by renal filtration.

4) BNP is cleared by additional mechanisms (the clearance receptor NPR-C and the enzyme neprilysin).

Note, it is important that all equations given below use molar concentrations.

Figure 3.1 shows a schematic to describe the process behind production and clearance rates of BNP and NT-proBNP.

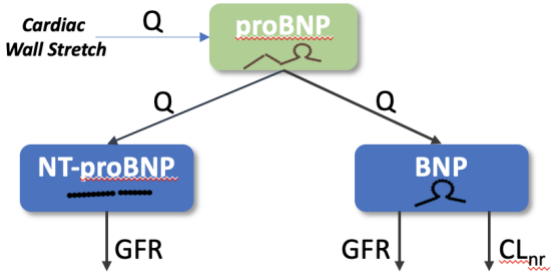

Figure 3.1. Schematic to describe production and clearance rates of BNP and NT-proBNP.

We then integrated these relationships into a larger cardiorenal quantitative systems pharmacology (QSP) model that couples previously published cardiac models and a model of renal function and volume homeostasis to allow for interactions between cardiac and renal functions. These individual portions of the model are coupled through blood volume (regulated by the kidneys through control of excretion of water and sodium and mean arterial pressure which determines GFR) [48].

The complexity of integrated functions of the heart, kidney, and neurohormonal mechanisms makes it difficult to fully understand the interplay between them, especially when one or many states are in dysfunction. In heart failure, as previously mentioned, heart and kidney dysfunction usually coexist, and drugs to treat heart failure act through renal mechanisms but could have unexpected effects on cardiac function. We use mathematical models to investigate the

integrated function of the 2 systems and understand the effect of interventions [80]. In addition, the model can describe cardiac function and remodeling due to hypertrophy and volume homeostasis in heart failure.

3.2.1 Mathematical relationship between NT-proBNP and GFR

Under the above assumptions, the rate of change of the amount of plasma NT-proBNP is the difference between the rate of cardiac proBNP production *Q* and the rate of renal filtration of NT-proBNP. Under the assumption of free filtration, the rate of filtration is the product of GFR and the plasma concentration of NT-proBNP.

$$V_N \frac{dNTP}{dt} = Q - GFR * NTP \qquad \text{Eq. 3.1}$$

Here, NTP is the plasma concentration of NT-proBNP, and V_N is the volume of distribution of NT-proBNP. At steady state (or any approximation of steady state where *Q* and GFR are not changing rapidly)

$$Q = GFR * NTP, \qquad \text{Eq. 3.2}$$

Moreover, this relationship generally applies at any steady state i

$$Q_i = GFR_i * NTP_i. \qquad \text{Eq. 3.3}$$

Consider a situation in which GFR is decreased, but cardiac production of proBNP is unchanged. Let GFR_{ref} and NTP_{ref} denote the typical levels of GFR and NT-proBNP in a healthy subject. Then, at any new steady state *i*,

$$Q_{ref} = Q_i.$$

From Eq. 3.3,

$$GFR_{ref} NTP_{ref} = GFR_i * NTP_i.$$

Thus, at any new steady state *i*, the new steady-state concentration of NT-proBNP can be determined for any new value of GFR

$$NTP = \frac{GFR_{ref}}{GFR} * NTP_{ref}. \quad \text{Eq. 3.4}$$

In other words, given known reference values of GFR and NTP-proBNP, the NT-proBNP that will occur if there is a change in GFR but no change in cardiac stretch (i.e. proBNP release rate *Q*) can be predicted.

Conversely, and perhaps more usefully, given an observed NT-proBNP concentration and GFR, the NT-proBNP concentration that would exist at the same cardiac production rate but at the reference GFR can be determined. Let NTP_i and GFR_i be the observed NT-proBNP and GFR, and NTP_{adj} be the NT-proBNP level that would occur at the same production rate but normal GFR. Then

$$Q_i = NTP_i GFR_i = NTP_{adj} GFR_{ref}$$

and

$$NTP_{adj} = NTP_1 \frac{GFR_1}{GFR_{ref}}. \quad \text{Eq. 3.5}$$

Thus, NT-proBNP can be adjusted for GFR simply by multiplying by the ratio of observed and normal GFR. This equation is basically the inverse of Eq. 3.4 and allows determination of the contribution of renal function to observed NT-proBNP values.

3.2.2 Mathematical Relationship between BNP and GFR

We then applied a similar analysis to BNP. Under the assumptions stated earlier, BNP is produced by myocardial release of proBNP at the same molar rate *Q* as NT-proBNP. BNP is cleared by both renal filtration and non-renal clearance mechanisms. Let CL_{nr} represent the non-renal clearance rate of BNP. Then, the rate of change of the amount of plasma BNP is given by

$$V_B \frac{dBNP}{dt} = Q - GFR * BNP - CL_{nr} * BNP. \quad \text{Eq. 3.6}$$

Here, *BNP* is the plasma concentration of BNP, and V_N is the volume of distribution of BNP. At steady state *I* (or any approximation of steady state where *Q* and GFR are not changing rapidly):

$$Q_i = GFR_i * BNP_i + CL_{nr} * BNP_i \quad \text{Eq. 3.7}$$

Because BNP and NT-proBNP are formed from proBNP at the same molar rate, then from Eq. 3.2 above, $Q = GFR \times NTP$. Plugging into the previous equation and solving for CL_{nr} gives:

$$CL_{nr} = \frac{GFR*NTP - GFR*BNP}{BNP}$$

Let GFR_{ref}, BNP_{ref}, and NTP_{ref} denote the normal levels of GFR, BNP, and NT-proBNP. Then, plugging in and rearranging the above equation, non-renal clearance of BNP CL_{nr} can be written as

$$CL_{nr} = \left(\frac{NTP_{ref}}{BNP_{ref}} - 1\right) * GFR_{ref} \, . \quad \text{Eq. 3.8}$$

The molar ratio of NT-proBNP to BNP in normal subjects reported in various studies ranges from 1.3 to 2 (which is equivalent to a mass ratio of 3.2 to 5.4). Thus, according to equation 10, the non-renal clearance rate of BNP likely falls somewhere between 30 to 100% of GFR. This also means that GFR is responsible for at least half (if CL_{nr} = GFR) and up to 75% (if CL_{nr} = 0.3*GFR) of BNP clearance.

Let us assume non-renal clearance of BNP is constant and does not change as GFR changes. Then, at any state i,

$$Q_i = GFR_i * BNP_i + CL_{nr} * BNP_i \quad \text{Eq. 3.9}$$

Cardiac production Q_i can also be expressed in terms of GFR and NT-proBNP, from Eq. 3.3. If *Q* is constant, then for any new value of GFR, the new steady-state concentration of BNP can be determined:

$$GFR_{ref}NTP_{ref} = GFR_i * BNP_i + CL_{nr} * BNP_i.$$

Rearranging and substituting in Eq. 3.8 for CL_{nr} gives

$$BNP_i = \frac{NTP_{ref} GFR_{ref}}{\mathrm{GFR_i} + \left(\frac{NTP_{ref}}{BNP_{ref}} - 1\right) * GFR_{ref}}. \qquad \text{Eq. 3.10}$$

3.2.3 Mathematical Relationship between ratio of NT-proBNP to BNP and GFR

Returning to Equations 3.2 and 3.7, we can also determine the ratio of NT-proBNP to BNP at any GFR

$$Q_i = GFR_i * NTP_i = \ GFR_i * BNP_i + CL_{nr} * BNP_i \ .$$

Solving for the ratio gives

$$\frac{NTP_i}{BNP_i} = \frac{GFR_i + CL_{nr}}{GFR_i}. \qquad \text{Eq. 3.11}$$

Note that the ratio does not depend on production rate *Q*. Thus, while changes in cardiac production of proBNP affect the concentrations of each peptide, it has no effect on their ratio. The ratio depends only on GFR (and on non-renal BNP clearance, but we are assuming that it is constant). Assuming constant non-renal clearance rate and plugging in Eq. 3.8 gives

$$\frac{NTP_i}{BNP_i} = \frac{GFR_i + \left(\frac{NTP_{ref}}{BNP_{ref}} - 1\right) * GFR_{ref}}{GFR_i}.$$

This can be rearranged to give

$$\frac{NTP_i}{BNP_i} = 1 + \frac{GFR_{ref}}{GFR_i}\left(\frac{NTP_{ref}}{BNP_{ref}} - 1\right). \qquad \text{Eq. 3.12}$$

Note that this equation describes the molar ratio, not the mass ratio. Because the molecular weights of NT-proBNP and BNP are 8.5 and 3.464 kDa, the mass ratio can be obtained by multiplying by 8.5/3.464 or 2.45. This is important since concentrations are typically reported in units of pg/ml rather than pmol/L.

3.3 Results

3.3.1 Mathematical Relationship between NT-proBNP and GFR

The predicted relationships from Eqs. 4 and 5 are shown graphically in **Figure 3.2**. A GFR of 100 ml/min and NT-proBNP of 5.88 pmol/L (50 pg/ml) is used as the reference point. Eq. 3.4 predicts that NT-proBNP increases non-linearly as GFR declines at constant *Q* (**Figure 3.2a**). A concentration of 125 pg/ml is often referenced as the upper limit of normal for NT-proBNP. However, this figure illustrates that in subjects with GFR less than 40 ml/min, NT-proBNP should be expected to be above this level even if there is no change at all in cardiac stretch and proBNP production, simply because of reduced renal clearance. **Figure 3.2b** shows the effect of adjusting observed NT-proBNP for observed GFR (Eq. 3.5). The adjusted value (the value that would be observed if GFR were normal), is linearly related to observed GFR. As GFR goes down, the adjusted NT-proBNP decreases relative to observed (or in other words, a smaller NT-proBNP would be observed if GFR were normal). As GFR increases above normal (i.e. hyperfiltration), adjusted NT-proBNP increases.

These simple mechanistic equations are generally consistent with a previous analysis of the effect of eGFR on NT-proBNP in 204 male subjects in Germany [81]. This study determined an empirical formula for correcting for GFR through regression analysis: $NTP_{adj} = \frac{NTP}{e^{1.892-0.025\times eGFR}}$. This relationship is also shown in **Figure 3.2b** for comparison. There is good agreement between the two relationships, although they diverge at low and high GFR levels. The mechanistic relationship developed here suggests that the effect of GFR on NT-proBNP is more nonlinear and suggests that the empirical relationship may underestimate NT-proBNP at very low GFRs while overestimating it in hyperfiltering subjects.

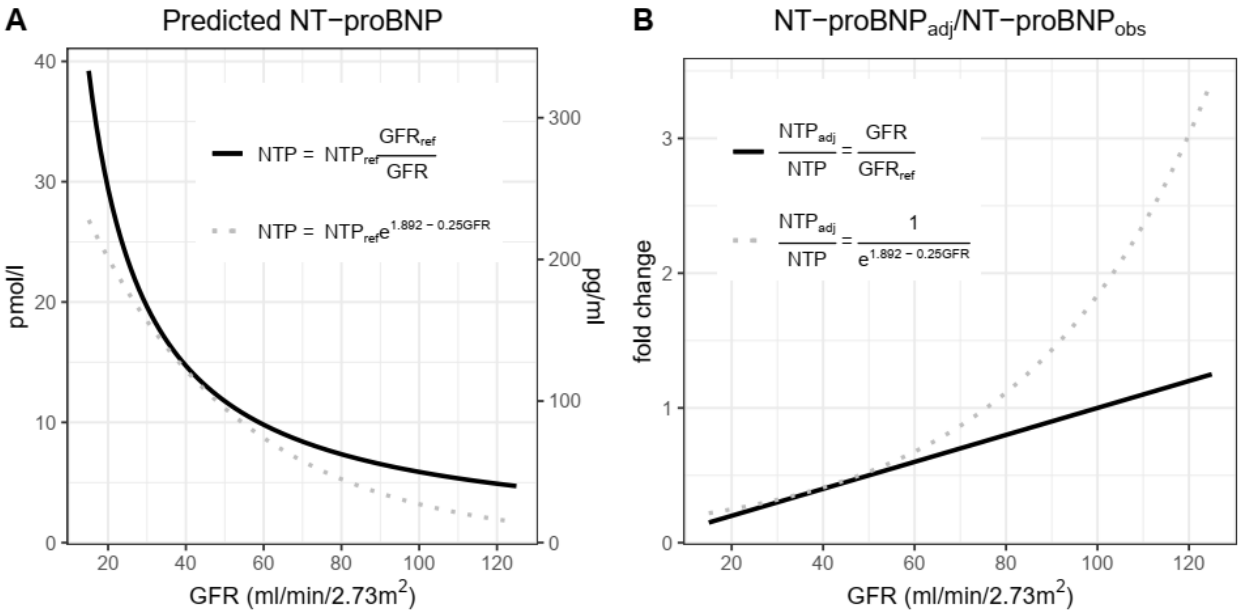

Figure 3.2. *A) Holding cardiac pro-BNP production rate Q constant, NT-proBNP is predicted to increase nonlinearly with decreasing eGFR (Eq. 3.4). B) Predicted ratio of GFR-adjusted to non-adjusted NT-proBNP (Eq. 3.5). For comparison, the regression equation from Luchner et al [81] is also shown (gray dashed curves). Both simulations assume reference GFR of 100 ml/min and reference NT-proBNP of 50 pg/ml (5.88 pmol/L).*

The adjusted NT-proBNP calculated by Eq. 3.5 is determined relative to a reference GFR, which we have up until now assumed to be the typical value seen in normal healthy subjects. However, the same relationship can more generally be applied to adjust NT-proBNP for a change in renal function relative to ANY previously measured GFR. For instance, if a subject's NT-proBNP rises over a certain time period, but GFR falls over the same time period, a portion of the rise in NT-proBNP is a consequence of reduced clearance, and the rest is due to a change in cardiac production of proBNP. It may be useful to calculate the NT-proBNP that would have been observed if GFR had stayed constant. To do this, let NTP_0, GFR_0, and Q_0, be the initial NT-proBNP, GFR, and cardiac production rate. Let NTP_1, GFR_1, and Q_1 be the final NT-proBNP, GFR, and proBNP production rates. Let NTP_x be the NT-proBNP that would exist if GFR had remained at GFR_0 but proBNP production rate is Q_1.

From Eq. 3.3,

$$Q_1 = NTP_1 GFR_1$$

and

$$Q_1 = NTP_x GFR_0 \,.$$

Therefore

$$NTP_x = \frac{NTP_1 GFR_1}{GFR_0}. \qquad \text{Eq. 3.13}$$

Thus, for any observed NT-proBNP and GFR, the NT-proBNP that would exist if cardiac proBNP production remained the same, but GFR were different can be calculated. This is a generalization of Eq. 3.5.

In addition, we can also determine how much cardiac production has changed between these two states. At the initial state,

$$Q_0 = NTP_0 GFR_0$$

Therefore, the ratio of cardiac production after (1) vs. before (0) is:

$$\frac{Q_1}{Q_0} = \frac{NTP_1}{NTP_0}\frac{GFR_1}{GFR_0} \qquad \text{Eq. 3.14}$$

These relationships can be quite useful in improving the interpretation and information that can be obtained from NT-proBNP.

3.3.2 Mathematical Relationship Between BNP and GFR

This predicted relationship between GFR and BNP at constant *Q* is shown graphically in **Figure 3.3**, assuming GFR_{ref} is 100 ml/min, NTP_{ref} is 5.88 pmol/L (50 pg/ml), and BNP_{ref} is 2.9 pmol/L (10 pg/ml). Compared to NT-proBNP (**Figure 3.2**), the curve for BNP is much less steep.

Inspecting equation 3.10, if we assume a molar ratio of normal NT-proBNP to BNP of approximately 2 (5.9/2.9 pmol/L), non-renal clearance CL_{nr} is equal to GFR_{ref}, and BNP is cleared half renally and half non-renally, compared to NT-proBNP which is cleared completely renally. As GFR falls, the non-renal clearance of BNP is maintained, and thus BNP rises less.

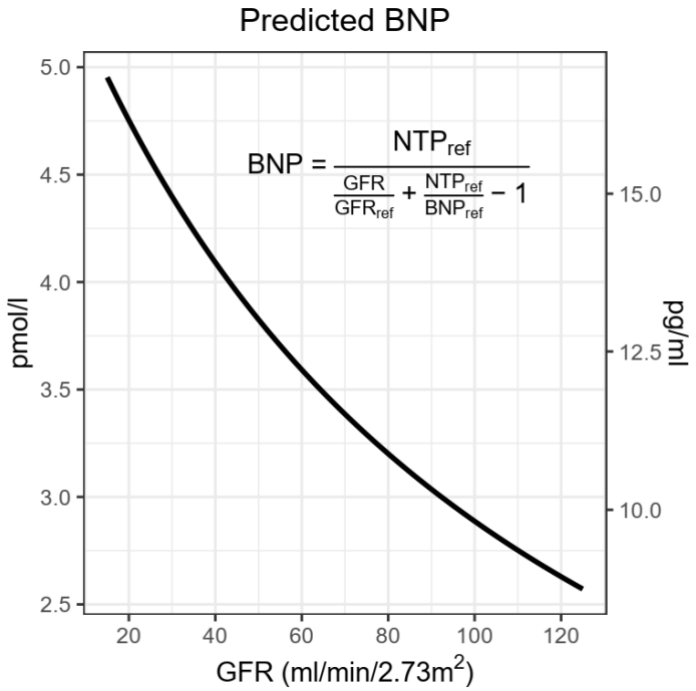

Figure 3.3. *Predicted effect of GFR on BNP at constant pro-BNP release rate Q (Eq. 3.10). Simulation assumes normal GFR of 100 ml/min, normal NT-proBNP of 50 pg/ml (5.88 pmol/L), and normal BNP of 10 pg/ml.*

3.3.3 Mathematical Relationship Between Ratio of NT-proBNP to BNP and GFR

Study	**N**	**Population**	**NT-proBNP Assay**	**BNP Assay**	**GFR groups (ml/min/1.73 m²)**
PARADIGM-HF [37]	6438	HF-rEF (non-Afib subgroup)	ECLIA on Elecsys analyzer (Roche Diagnostics)	Advia Centaur (Bayer Diagnostics)	eGFR < 60 eGFR 60-89 eGFR ≥ 90
Vickery 2005 [38]	219	Stage 3-5 CKD	ECLIA on Elecsys analyzer (Roche Diagnostics)	Advia Centaur (Bayer Diagnostics)	eGFR < 15 eGFR 15-29 eGFR 30-60

Val-HeFT [39]	3916	HF-rEF	ECLIA on Elecsys analyzer (Roche Diagnostics)	IRMA, Shionoria, Shionogi, Japan	eGFR < 30 eGFR 30-59 eGFR 60-89 eGFR ≥ 90
van Kimmenade 2009 [36]	165	Hypertensive subjects with suspected renal stenosis	ECLIA on Elecsys analyzer (Roche Diagnostics)	IRMA, Shionoria, Shionogi, Japan	Individual data, eGFR 11- 134

Table 3.1. *Clinical studies reporting dependence of ratio of NT-proBNP to BNP on GFR*

We compared the relationship predicted by Eq. 3.12 to observations from four different clinical studies (**Figure 3.4**). The details of each clinical study are summarized in Table 1. While all four studies considered measured NT-proBNP using the same assay, two different assays were used for BNP. The automated immunoassay used in PARADIGM-HF [37] and Vickery et al [38] has been shown to report BNP values 10-15% higher than the earlier manual immunoradiometric assay used in Val-HeFT[39] and van Kimmenade et al [36], which means the ratio of NT-proBNP to BNP will be 10-15% lower in these studies. In applying Eq. 3.12, BNP_{ref} was 10 pg/ml (2.88 pmol/L) in the first two studies, and 9 pg/ml (2.6 pmol/L) in the last two. GFR_{ref} was 100 ml/min and NTP_{ref} was 50 pg/ml (5.88 pmol/L) for all four studies.

As shown in **Figure 3.4**, Eq. 3.14 performed well in predicting the increasing ratio of NT-proBNP to BNP with decreasing GFR across the different studies, which together included a wide range of eGFR. The ability to predict the change in ratios across studies and across GFR provides confidence that the assumptions used in developing the equations are reasonable. The equation assumes the production rates of BNP and NT-proBNP are always equal but makes no assumptions about how cardiac proBNP production changes with GFR – the ratio is independent of production rate. Cardiac stretch and thus cardiac proBNP production rate may increase in many subjects as

GFR declines, as poor renal function puts more stress on the heart, but this does not impact the biomarker ratio.

The increasing ratio can be explained by decreasing GFR alone, without requiring any changes in non-renal BNP clearance, supporting the assumption of constant non-renal clearance. However, the equation can also be applied to suggest a possible role for changes in non-renal clearance.

In PARADIGM-HF, the subgroup with atrial fibrillation (Afib) had a higher ratio across all GFR levels compared to patients without Afib. Because the ratio is independent of production, this difference cannot be explained by differences in cardiac production in Afib patients (although production may indeed be influenced by Afib). However, this difference could be reproduced mathematically if non-renal BNP clearance in the Atrial fibrillation group is assumed to be increased, as shown in **Figure 3.3a** (green curve – non-renal clearance increased 65%). While this is currently only a mathematical hypothesis, NPR-C is the most highly expressed receptor in the atrium and has been found to be protective against Afib. One could speculate that atrial NRP-C could be upregulated as an adaptive mechanism in Afib patients, resulting in increased BNP non-renal clearance, and thus a higher ratio.

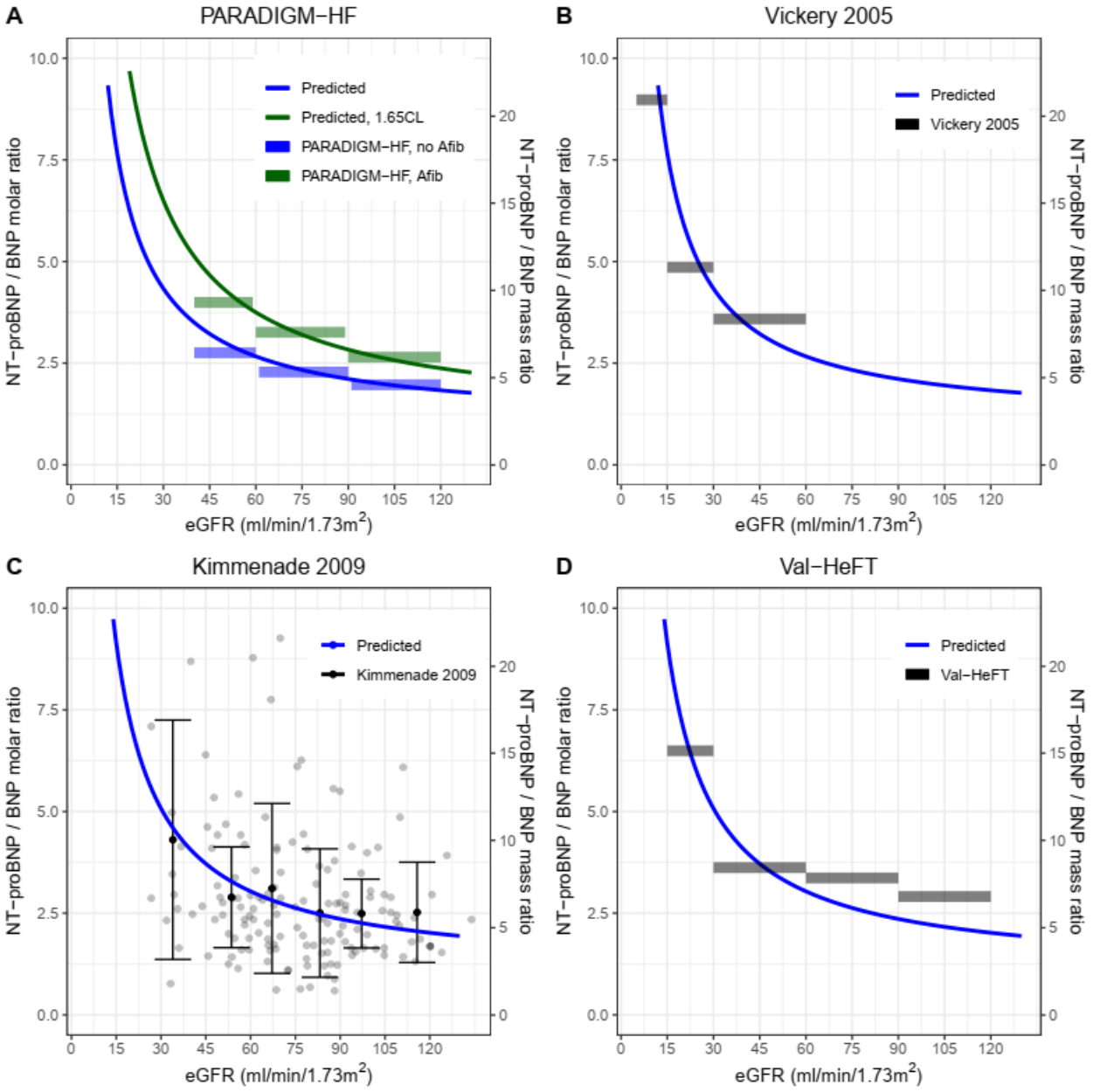

Figure 3.4. *Mechanistic relationship between NT-proBNP to BNP ratio and GFR (Equation 13,14) explains observations from 4 clinical studies. In A), a second prediction is shown (green) representing increased non-renal clearance (x1.65). For PARADIGM (A), Vickery et al (B), and Val-HeFT (D), ratios were reported by GFR range or CKD class. Horizontal bars represent the mean reported value for each category. Predicted curves assume* NTP_{ref} *= 50 pg/ml,* BNP_{ref} *= 10 pg/ml, and* $eGFR_{ref}$ *= 100 ml/min/1.73m*^{2}*.* CL_{nr} *was calculated using Eq. 3.8.*

3.4 Discussion and Conclusion

This analysis developed a straightforward mechanistic approach to account for renal effects on natriuretic peptides biomarkers BNP and NT-proBNP. We showed that we were able to use a mathematical function to describe the production and clearance rates of BNP and NT-proBNP and their relationship with kidney function (measured by GFR). The renal effect makes interpretation of BNP and NT-proBNP difficult since thresholds are usually stratified by patient characteristics. However, correcting for GFR may be more useful as GFR decreases with age. These equations require a few assumptions, but the BNP equations are not sensitive to the assumption of the initial NT-proBNP to BNP ratio. The ability of our equations to reproduce data seen in multiple studies provides confidence that our equations and assumptions are reasonable.

CHAPTER 4

Integrating a Model Relating Natriuretic Peptide Biomarkers and Kidney Function into a Larger Cardiorenal Model and Validating the Response to Therapy

Introduction

Computational models have been developed by Guyton, Coleman, Bovendeerd, and Cox to represent cardiac structure, and improvements over the years have allowed these models to capture changes in geometry of the heart as well as calculate EF and important biomarkers and blood pressure. The Hallow Lab developed an integrated quantitative systems pharmacology model (QSP) to link cardiac function with renal function to simulate renal hemodynamics for a wide range of heart conditions and investigate the effect of therapies on this system.

QSP models incorporate data from multiple sources to computationally represent a biological system and predict outcomes without the need for costly and time-consuming experiments. While not perfect, they allow researchers to gather a qualitative understanding of the system as well as how that system responds to various therapies. Each parameterization of a QSP model can be viewed as a virtual patient (VPs) and populations of VPs (VPops) can be used to analyze uncertainty within QSP models and explore the range of possible outcomes. VPops can be constructed to "match" distributions of clinical data based on the available outputs, and several methods exist for creating such VPops. Since natriuretic peptide (NPs) are used as surrogate measures of HF severity and pressure within the heart due to fluid buildup, relationships to link cardiac stress and kidney dysfunction to changes in NPs were developed and integrated into a larger cardiorenal model. The goal of this aim was to gather a set of HF-rEF virtual patients and

simulate the effects of therapy (ARB) and compare to a published clinical trial. In addition, we aimed to identify the parameters that were most influential in explaining that response to therapy by conducting a Sobol Sensitivity analysis.

The relationships among cardiac stress, kidney dysfunction and natriuretic peptides were developed in a smaller mechanistic model in aim 2. We saw our model was able to reproduce relationships between kidney dysfunction and NPs as seen in multiple clinical studies with relevant data. Specifically, NP concentrations increased as GFR decreased. We then incorporated these relationships into the larger cardiorenal model and produced a set of virtual patients that closely matched a clinical dataset. This VPop was simulated according to the Val-HeFT protocol and was shown to have very similar predicted effects on BNP as seen in the trial (37% placebo-adjusted change in Val-HeFT vs. 39 – 44% in VPop). In addition, our Sobol Sensitivity analysis showed contractility as the most influential in predicting BNP response, while nephron loss was most influential in predicting GFR and LV EDS response to therapy.

4.1 Methods

4.1.1 Deriving relationship between wall stress and natriuretic peptides.

The objective of this aim is to expand upon the previously described relationships between BNP/NT-proBNP and GFR and incorporate them into a larger cardiorenal model. We then used these relationships to validate the QSP cardiorenal model by simulating a set of clinically representative virtual patients and their response to therapy. Previous methods only derived equations for kidney function and natriuretic peptides, but never formally derived the production rates.

As previously described, the rate of change of the amount of plasma NT-proBNP is the difference between the rate of production Q and the rate of renal filtration. Under the assumption of free filtration, the rate of filtration is the product of GFR and the plasma concentration of NT-proBNP is given by

$$V_N \frac{dNTP}{dt} = Q - GFR * NTP \qquad \text{Eq. 4.1}$$

and the rate of change of the amount of plasma BNP is given by

$$V_B \frac{dBNP}{dt} = Q - GFR * BNP - CL_{nr} * BNP. \qquad \text{Eq. 4.2}$$

We derived steady state equations for production in Chapter 3, adjusted BNP and NT-proBNP concentrations and the non-renal clearance constant for BNP. We briefly mentioned in the previous chapter that production was related to cardiac wall stress but failed to derive the relationship and will do so in this chapter. We assume that proBNP cardiac production rate increases in response to increases in passive stretch of the ventricle wall during diastole, so that the rate of production Q is a function of left ventricle end diastolic wall stress:

$$Q = Q_{ref} + m * (LV\ EDS - LV\ EDS_{ref}) . \qquad \text{Eq. 4.3}$$

Here, LV EDS_{ref} is the left ventricular (LV) end diastolic wall stress under normal conditions, Q_{ref} is the basal rate of proBNP production at normal LV EDS, and m defines the slope of the relationship between LV EDS and proBNP production.

To define the relationship between LV EDS and proBNP production in Eq. 4.3, the model was fit to data reported by Iwanaga et al. 2007 who reported a very strong linear relationship between end diastolic wall stress and BNP [33]. Iwanaga et al measured BNP in 160 consecutive patients admitted to a local medical center for congestive heart failure. BNP was measured using an immunoassay technique, LV EDP, Volume, and ejection fraction were measured during cardiac

catheterization, and echocardiography was used to calculate LV mass. End-diastolic wall stress was calculated combining catheter and echocardiography data from a expression derived in [82]

$$EDWS = 0.334 \times P \times (LVID)/WT \times (1 + WT/LVID), \qquad \text{Eq. 4.4}$$

where EDWS = end-diastolic wall stress, P = LV pressure, LVID = LV internal dimension, WT = wall thickness.

We then examined the presented relationship between end-diastolic wall stress (EDWS) and BNP and performed simple linear regression to obtain a slope to relate BNP to EDWS (**Figure 4.1**). The resulting equation of the line is BNP = 0.037*LVEDS – 0.055 with a R^2 value of 0.88.

Our relationship is further qualified by data seen in Alter et al. 2007 which shows a similar trend as Iwanaga's work [83]. Alter et al. enrolled 34 patients with suspected cardiomyopathy, and showed BNP levels binned across the range of EDS. In addition, parameter values used in the model and baseline concentrations are given in **Table 4.1** and **Figure 4.2**, respectively.

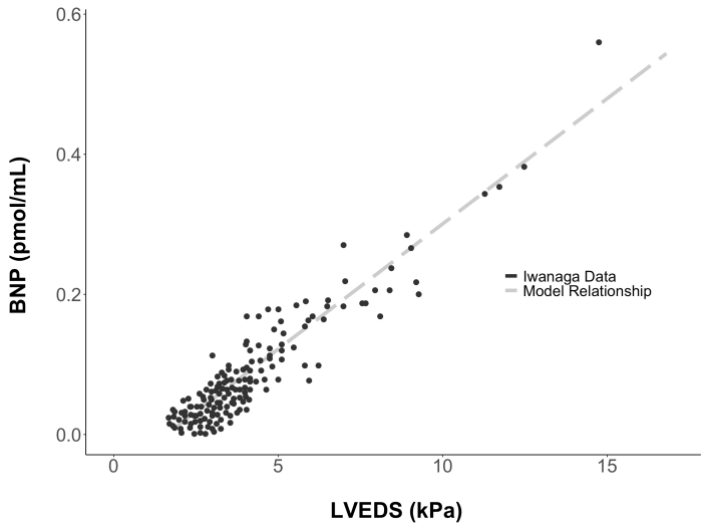

Figure 4.1. *Model reproduces the same EDS – BNP relationship as seen in Iwanaga's data. This relationship is further qualified by comparing results to that of Alter et al and reproducing similar relationship across binned stress levels.*

Parameter	Definition	Value
GFR_{ref}	Reference Glomerular filtration rate	100 mL/min/1.73m^2
LV EDS_{ref}	Reference left ventricular end diastolic stress	1.8 kPa
BNP_{ref}	Reference BNP	10 pg/mL(2.9 pmol/L)
NT-$proBNP_{ref}$	Reference NT-proBNP	50 pg/mL(5.9 pmol/L)
CL_{nr}	Non-renal clearance of BNP	0.101mL/min/1.73m^{2-1}
Q_{ref}	Reference proBNP production Rate	0.59 pmol/min
m	Slope relating LV EDS to BNP (from Iwanaga)	0.036 pmol / Pa

Table 4.1. BNP / NT-proBNP Submodel Parameters

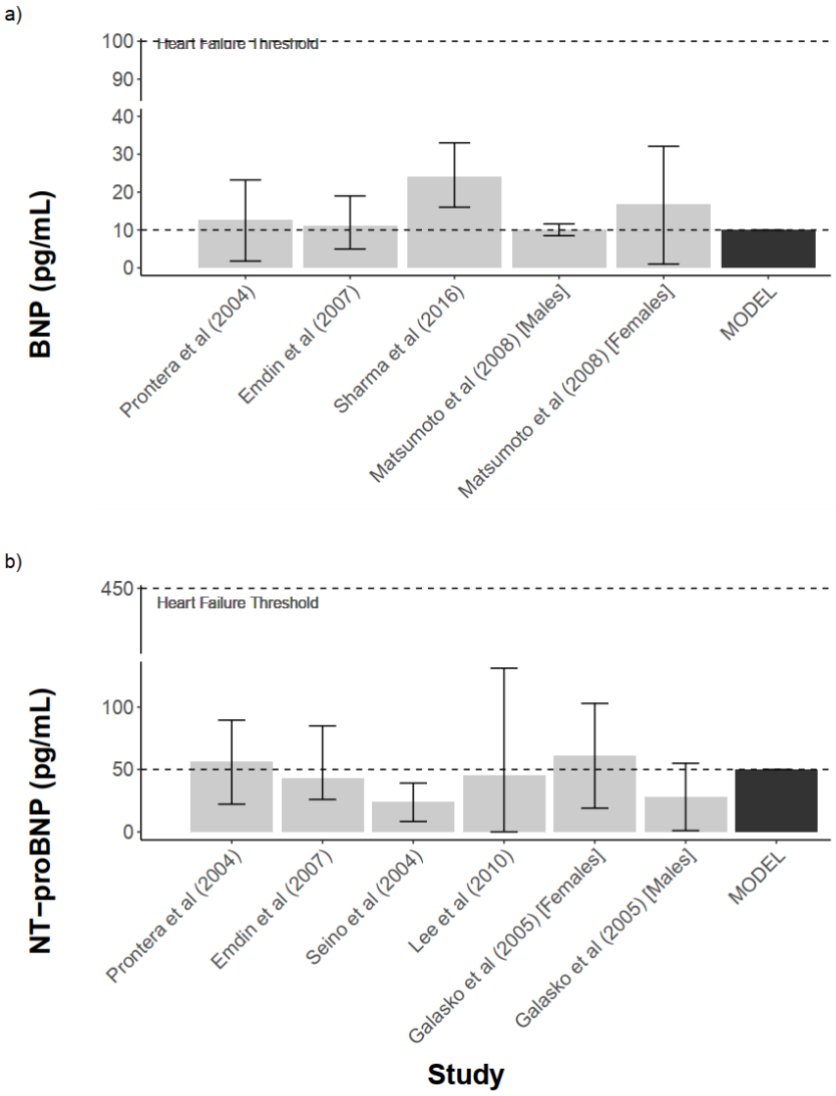

Figure 4.2. *Baseline values of BNP and NT-proBNP across multiple studies [84-91]. Based on these studies, reference BNP and NT-proBNP concentrations were set to 10 pg/mL (2.9 pmol/L) and 50 pg/mL (5.9 pmol/L), respectively [84-92]. Error bars represent reported measure of variability (median + IQR or mean +/- SD). Only studies that used Shionogi assay to measure BNP and Elecsys 2010 analyzer for NT-proBNP are included.*

The cardiorenal model calculated LV EDS and GFR dynamically, as a function of their underlying physiological determinants. The BNP/NT-proBNP submodel equations were incorporated into the larger cardiorenal model, with the dynamic model-calculated LV EDS and GFR as inputs into the BNP and NT-proBNP equations.

4.1.2 Validation of Integrated Model: Simulation of Val-HeFT Clinical Trial (Overview)

To validate the integrated model, we evaluated whether the model could reproduce the changes in BNP in HF-rEF patients treated with valsartan in the Val-HeFT clinical trial. To do this, we created a large set of virtual patients (VP's) with HF-rEF, using our previously described methodology, which we refer to as the "plausible" population [80]. From this plausible population, we selected a subset to match the baseline characteristics of the Val-HeFT clinical population. Because only summary level data has been published for Val-HeFT, we also utilized a second clinical dataset with mean baseline characteristics very similar to those of Val-HeFT, but with individual-level data available (described below), with the assumption that the distributions and correlations (or lack of correlation) between baseline characteristics is similar between the two study populations. From the plausible population, we selected a subset by matching the distributions of virtual population baseline ejection fraction and NT-proBNP to the clinical dataset. We then simulated the Val-HeFT protocol in these virtual patients, as described below, and compared model-predicted and observed placebo-adjusted changes in BNP with valsartan treatment.

4.1.3 Val-HeFT Study

Val-HeFT was a randomized, double-blind, placebo-controlled, phase III clinical trial. Eligible patients had a history of heart failure (documented left ventricular dysfunction with an ejection fraction less than 40%) and had to have been on a fixed-dose drug regimen that included ACE inhibitors, diuretics, digoxin, or beta-blockers for at least 2 weeks prior to randomization. A total of 5010 patients were randomized to receive either oral valsartan (initiated at 40mg twice daily and doubled every 2 weeks until 160 mg twice daily dosage was reached) or placebo (with similar dose-equivalent adjustments). Of the enrolled participants, 92.7% were on an ACE inhibitor, 34.9% were on a beta-blocker. Plasma BNP was reported in a sub-study at baseline and at 4 months, 1 year, 2 years, and study endpoint [93, 94].

4.1.4 Clinical Dataset

Because Val-HeFT only reported summary level information, we used published data from Spinar et el. with baseline characteristics similar to Val-HeFT to represent the Val-HeFT study population [95]. These data contained individual-level demographic information, medication history, survival outcomes, and more importantly, biomarkers of HF severity such as ejection fraction, NT-proBNP, and eGFR. In addition to accessibility, the common characteristics between this study and Val-HeFT's baselines were comparable, although the clinical dataset contained a slightly higher proportion of diabetic patients (41.4% vs. 25.5% in Val-HeFT) [95].

4.1.5 Virtual Patient Generation, Selection, and Trial Simulation

Virtual patients were generated using our previously described methodology [80], so parameters were calibrated to ensure the distribution of simulated variables of interest adequately covered the full range of the clinical dataset. Since nearly all patients in Val-HeFT (92.7%) and the clinical dataset (95%) were co-medicated with an ACE inhibitor (ACEi) or angiotensin-

receptor blocker (ARB), all VPs were simulated on ACEi therapy before study baseline. This process produced 12,000 plausible virtual patients (PP's).

From this plausible population, a subset of virtual patients was then selected to reconstruct the clinical dataset by matching distributions of a couple key variables (ejection fraction and NT-proBNP) using the accept-reject sampling technique [96]. Bivariate distributions for EF and NT-proBNP were calculated in the plausible population and clinical data, and each PP's individual density was compared between the 2 populations. The ratio of clinical density to plausible population density was calculated, so that higher values indicated a high likelihood of inclusion since similar patients were contained in the clinical dataset. Similarly, low ratio values indicated similar patients were not contained in the clinical population, thus very likely to be excluded. Sampling was performed without replacement; thus, all selected VPs were unique. This process was intended to ensure that important variables' distributions were matched sufficiently well to ensure we had a representative virtual population. The lowest possible value for NT-proBNP in the model was 50 pg/mL, thus it was impossible to capture any patients in the clinical dataset with values less than that. Extremely skewed variables (e.g. NT-proBNP with values > 10,000 pg/mL in clinical data) would be matched on the log scale, but we were not concerned with fully capturing these patients, thus resulting in inflated KS values, and therefore extreme values were retained. In addition, the KS test is sensitive to large sample size, thus leading to over significance in p-values. Other variables of interest were mean arterial pressure and GFR, but since those were not included in the initial selection process, our goal was to ensure at least they matched moderately well between the matched VP's and the clinical data. Resulting distributions were examined visually and any Kolmogorov-Smirnov test statistics < 0.2 were generally considered to be good matches.

Each selected virtual patient was simulated on a 160 mg dose of valsartan and placebo twice daily for 4 months. Valsartan and ACEi treatment were modeled as described previously [55]. Placebo-adjusted changes in simulated and GFR-corrected BNP and NT-proBNP were compared between the simulations and Val-HeFT. Four-month changes in NT-proBNP are not reported in Val-HeFT, thus only simulated and GFR-corrected results are presented.

4.1.6 Model Application: Sobol Sensitivity Analysis

A sensitivity analysis is conducted to identify the parameters that have the largest influence on a given model output's variability. A Sobol global sensitivity analysis is used and identifies influential parameters by decomposing the output variance into summands of the parameters' variances. We can estimate the contributions of each parameter and their interactions using

$$D(\boldsymbol{f}) = \sum_i D_i + \sum_{i<j} D_{ij} + \sum_{i<j<k} D_{ijk} + \cdots + D_{ijk,\ldots p},$$

where D(f) is the total variance of the model output, D_i indicates the first order variance contribution, D_{ij} is the 2nd order variance contribution (or the interactions between parameters) and remaining terms are the higher-order interactions between inputs (up to p, the number of input parameters). First order and total order indices are defined as follows:

$$S_i = \frac{D_i}{D}$$

$$S_{Ti} = 1 - \frac{D_i}{D}$$

A benefit of using Sobol sensitivity analysis is that there are no underlying assumptions about the relationship between input and output.

If we consider our ODE model to be

$$\dot{\boldsymbol{Y}} = f(\boldsymbol{Y}, \boldsymbol{x})\ ;\ \ \boldsymbol{Y}(\boldsymbol{0}) = y_0,$$

where Y is our output, and $\boldsymbol{x} = x_1 \dots x_p$ are our input parameters with probability distributions **P**. Since we are measuring the relative importance of each input parameter using a variance decomposition technique, the influence of a parameter, X_i is fixed at x_i* is described by the conditional variance

$$V_{x_{-i}}(Y|X_i = x_i^*).$$

The variance is calculated over the input parameter space of the other $p - 1$ parameters, and we use the law of total variance as the framework for the Sobol analysis:

$$V(Y) = V_{X_i}\left(E_{X_i}(Y|X_i)\right) + E_{X_i}(V_{X_i}(Y_{X_i})).$$

After normalizing (so variance totals to 1), dividing both sides by V(Y), we obtain

$$1 = \frac{V_{X_i}\left(E_{X_{-i}}(Y|X_i)\right)}{V(Y)} + \frac{E_{X_i}\left(V_{(X_{-i})}(Y_{X_i})\right)}{V(Y)}.$$

Thus, the first order index is

$$S_i = \frac{V_{X_i}\left(E_{X_{-i}}(Y|X_i)\right)}{V(Y)}$$

and total order index is

$$S_{Ti} = \frac{E_{X_i}\left(V_{X_{-i}}(Y_{X_i})\right)}{V(Y)} = 1 - \frac{V_{X_i}\left(E_{X_{-i}}(Y|X_i)\right)}{V(Y)}$$

Thus, the following property that must be satisfied:

$$0 \leq S_i \leq S_{Ti} \leq 1$$

The first term in the expression above is the first order sensitivity, the second is the total order effect, which is the variance of the expected value of Y conditioning on all the variables except the ith variable. The first order, S_i, represents, the expected reduction in overall variance, V(Y), if

the variables in X_i are fixed. In other words, it's the percentage of the variance that can be explained by each respective input parameter.

In practice, calculating these variances, expectations, and indices is impossible to do directly. Thus, Monte Carlo simulations are conducted to estimate the Sobol indices, specifically Azzini's method of calculating Sobol indices [97]. The indices are based on 2 matrices of N parameter sets, X_A and X_B ($N \times p$ matrices). The A and B matrices are created by identically *distributed* input vectors where the elements of the matrices are formed by the quasi-random numbers to fill the input space quicker more quickly than a Latin Hypercube Sampling technique, or completely random number sequence. If we let $j_1, \cdots, j_p$ be the i[th] sample of variable p, and define a 3[rd] and 4[th] parameter set matrix, X_{AB} and X_{BA}. X_{AB} for instance is the A matrix repeated p times, but with each iteration, column p in X_A is replaced with the same column from X_B. The p iterative matrices are then combined to form a $pN\ x\ p\ matrix$. A similar procedure is done to create the X_{BA} matrix (also a $pN\ x\ p$). In total then, $2N(p+1)$ simulations are required to estimate the indices.

The result is 4 sets of output:

$$Y_A = f(X_A)$$

$$Y_B = f(X_B)$$

$$Y_{AB} = f(X_{AB})$$

$$Y_{BA} = f(X_{BA})$$

$$X_A = \begin{bmatrix} X_{11} & \cdots & X_{1p} \\ \vdots & \ddots & \vdots \\ X_{N1} & \cdots & X_{Np} \end{bmatrix}, \qquad X_B = \begin{bmatrix} X_{11} & \cdots & X_{1p} \\ \vdots & \ddots & \vdots \\ X_{N1} & \cdots & X_{Np} \end{bmatrix}$$

$$X_{AB}^{(k)} = \begin{bmatrix} X_{11} & \cdots & X_{1p} \\ \vdots & \ddots & \vdots \\ X_{N1} & \cdots & X_{Np} \end{bmatrix}, \qquad X_{AB}^{p} = \begin{bmatrix} X_{11} & \cdots & X_{1p} \\ \vdots & \ddots & \vdots \\ X_{N1} & \cdots & X_{Np} \end{bmatrix}$$

$$X_{BA}^{(k)} = \begin{bmatrix} X_{11} & \cdots & X_{1p} \\ \vdots & \ddots & \vdots \\ X_{N1} & \cdots & X_{Np} \end{bmatrix}, \qquad X_{BA}^{p} = \begin{bmatrix} X_{11} & \cdots & X_{1p} \\ \vdots & \ddots & \vdots \\ X_{N1} & \cdots & X_{Np} \end{bmatrix}$$

There are versions of the Sobol sensitivity that can be calculated using either X_{AB} or X_{BA} alone. After calculating the 4 outputs, the Sobol sensitivity index using can be calculated by using Azzini's method as expressed by

$$\widehat{S_i} = \frac{\Sigma_{k=1}^{N}\left(f(X_B)_k - f\left(X_{BA}\right)_k^{(i)}\right)^2 + \left(f(X_A)_k - f\left(X_{AB}\right)_k^{(i)}\right)^2}{\Sigma_{k=1}^{N}\left(f(X_A)_k - f(X_B)_k\right)^2 + \left(f\left(X_{BA}\right)_k^{(i)} - f\left(X_{AB}\right)_k^{(i)}\right)^2}.$$

To ensure all outputs of sensitivities for the first and total order indices followed the assumptions and rule of Azzini's method, all simulations were run and analyzed by comparing full trajectories and ensuring all simulations had reached steady state before applying the drug effect, which, was ultimately the output used in the Sobol analysis. Multiple different sample sizes, N, were required to ensure non-negative sensitivities. Because N was then multiplied by $2N(p+1)$ to get the full number necessary simulations, all data was analyzed on a cluster computer and all outputs needed to be retrieved an analyzed in the correct order of analysis.

4.1.7 Software

The model was implemented in a free open-source programming R package RxODE package [98] (R 4.1.0). All data in this study are available from the corresponding author upon request.

4.2 Results

4.2.1 BNP-NT-proBNP Submodel Integration Validation

We incorporated the updated relationship between EDS and BNP and integrated these equations into the cardiorenal model along with the current formulas relating BNP and NT-

proBNP to GFR. After integration, as shown in results from the previous objective (3.4), we were able to obtain the stress-BNP relationships as seen in Iwanaga's work as well as the inverse relationship between GFR and the natriuretic peptides seen in multiple clinical studies. These results provide confidence that the model is performing as expected and further simulations were representative of human physiological function.

4.2.2 Virtual Patient Selection and Baseline Characteristics

Figure 4.3a shows the distributions of the baseline characteristics of 12909 plausible patients (PPs) and the 744 clinical patients including LVEF, log NT-proBNP, GFR, and MAP. Collectively, the created virtual patient population characteristics covered the range of baselines of the clinical dataset, though distributions of GFR and MAP differed slightly between our subset and the clinical dataset, but that is because our VPs were unable to capture the extreme ranges of these variables (in addition to NT-proBNP). **Figure 3.7b** showed that the baseline characteristics of the selected virtual population were like those in the clinical dataset, and thus likely to be similar to the Val-HeFT study population. **Table 4.2** gives summary statistics comparing the clinical dataset, Val-HeFT baseline characteristics, and our selected virtual patients where applicable. QSP models are unable to produce the range of values seen in real data, thus standard errors of virtual patients are less than that of clinical and Val-HeFT data. Virtual patient simulations would unpredictably fail to run; thus, a small surplus of virtual patients was selected to mimic distributions in the clinical dataset.

Variable Summarized	***Clinical Data (n = 744)***	***Val-HeFT Summary Data (n = 5010)***	***Virtual Patient Population (n = 1500)***
Ejection Fraction (%) (mean ± SD)	27.4 ± 6.4	26.7 ± 7.2	27.7 ± 5.8

BNP (pg/mL) (median [IQR])	243	181 ± 230 99 [41 – 242]	179.8 ± 130.1 138.4 [72.3 – 251.4]
NTP (ng/L) (median [IQR])	706.5	NA 895 [375 – 1985]	1129.1 ± 746.7 940.5 [527.7 – 1509.8]
SBP (mmHg) (mean ± SD)	126.4 ± 16.3	124.0 ± 19.0	128.3 ± 10.4
DBP (mmHg) (mean ± SD)	79.4 ± 10.6	76.0 ± 11.0	82.8 ± 6.4
Heart Rate (beats/min) (mean ± SD)	74.7 ± 13.0	73.0 ± 13.0	69.6 ± 8.1
Hypertension (%)	63.6%	6.1%	-
Diabetes (%)	41.4%	25.5%	-
Atrial Fibrillation (%)	34.3%	12.1%	-
Beta-Blockers (%)	94.8%	34.9%	-
Diuretics (%)	90.9%	85.5%	-
NYHA			
1	77 (9.7%)	0%	-
2	469 (59.1%)	62.1%	-
3	243 (30.6%)	36.1%	-
4	5 (0.6%)	1.7%	-

Table 4.2. *Comparison of baseline characteristics between clinical data, Val-HeFT summary data and virtual patient population. Pre-existing conditions included to show differences in health between Val-HeFT and clinical dataset (e.g. clinical data patients were more hypertensive).*

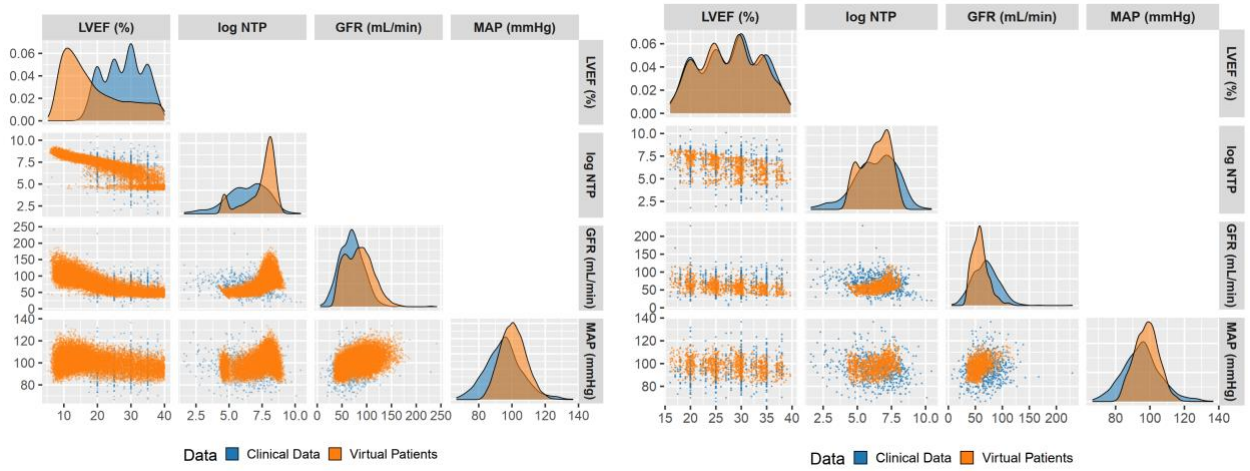

Figure 4.3. *Distributional characteristics of plausible population compared to the clinical dataset before and after selection of Virtual Patients.*

4.2.3 Virtual Patient Trial Simulation

Simulations reproduced very similar 4-month placebo-adjusted changes in BNP to that of Val-HeFT (**Figure 4.4)**. At 4 months Val-HeFT reported a mean placebo-adjusted change of 37 pg/mL compared to that in our simulations of 38.9 pg/mL of BNP and 44.2 pg/mL in the GFR-corrected BNP. This larger drop in BNP (and NT-proBNP) adjusted for GFR follows closely with what we expect since a slight drop in GFR with an ARB somewhat masks the full extent of improvement in BNP and NT-proBNP concentrations. **Figure 4.4** shows 4-month placebo-adjusted changes in GFR, LV EDP, and LV EDS with using an ARB. The simulated GFR's placebo-adjusted percent change of 10.2% is comparable to that reported in Val-HeFT (5.9%). Similarly, EDS and EDP show a placebo adjusted change of 16.7% and 14.1%, respectively.

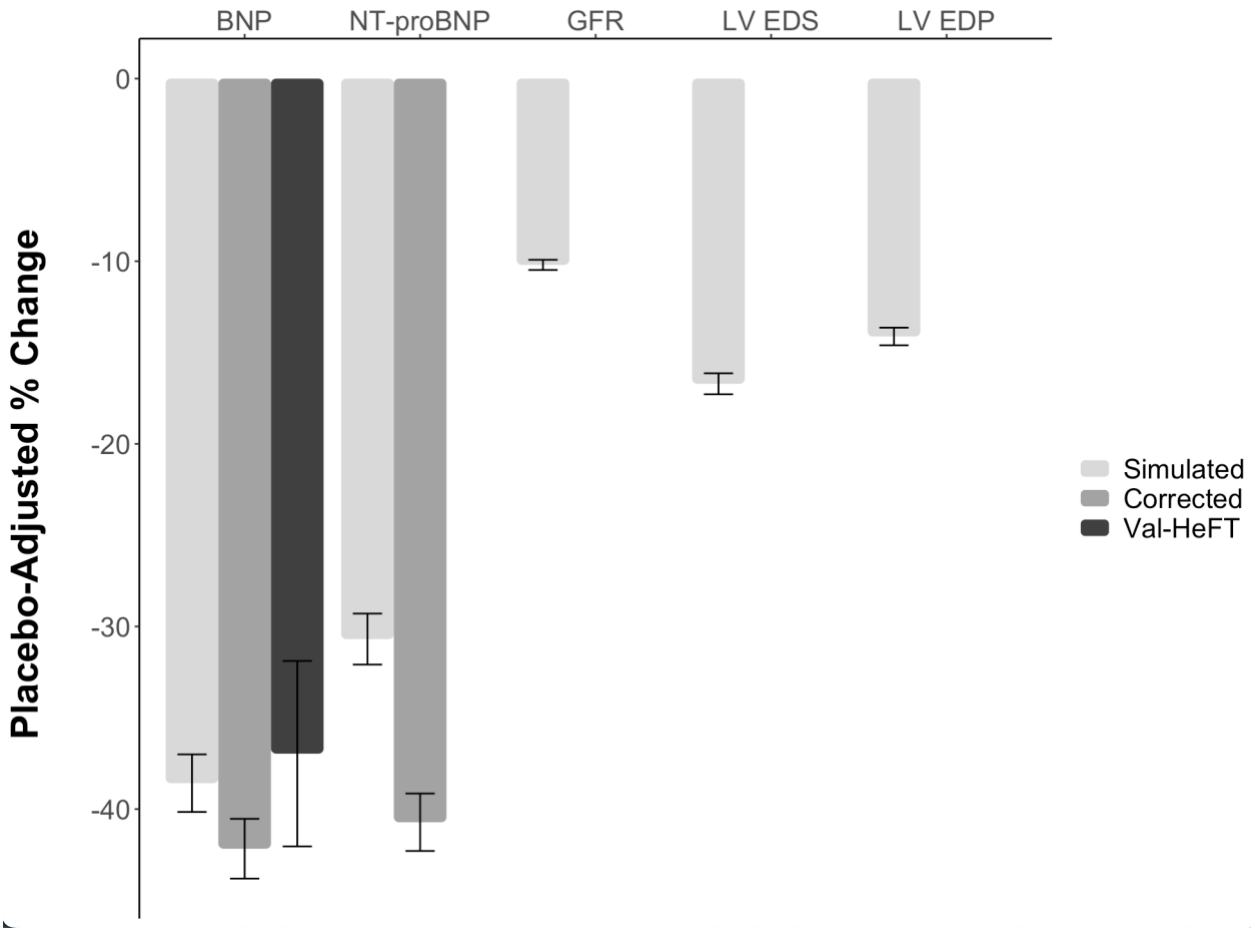

Figure 4.4. *Placebo-adjusted percent changes in BNP, NT-proBNP, GFR, LV EDS, and LV EDP. Changes in GFR are comparable to that seen in Val-HeFT (10% in simulations vs. 6% in Val-HeFT).*

4.2.4 Model Application

The Sobol Sensitivity Analysis using the QSP model was performed to analyze the parameters most influential in predicting the 4-month change of BNP, GFR, and LV EDS in response to use of an ARB. To see convergence of Sobol indices, different sample sizes ranging from 64 to 256 were tested to ensure convergence of the Sobol scores. When using Azzini's sampling scheme (see section 3.4.6), $2N(p+1) = 2 * 256 * 11 \; or \; 5632$ iterations were necessary to evaluate the indices. First order and total order sensitivities were calculated. The

ranges used for each parameter are listed in **Table 4.3.** First and total order indices for each parameter and their influence on BNP, GFR, and LV EDS are shown in (**Figure 4.5**). For BNP, contractility and nephron loss were responsible for 23% and 16% of the variance in BNP response. For GFR, over 80% was accounted for by nephron loss, and similarly to BNP, LV EDS was explained by nephron loss and contractility (25% and 21%, respectively).

Parameter Name	Range	Normal
HbA1c	5 – 15	4
LV Stiffness	1 – 1.48	1
LV Contractility	0.77 - 1	1
Nephron loss	0 – 0.755	0
Glomerulosclerosis	0 – 0.3	0
Peripheral resistance	1.26 – 1.36	1
CD Sodium Reabsorption	0.68 – 0.79	0.84
Proximal Tubule Na Reabsorption	0.55 – 0.66	0.7
CD Pressure Natriuresis	0.2 – 0.6	0.2
Proximal Tubule Pressure Natriuresis	0.2 – 0.6	0.2

Table 4.3. *Ranges of parameter values used in Sobol Sensitivity analysis*

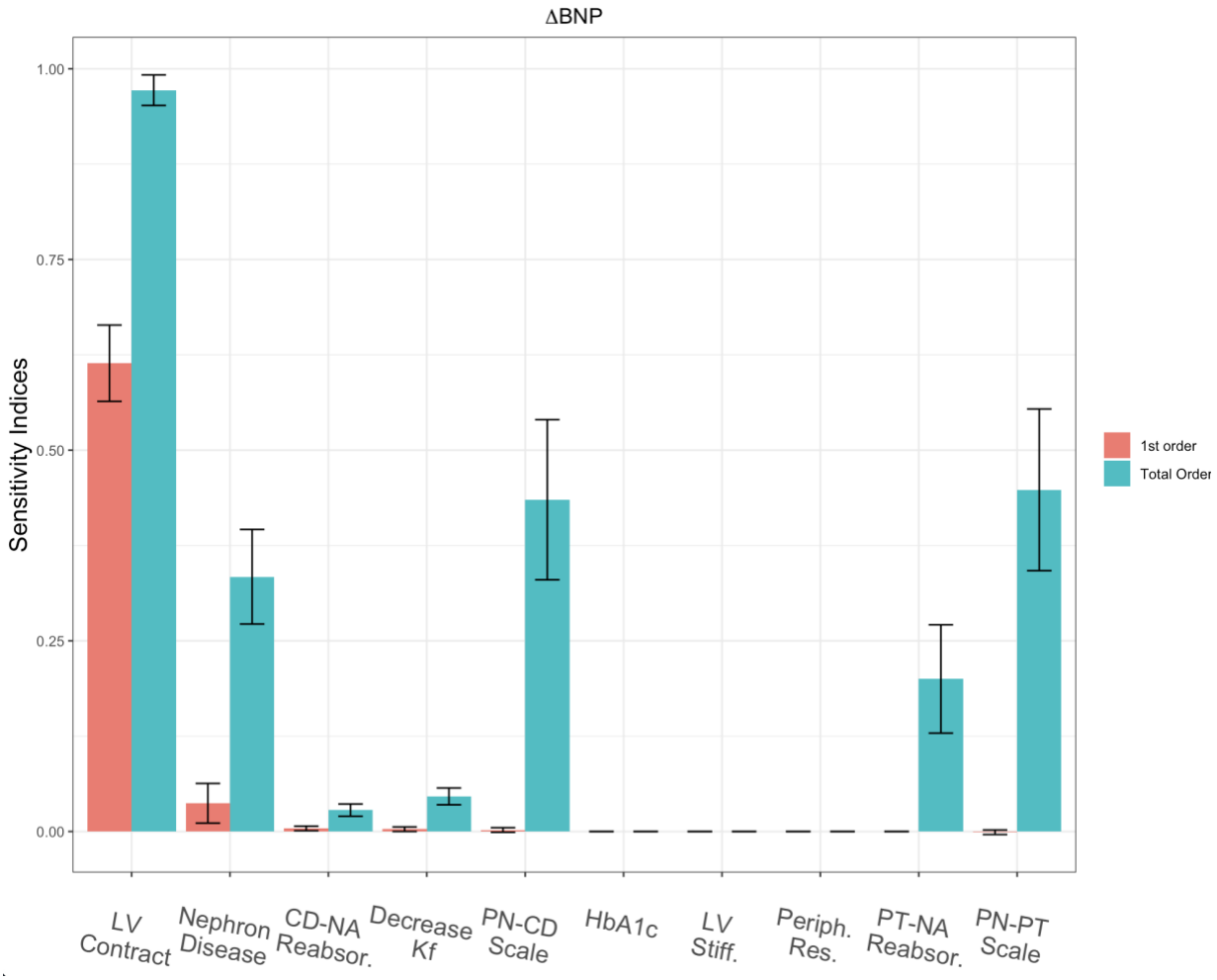

Figure 4.5a. *Sobol sensitivities (first order and total order) for each parameter on BNP Pink bars (first order) represent percentage of variance attributed to changes in that parameter, and green bars (total order) represent percentage of variance of all groups of variables that contain that input.*

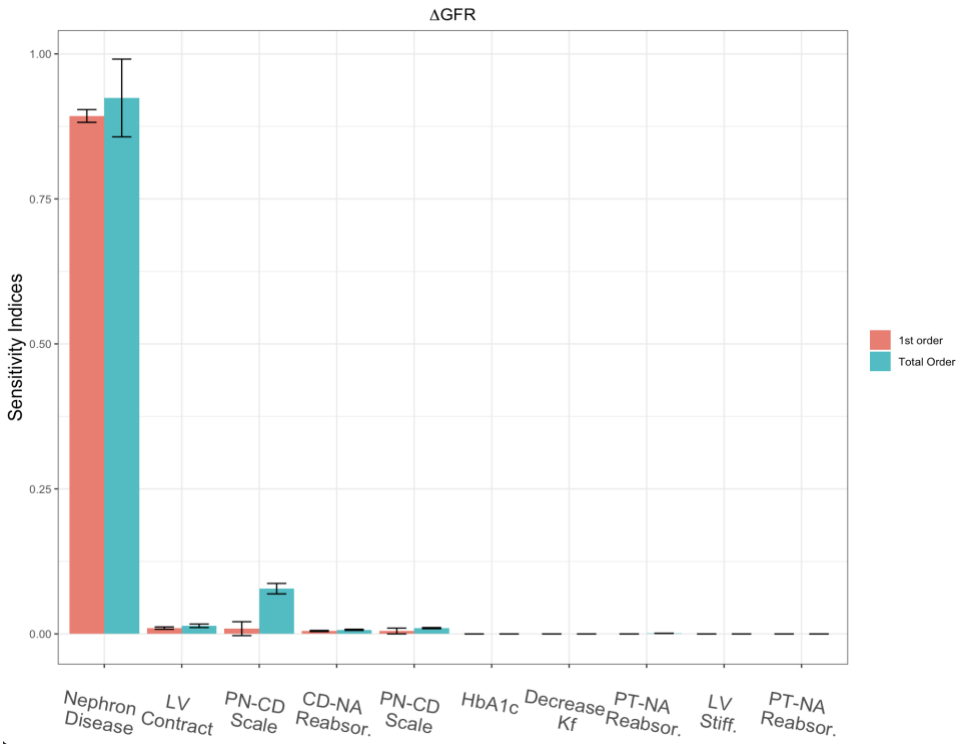

Figure 4.5b. *Sobol sensitivities (first order and total order) for each parameter on GFR.*

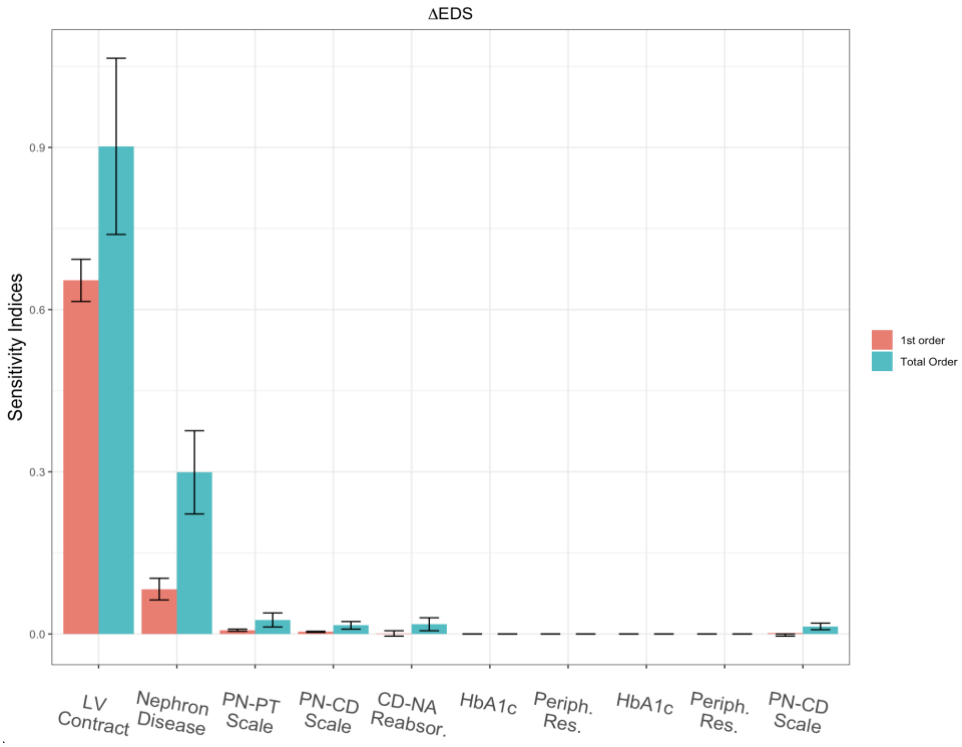

Figure 4.5c. *Sobol sensitivities (first order and total order) for each parameter on LV EDS.*

4.3 Discussion and Conclusions

We developed relationships between BNP, NT-proBNP, stress, and GFR and incorporated these relationships into a larger cardiorenal model. We described production rates as a function of stress and showed that the relationship derived was able to reproduce similar relationships in multiple studies. Incorporating these equations into the larger cardiorenal, we wanted to show that we can use these relationships and validate the response to therapy as seen in a published clinical trial. However, this study (Val-HeFT) did not report individual level data on all 5010 patients studied, only aggregated demographic and clinical data. Conveniently, a group of Czech researchers performed a study that measured NT-proBNP as a prognostic indicator of survival in heart failure and collected accessible individual level data. This data was used as surrogate dataset for the Val-HeFT data because baseline characteristics were similar between studies. We used our cardiorenal model to simulate plausible virtual patients and systematically selected them to reasonably match the distributions of common variables between the simulated and the clinical datasets. We then simulated our selected virtual patients on an ARB (like in Val-HeFT) and compared our response of BNP and NT-proBNP to that of Val-HeFT and used a machine learning method to determine parameters most influential in explaining the response to therapy.

When examining the results of the Sobol Sensitivity Analysis, we used Azzini's method to understand which parameters in our model were most influential in predicting 4-month changes in BNP, GFR, and LV EDS responses to therapy. Given the sampling scheme, 5632 iterations were necessary, and we saw that contractility was most influential in predicting BNP response while nephron loss / disease was most influential in predicting GFR and LV EDS response. Since contractility is important for powering the heart to pump blood adequately throughout the body, inability to distribute blood leads to fluid build up and thus, higher BNP. Therapies then, such as

ACEi and ARBs act to slow the heart rate and remodeling process in hopes of easing the stress within the heart allowing it to contract more strongly. In addition, since those treatments act through the kidneys in HF patients by maintaining water/sodium homeostasis and reducing volume retention. Moreover, while they are unable to spur the growth of nephrons, they can help with fluid retention and enable kidneys to hopefully filter more fluid quickly.

4.3.1 Limitations

Values for nominal BNP and NT-proBNP in healthy subjects varied widely, thus the values used are an estimate from the summary statistics presented in an ensemble of studies likely due to inconsistent assaying techniques to measure peptide levels. Moreover, PARADIGM's NT-proBNP to BNP ratio was higher than those predicted in our model which is likely because of an underlying effect of atrial fibrillation – among other conditions – that is not accounted for.

One limitation of this study is that use of a beta blocker was not considered in these simulations even though they also seemed to play an important role in the placebo response seen in Val-HeFT. For the given cardiorenal model, we assume the shape of the heart is a sphere, where cardiac valves were assumed to be perfect valves, thus oversimplifying some cardiac functions, such as speed of ejection during systole [80].When selecting a subset to match the Czech dataset, using only one variable to match distributions between the VP's and the Czech data led to very good matching and overlap in the resulting probability distributions, while sacrificing overlap in the remaining variables. Moreover, the lowest possible value for NT-proBNP in our model was 50 pg/mL; thus, it was impossible to capture any Czech patients with values less than that. Extremely skewed variables (e.g., NT-proBNP with values > 10,000 pg/mL in Czech data) would be matched on the log scale, but we were not concerned with fully capturing these patients, thus resulting in inflated KS values since all patients were retained. In addition, the KS test is sensitive to large

sample size, thus leading to over significance in p-values. Visually examining resulting distributions showed good overlap, thus any KS test statistics < 0.2 were generally considered to be good matches. Some virtual patient simulations would unpredictably fail to run; thus, a surplus of virtual patients was chosen to mimic distribution in the Czech dataset, but eventually down-sampled to adequately capture the original structure of the selected VPs' baseline characteristics.

CHAPTER 5

DISCUSSION, CONCLUSION, AND FUTURE DIRECTIONS

5.1 Discussion/Conclusion/Future Work

Several health conditions/diseases are present and costly to the population including heart failure, diabetes, hypertension, kidney disease, etc. These conditions are difficult to study because collecting data from these patients may prove difficult. To understand these conditions, mechanistic models in the form of ordinary differential equations can prove useful since they are a representation of reality, but some parameters in the model are not easily measured. Extensive work must be done with a combined effort between researchers and modelers to ensure completeness of these models while also understanding not everything will be able to be incorporated. As these models increase in size, computational cost increases accordingly, and researchers must be mindful of this increase in necessary resources. These models also come with a large amount of uncertainty and understanding the sensitivities of parameters in these types of models narrows down the scope of work to a degree. A significant amount of work has been done to quantify sensitivities of parameters – Latin hypercube sampling, variance-based methods such as Sobol indices, screening methods such as the Morris method, derivative based methods, and frequency methods are also considered. However, interactions between parameters aren't well studied and other methods to understand parameter interactions are required for future work.

Sensitivity analyses serve to "shrink" the model by enabling researchers to rank the parameters of interest and understanding what perturbing these parameters does to outputs of interest. After sensitive parameters are identified, it better informs researchers when

parameterizing the model and collecting simulations within reasonable ranges. When using different parameter sets (such as when conducting an Latin Hypercube Sampling tecnhique), each parameter set can be thought of as a belonging to a virtual patient since parameter values will vary across individuals. Collecting multiple iterations of the model with different parameter sets results in a group of plausible patients that combine to form a virtual population. From these Vpops, a subset based on quantities of interest is needed to cover a reasonable range of a clinical dataset to be representative of a real population. These Vpops contain different variables that match observables in clinical datasets, and selecting subsets to match these datasets are of great interest to researchers. When matching VP's to distributions, several methods exist that quantify the "distance" between the distributions (e.g. Kullback-Leibler Divergence, Jeffrys Divergence, Bhattacharya Distance) as well as tests that quantify the difference (Kolmogorov Smirnov and Cramer Von Mises tests). Divergences are not well understood and not intuitive, so KS and CVM tests are more easily explained and understood. 1- and 2-sample tests (comparing between sample and reference, or 2 samples) exist and are well formulated, but KS tests in higher dimensions (comparing bivariate distributions and higher) are not well researched. Being able to compare combinations of variables would better inform researchers about matching techniques and increase their confidence that their selected subset of VP's is, indeed, representative of a real / clinical population.

References

1. Emmert-Streib, F. and M. Dehmer, *Networks for systems biology: conceptual connection of data and function.* IET Syst Biol, 2011. **5**(3): p. 185-207.
2. Putnins, M., et al., *From data to QSP models: a pipeline for using Boolean networks for hypothesis inference and dynamic model building.* J Pharmacokinet Pharmacodyn, 2022. **49**(1): p. 101-115.
3. Allen, R., T. Rieger, and C. Musante, *Efficient Generation and Selection of Virtual Populations in Quantitative Systems Pharmacology Models.* CPT: Pharmacometrics & Systems Pharmacology, 2016. **5**(3): p. 140-146.
4. Huang, C., et al., *Clinical features of patients infected with 2019 novel coronavirus in Wuhan, China.* Lancet (London, England), 2020. **395**(10223): p. 497-506.
5. Passarella, P., et al., *Hypertension Management in Diabetes: 2018 Update.* Diabetes spectrum : a publication of the American Diabetes Association, 2018. **31**(3): p. 218-224.
6. Whelton, P.K., et al., *2017 ACC/AHA/AAPA/ABC/ACPM/AGS/APhA/ASH/ASPC/NMA/PCNA Guideline for the Prevention, Detection, Evaluation, and Management of High Blood Pressure in Adults: Executive Summary: A Report of the American College of Cardiology/American Heart Association Task Force on Clinical Practice Guidelines.* Circulation, 2018. **138**(17): p. e426-e483.
7. Guo, J., et al., *Coronavirus Disease 2019 (COVID-19) and Cardiovascular Disease: A Viewpoint on the Potential Influence of Angiotensin-Converting Enzyme Inhibitors/Angiotensin Receptor Blockers on Onset and Severity of Severe Acute Respiratory Syndrome Coronavirus 2 Infection.* J Am Heart Assoc, 2020. **9**(7): p. e016219.
8. de Abajo, F.J., et al., *Use of renin-angiotensin-aldosterone system inhibitors and risk of COVID-19 requiring admission to hospital: a case-population study.* Lancet, 2020. **395**(10238): p. 1705-1714.
9. Son, M., J. Seo, and S. Yang, *Association Between Renin-Angiotensin-Aldosterone System Inhibitors and COVID-19 Infection in South Korea.* Hypertension, 2020. **76**(3): p. 742-749.
10. Trifirò, G., et al., *Renin-Angiotensin-Aldosterone System Inhibitors and Risk of Death in Patients Hospitalised with COVID-19: A Retrospective Italian Cohort Study of 43,000 Patients.* Drug safety, 2020. **43**(12): p. 1297-1308.
11. Bozkurt, B., R. Kovacs, and B. Harrington, *Joint HFSA/ACC/AHA Statement Addresses Concerns Re: Using RAAS Antagonists in COVID-19.* Journal of Cardiac Failure, 2020. **26**: p. 370.
12. Derington, C.G., et al., *Trends in Antihypertensive Medication Monotherapy and Combination Use Among US Adults, National Health and Nutrition Examination Survey 2005–2016.* Hypertension, 2020. **75**(4): p. 973-981.
13. Verdecchia, P., et al., *The pivotal link between ACE2 deficiency and SARS-CoV-2 infection.* Eur J Intern Med, 2020. **76**: p. 14-20.
14. Dandona, P., et al., *Angiotensin II and inflammation: the effect of angiotensin-converting enzyme inhibition and angiotensin II receptor blockade.* J Hum Hypertens, 2007. **21**(1): p. 20-7.

15. Simões e Silva, A.C., et al., *ACE2, angiotensin-(1-7) and Mas receptor axis in inflammation and fibrosis.* Br J Pharmacol, 2013. **169**(3): p. 477-92.
16. Fang, L., G. Karakiulakis, and M. Roth, *Are patients with hypertension and diabetes mellitus at increased risk for COVID-19 infection?* The Lancet. Respiratory medicine, 2020. **8**(4): p. e21-e21.
17. Sriram, K. and P.A. Insel, *Risks of ACE Inhibitor and ARB Usage in COVID-19: Evaluating the Evidence.* Clinical Pharmacology & Therapeutics, 2020. **108**(2): p. 236-241.
18. Tay, M.Z., et al., *The trinity of COVID-19: immunity, inflammation and intervention.* Nature Reviews Immunology, 2020. **20**(6): p. 363-374.
19. Zambelli, V., et al., *Angiotensin-(1-7) improves oxygenation, while reducing cellular infiltrate and fibrosis in experimental Acute Respiratory Distress Syndrome.* Intensive Care Med Exp, 2015. **3**(1): p. 44.
20. Imai, Y., K. Kuba, and J.M. Penninger, *The discovery of angiotensin-converting enzyme 2 and its role in acute lung injury in mice.* Exp Physiol, 2008. **93**(5): p. 543-8.
21. Imai, Y., et al., *Angiotensin-converting enzyme 2 protects from severe acute lung failure.* Nature, 2005. **436**(7047): p. 112-6.
22. Gaddam, R.R., S. Chambers, and M. Bhatia, *ACE and ACE2 in inflammation: a tale of two enzymes.* Inflamm Allergy Drug Targets, 2014. **13**(4): p. 224-34.
23. Wysocki, J., et al., *ACE and ACE2 activity in diabetic mice.* Diabetes, 2006. **55**(7): p. 2132-9.
24. Anguiano, L., et al., *Circulating angiotensin-converting enzyme 2 activity in patients with chronic kidney disease without previous history of cardiovascular disease.* Nephrol Dial Transplant, 2015. **30**(7): p. 1176-85.
25. Xie, X., et al., *Age- and gender-related difference of ACE2 expression in rat lung.* Life Sci, 2006. **78**(19): p. 2166-71.
26. Yoon, H.E., et al., *Age-Associated Changes in the Vascular Renin-Angiotensin System in Mice.* Oxid Med Cell Longev, 2016. **2016**: p. 6731093.
27. Kuba, K., et al., *A crucial role of angiotensin converting enzyme 2 (ACE2) in SARS coronavirus-induced lung injury.* Nat Med, 2005. **11**(8): p. 875-9.
28. Wrapp, D., et al., *Cryo-EM structure of the 2019-nCoV spike in the prefusion conformation.* Science (New York, N.Y.), 2020. **367**(6483): p. 1260-1263.
29. Collinson, P., *Natriuretic Peptides - A Review*. European Cardiology 2005;1(1):66-9, 2005.
30. Ponikowski, P., et al., *2016 ESC Guidelines for the diagnosis and treatment of acute and chronic heart failure: The Task Force for the diagnosis and treatment of acute and chronic heart failure of the European Society of Cardiology (ESC). Developed with the special contribution of the Heart Failure Association (HFA) of the ESC.* Eur J Heart Fail, 2016. **18**(8): p. 891-975.
31. Januzzi, J.L., et al., *NT-proBNP testing for diagnosis and short-term prognosis in acute destabilized heart failure: an international pooled analysis of 1256 patients: the International Collaborative of NT-proBNP Study.* Eur Heart J, 2006. **27**(3): p. 330-7.
32. Cao, Z., Y. Jia, and B. Zhu, *BNP and NT-proBNP as Diagnostic Biomarkers for Cardiac Dysfunction in Both Clinical and Forensic Medicine.* Int J Mol Sci, 2019. **20**(8).
33. Iwanaga, Y., et al., *B-type natriuretic peptide strongly reflects diastolic wall stress in patients with chronic heart failure: comparison between systolic and diastolic heart failure.* J Am Coll Cardiol, 2006. **47**(4): p. 742-8.

34. Krittayaphong, R., et al., *Correlation Between NT-pro BNP levels and left ventricular wall stress, sphericity index and extent of myocardial damage: a magnetic resonance imaging study.* J Card Fail, 2008. **14**(8): p. 687-94.
35. Kroll, M.H. and P. Srisawasdi, *The clearance of BNP modeled using the NT-proBNP–BNP relationship.* Biosystems, 2007. **88**(1): p. 147-155.
36. van Kimmenade, R.R., et al., *Renal clearance of B-type natriuretic peptide and amino terminal pro-B-type natriuretic peptide a mechanistic study in hypertensive subjects.* J Am Coll Cardiol, 2009. **53**(10): p. 884-90.
37. Rorth, R., et al., *Comparison of BNP and NT-proBNP in Patients With Heart Failure and Reduced Ejection Fraction.* Circ Heart Fail, 2020. **13**(2): p. e006541.
38. Vickery, S., et al., *B-type natriuretic peptide (BNP) and amino-terminal proBNP in patients with CKD: relationship to renal function and left ventricular hypertrophy.* Am J Kidney Dis, 2005. **46**(4): p. 610-20.
39. Masson, S., et al., *Direct comparison of B-type natriuretic peptide (BNP) and amino-terminal proBNP in a large population of patients with chronic and symptomatic heart failure: the Valsartan Heart Failure (Val-HeFT) data.* Clin Chem, 2006. **52**(8): p. 1528-38.
40. Farnsworth, C.W., et al., *Diagnostic concordance between NT-proBNP and BNP for suspected heart failure.* Clinical Biochemistry, 2018. **59**: p. 50-55.
41. Cunningham, J.W. and P.L. Myhre, *NT-proBNP Response to Heart Failure Therapies: An Imperfect Surrogate.* J Am Coll Cardiol, 2021. **78**(13): p. 1333-1336.
42. Guyton, A.C., *Regulation of cardiac output.* Anesthesiology, 1968. **29**(2): p. 314-26.
43. Suga, H. and K. Sagawa, *Instantaneous pressure-volume relationships and their ratio in the excised, supported canine left ventricle.* Circ Res, 1974. **35**(1): p. 117-26.
44. Tsuruta, H., et al., *Mathematical model of cardiovascular mechanics for diagnostic analysis and treatment of heart failure: Part 1. Model description and theoretical analysis.* Med Biol Eng Comput, 1994. **32**(1): p. 3-11.
45. Stergiopulos, N., B.E. Westerhof, and N. Westerhof, *Total arterial inertance as the fourth element of the windkessel model.* Am J Physiol, 1999. **276**(1): p. H81-8.
46. Smith, B.W., et al., *Minimal haemodynamic system model including ventricular interaction and valve dynamics.* Med Eng Phys, 2004. **26**(2): p. 131-9.
47. Bovendeerd, P.H., et al., *Dependence of intramyocardial pressure and coronary flow on ventricular loading and contractility: a model study.* Ann Biomed Eng, 2006. **34**(12): p. 1833-45.
48. Hallow, K.M., et al., *Cardiorenal Systems Modeling: Left Ventricular Hypertrophy and Differential Effects of Antihypertensive Therapies on Hypertrophy Regression.* Front Physiol, 2021. **12**: p. 679930.
49. Allen, R.J., T.R. Rieger, and C.J. Musante, *Efficient Generation and Selection of Virtual Populations in Quantitative Systems Pharmacology Models.* CPT Pharmacometrics Syst Pharmacol, 2016. **5**(3): p. 140-6.
50. Rice, G.I., et al., *Evaluation of angiotensin-converting enzyme (ACE), its homologue ACE2 and neprilysin in angiotensin peptide metabolism.* Biochem J, 2004. **383**(Pt 1): p. 45-51.
51. Vickers, C., et al., *Hydrolysis of biological peptides by human angiotensin-converting enzyme-related carboxypeptidase.* J Biol Chem, 2002. **277**(17): p. 14838-43.

52. Bhuiyan, M.A., et al., *Engineered mutation of some important amino acids in angiotensin II type 1 (AT1) receptor increases the binding affinity of AT1-receptor antagonists.* J Pharmacol Sci, 2010. **113**(1): p. 57-65.
53. Santos, R.A.S., et al., *Angiotensin-(1–7) is an endogenous ligand for the G protein-coupled receptor Mas.* Proceedings of the National Academy of Sciences, 2003. **100**(14): p. 8258-8263.
54. Kocks, M.J., et al., *Sodium status and angiotensin-converting enzyme inhibition: effects on plasma angiotensin-(1-7) in healthy man.* J Hypertens, 2005. **23**(3): p. 597-602.
55. Gebremichael, Y., et al., *Benchmarking renin suppression and blood pressure reduction of direct renin inhibitor imarikiren through quantitative systems pharmacology modeling.* J Pharmacokinet Pharmacodyn, 2019. **46**(1): p. 15-25.
56. Yamamoto, K., et al., *In vivo metabolism of angiotensin I by neutral endopeptidase (EC 3.4.24.11) in spontaneously hypertensive rats.* Hypertension, 1992. **19**(6 Pt 2): p. 692-6.
57. Hallow, K.M., et al., *A model-based approach to investigating the pathophysiological mechanisms of hypertension and response to antihypertensive therapies: extending the Guyton model.* Am J Physiol Regul Integr Comp Physiol, 2014. **306**(9): p. R647-62.
58. Bayes-Genis, A., J. Barallat, and A.M. Richards, *A Test in Context: Neprilysin: Function, Inhibition, and Biomarker.* J Am Coll Cardiol, 2016. **68**(6): p. 639-653.
59. Hamming, I., et al., *Tissue distribution of ACE2 protein, the functional receptor for SARS coronavirus. A first step in understanding SARS pathogenesis.* J Pathol, 2004. **203**(2): p. 631-7.
60. Roca-Ho, H., et al., *Characterization of ACE and ACE2 Expression within Different Organs of the NOD Mouse.* Int J Mol Sci, 2017. **18**(3).
61. Yamaleyeva, L.M., et al., *Differential regulation of circulating and renal ACE2 and ACE in hypertensive mRen2.Lewis rats with early-onset diabetes.* Am J Physiol Renal Physiol, 2012. **302**(11): p. F1374-84.
62. Yamamoto, K., et al., *In vivo metabolism of angiotensin I by neutral endopeptidase (EC 3.4.24.11) in spontaneously hypertensive rats.* Hypertension, 1992. **19**(6_pt_2): p. 692-696.
63. Glowacka, I., et al., *Differential downregulation of ACE2 by the spike proteins of severe acute respiratory syndrome coronavirus and human coronavirus NL63.* J Virol, 2010. **84**(2): p. 1198-205.
64. Soro-Paavonen, A., et al., *Circulating ACE2 activity is increased in patients with type 1 diabetes and vascular complications.* J Hypertens, 2012. **30**(2): p. 375-83.
65. Anguiano, L., et al., *Circulating angiotensin-converting enzyme 2 activity in patients with chronic kidney disease without previous history of cardiovascular disease.* Nephrol Dial Transplant, 2015. **30**(7): p. 1176-85.
66. Reich, H.N., et al., *Decreased glomerular and tubular expression of ACE2 in patients with type 2 diabetes and kidney disease.* Kidney Int, 2008. **74**(12): p. 1610-6.
67. Konoshita, T., et al., *Tissue gene expression of renin-angiotensin system in human type 2 diabetic nephropathy.* Diabetes Care, 2006. **29**(4): p. 848-52.
68. Lely, A., et al., *Renal ACE2 expression in human kidney disease.* 2004. **204**(5): p. 587-593.
69. Ye, M., et al., *Increased ACE 2 and decreased ACE protein in renal tubules from diabetic mice: a renoprotective combination?* Hypertension, 2004. **43**(5): p. 1120-5.
70. Crackower, M.A., et al., *Angiotensin-converting enzyme 2 is an essential regulator of heart function.* Nature, 2002. **417**(6891): p. 822-8.

71. Swärd, P., et al., *Age and sex differences in soluble ACE2 may give insights for COVID-19.* Crit Care, 2020. **24**(1): p. 221.
72. Bunyavanich, S., A. Do, and A. Vicencio, *Nasal Gene Expression of Angiotensin-Converting Enzyme 2 in Children and Adults.* JAMA, 2020. **323**(23): p. 2427-2429.
73. Flacco, M.E., et al., *Treatment with ACE inhibitors or ARBs and risk of severe/lethal COVID-19: a meta-analysis.* Heart (British Cardiac Society), 2020. **106**(19): p. 1519-1524.
74. Tikellis, C., et al., *Improved islet morphology after blockade of the renin- angiotensin system in the ZDF rat.* Diabetes, 2004. **53**(4): p. 989-97.
75. Zambelli, V., et al., *Angiotensin-(1-7) improves oxygenation, while reducing cellular infiltrate and fibrosis in experimental Acute Respiratory Distress Syndrome.* Intensive care medicine experimental, 2015. **3**(1): p. 44-44.
76. Klein, N., et al., *Angiotensin-(1-7) protects from experimental acute lung injury.* Crit Care Med, 2013. **41**(11): p. e334-43.
77. Supé, S., et al., *Therapeutic time window for angiotensin-(1-7) in acute lung injury.* Br J Pharmacol, 2016. **173**(10): p. 1618-28.
78. Sechi, L.A., et al., *Tissue-specific regulation of type 1 angiotensin II receptor mRNA levels in the rat.* Hypertension, 1996. **28**(3): p. 403-8.
79. Bastien, N.R., et al., *Downregulation of cardiac AT1-receptor expression and angiotensin II concentrations after long-term blockade of the renin-angiotensin system in cardiomyopathic hamsters.* J Cardiovasc Pharmacol, 1999. **34**(3): p. 402-6.
80. Yu, H., S. Basu, and K.M. Hallow, *Cardiac and renal function interactions in heart failure with reduced ejection fraction: A mathematical modeling analysis.* PLoS Comput Biol, 2020. **16**(8): p. e1008074.
81. Luchner, A., et al., *Improvement of the cardiac marker N-terminal-pro brain natriuretic peptide through adjustment for renal function: a stratified multicenter trial.* Clin Chem Lab Med, 2010. **48**(1): p. 121-8.
82. Douglas, P.S., et al., *Comparison of echocardiographic methods for assessment of left ventricular shortening and wall stress.* J Am Coll Cardiol, 1987. **9**(4): p. 945-51.
83. Alter, P., et al., *Relation of B-type natriuretic peptide to left ventricular wall stress as assessed by cardiac magnetic resonance imaging in patients with dilated cardiomyopathy.* Can J Physiol Pharmacol, 2007. **85**(8): p. 790-9.
84. Prontera, C., et al., *Analytical performance and diagnostic accuracy of a fully-automated electrochemiluminescent assay for the N-terminal fragment of the pro-peptide of brain natriuretic peptide in patients with cardiomyopathy: comparison with immunoradiometric assay methods for brain natriuretic peptide and atrial natriuretic peptide.* Clin Chem Lab Med, 2004. **42**(1): p. 37-44.
85. Emdin, M., et al., *Comparison of brain natriuretic peptide (BNP) and amino-terminal ProBNP for early diagnosis of heart failure.* Clin Chem, 2007. **53**(7): p. 1289-97.
86. Seino, Y., et al., *Application of NT-proBNP and BNP measurements in cardiac care: a more discerning marker for the detection and evaluation of heart failure.* Eur J Heart Fail, 2004. **6**(3): p. 295-300.
87. Sharma, V., et al., *Plasma brain natriuretic peptide concentrations in patients with valvular heart disease.* Open Heart, 2016. **3**(1): p. e000184.
88. Li, S., et al., *Establishment of normal reference values of NT-proBNP and its application in diagnosing acute heart failure in children with severe hand foot and mouth disease [corrected].* Medicine (Baltimore), 2018. **97**(36): p. e12218.

89. Galasko, G.I., et al., *What is the normal range for N-terminal pro-brain natriuretic peptide? How well does this normal range screen for cardiovascular disease?* Eur Heart J, 2005. **26**(21): p. 2269-76.
90. Lee, K.H., et al., *N-Terminal Pro-B-type Natriuretic Peptide Levels in the Korean General Population.* Korean Circ J, 2010. **40**(12): p. 645-50.
91. Matsumoto, M., et al., *Anemia as a factor that elevates plasma brain natriuretic peptide concentration in apparently healthy subjects.* Int Heart J, 2008. **49**(5): p. 577-86.
92. Ohashi, N., et al., *Salt intake causes B-type natriuretic peptide elevation independently of blood pressure elevation in the general population without hypertension and heart disease.* Medicine (Baltimore), 2021. **100**(19): p. e25931.
93. Cohn, J.N. and G. Tognoni, *A Randomized Trial of the Angiotensin-Receptor Blocker Valsartan in Chronic Heart Failure.* New England Journal of Medicine, 2001. **345**(23): p. 1667-1675.
94. Latini, R., et al., *Effects of valsartan on circulating brain natriuretic peptide and norepinephrine in symptomatic chronic heart failure: the Valsartan Heart Failure Trial (Val-HeFT).* Circulation, 2002. **106**(19): p. 2454-8.
95. Spinar, J., et al., *Prognostic value of NT-proBNP added to clinical parameters to predict two-year prognosis of chronic heart failure patients with mid-range and reduced ejection fraction - A report from FAR NHL prospective registry.* PLoS One, 2019. **14**(3): p. e0214363.
96. Casella, G., C.P. Robert, and M.T. Wells, *Generalized Accept-Reject Sampling Schemes.* Lecture Notes-Monograph Series, 2004. **45**: p. 342-347.
97. Azzini, I. and R. Rosati, *Sobol' main effect index: an Innovative Algorithm (IA) using Dynamic Adaptive Variances.* Reliability Engineering & System Safety, 2021. **213**: p. 107647.
98. Wang, W., K.M. Hallow, and D.A. James, *A Tutorial on RxODE: Simulating Differential Equation Pharmacometric Models in R.* CPT Pharmacometrics Syst Pharmacol, 2016. **5**(1): p. 3-10.